universität wien

DISSERTATION / DOCTORAL THESIS

Titel der Dissertation /Title of the Doctoral Thesis

„Bioluminescent and fluorescent reporter constructs for tracking signalling pathways *in vitro* and tumour growth *in vivo*“

verfasst von / submitted by

Julia Maier, MSc

angestrebter akademischer Grad / in partial fulfilment of the requirements for the degree of

Doctor of Philosophy (PhD)

Wien, 2019 / Vienna 2019

Studienkennzahl lt. Studienblatt / degree programme code as it appears on the student record sheet:	A 794 685 437
Dissertationsgebiet lt. Studienblatt / field of study as it appears on the student record sheet:	Biologie / Biology
Betreut von / Supervisor:	Univ. Prof. Dipl. Ing. Dr. Manfred Ogris

Acknowledgements

First, my thanks to Manfred and all the lessons he taught me about life, and for the many opportunities that I was given due to his choice of accepting me. Thanks also go to Sebastian, who taught me the value of making decisions. I also want to mention Alexandra Elbakyan, whose work inspired me greatly in my scientific endeavours.

There are a lot of people that helped me on my way; people from my past, people I only wrote emails with and have never seen, people that always helped out with things when I was in dire need. I am grateful to all of them.

A deep “thank you” goes to my students. I like to think that Timo, Erna, Rabia, Nawid, Islam and Katarina have taught me more than I taught them. I also thank all the other students in our lab that made the time there so precious and instructive, and who I had the honour to be trusted by.

I want to thank Haider for his advice and kindness, Anna for her open ears and patience, and Susi for being the amazing person that she is.

To my great fortune I did not only find excellent co-workers in our lab, but a family. In this new lab that we built with our hands and hearts, we shared sadness and happiness, a microwave and cinnamon, and sometimes even labelled knifes. Alex, Antonia and Magda, you shaped me, and I shaped you, and this is a thing of true beauty. You will be a part of me always.

The deepest gratitude is reserved for my other half, who holds me in perpetual love and kindness. Thank you.

Table of Contents

Acknowledgements ..... **i**

Table of Contents **2**

1 Abstract **4**

2 Zusammenfassung **5**

3 Introduction **6**

3.1 Part One: Reporter systems 6

3.1.1 Promoters in reporter constructs 6

3.1.2 Bioluminescent and fluorescent protein reporter genes 8

3.1.3 Reporter systems for assessing protein-protein-interactions: BRET and FRET 9

3.1.4 Reporter assay normalization 10

3.1.5 Construction and delivery of reporter systems 11

3.2 Part Two: Developmental pathways in cancer research 13

3.2.1 The Wnt pathway 14

3.2.2 The Hedgehog pathway 16

3.2.3 The Notch pathway 17

3.3 Part Three: Optical and imaging techniques - from single cell to multimodal *in vivo* methods 19

3.3.1 High-throughput single cell investigation: flow cytometry 19

3.3.2 Luciferase multicolour combinations 21

3.3.3 Multimodal *in vivo* imaging techniques 22

3.4 Part Four: Gene delivery 23

3.4.1 Lentiviruses 24

3.4.2 LPEI 27

4 Publications **29**

2.1 Luminescent and Fluorescent Triple Reporter Plasmid Constructs for Wnt, Hedgehog and Notch Pathway 29

2.2 Multimodal Fluorescence and Bioluminescence Imaging Reveals Transfection Potential of Intratracheally Administered Polyplexes for Breast Cancer Lung Metastases 68

2.3 Up-Scaled Synthesis and Characterization of Nonviral Gene Delivery Particles for Transient *In Vitro* and *In Vivo* Transgene Expression 84

5 Discussion 96

6 References 109

Disclaimer 117

1 Abstract

The use of reporter systems has become a central method for research in molecular biology. In these, a promoter that is sensitive to a biological process is coupled to an output gene whose expression is easy to detect. Since the molecular discovery of firefly luciferase and green fluorescent protein, luciferases as well as fluorescent proteins have become standard equipment in reporter systems. Often, such systems are employed to uncover the activity of signalling pathways, such as the Wnt, Hedgehog or Notch pathway. Additionally, specific constructs can be utilized to analyse processes *in vivo*, using imaging techniques.

In this work, we develop reporter constructs for visualizing the activity of the three central developmental pathways Wnt, Hedgehog and Notch. For this, we design fluorescent as well as luminescent reporter constructs for each pathway. The generated single-pathway reporters are tested and compared to constructs already described in the literature. After their successful evaluation, we develop and clone a fluorescent and a luminescent multi-pathway reporter construct that each include reporters for all three pathways, and rigorously investigate their performance. In another project, we employ multimodal fluorescence and bioluminescence imaging to visualize the *in vivo* growth as well as the transfection efficiency of fluorescently labelled breast cancer metastases in the lung. Lastly, we develop and evaluate an approach to facilitate easy and reproducible generation of polyplexes, a non-viral gene delivery vehicle, for *in vitro* and *in vivo* purposes.

The broad spectrum of reporter systems employed allows a detailed discussion of e.g. fluorescent proteins and luciferases as reporter genes, as well as the promotor performance in terms of specificity and sensitivity. Also, we discuss how to improve our reporter constructs in follow-up projects, and give an outlook on the future utilization of such constructs for the identification and evaluation of novel therapeutic substances.

2 Zusammenfassung

Reportersysteme sind mittlerweile ein fundamentaler Bestandteil der molekularbiologischen Forschung. In solchen Systemen wird ein Promotor, der auf einen biologischen Prozess reagiert, mit einem Output Gen gekoppelt, dessen Expression leicht zu detektieren ist. Seit der Entdeckung der Firefly Luciferase und des Green Fluorescent Protein werden fluoreszente Proteine sowie Luciferasen sehr häufig in Reportersystemen verwendet. Oft werden solche Systeme eingesetzt, um die Aktivität von Signalwegen zu untersuchen. Ebenso können bestimmte Konstrukte auch zur Analyse von Prozessen *in vivo* mittels bildgebender Verfahren verwendet werden.

In dieser Arbeit wurden Reporterkonstrukte generiert, um die Aktivität der drei entwicklungsbiologisch zentralen Signalwege Wnt, Hedgehog und Notch zu visualisieren. Hierfür wurden für jeden Signalweg fluoreszierende sowie lumineszierende Reporterkonstrukte erstellt. Die daraus entstehenden Reporter für einzelne Signalwege wurden dann mit bereits in der Literatur beschriebenen Konstrukten verglichen. Nach erfolgreicher Evaluierung wurden Multi-Signalweg-Reporter kloniert und evaluiert, welche alle drei Signalwege auf einmal detektieren können, und zwar jeweils einen aus fluoreszierenden Proteinen und einen aus Luciferase-Reportern. In einem weiteren Projekt wurde Fluoreszenz- und Biolumineszenzimaging eingesetzt, um das *in vivo* Wachstum und die Transfektion von fluoreszenzmarkierten Brustkrebszell-Metastasen in der Lunge zu visualisieren. Letztendlich wurde eine Methode, mit der einfach und reproduzierbar Polyplexe für nicht-virale Transfektion *in vitro* und *in vivo* hergestellt werden können, evaluiert.

Das breite Spektrum der gesamt verwendeten Reportersysteme erlaubt eine detailreiche Diskussion, wie etwa einen Vergleich von fluoreszierenden Proteinen und Luciferasen, sowie die Eignung der benutzten Promotoren in Bezug auf Spezifität und Empfindlichkeit. Zuletzt wird diskutiert, wie die generierten Reporterkonstrukte in nachfolgenden Projekten optimiert werden können, und ein Ausblick auf die Nutzung solcher Konstrukte zur Identifizierung und Evaluierung neuer therapeutischer Wirkstoffe gegeben.

3 Introduction

3.1 Part One: Reporter systems

The observation of living systems is the driving force of biology. In molecular biology specifically, it is hard to observe most events directly, and scientists often resort to lysing, fixing or, more generally, sacrificing the object of study to investigate it further. A workaround for this challenge are so-called reporter systems. In a reporter system, a biological signal is re-routed to an output that can be more readily measured, for example a visible entity. As such, reporter systems offer a method of observing molecular processes, such as gene expression or regulation, often also in living specimen.

On the molecular level, a reporter in molecular biology is a dedicated DNA construct that consists two parts. A signal receiver, such as a promotor that is sensitive to the process to be investigated, regulates expression of the output (1, 2). The second part, the output reporter gene, is matched to the organism of study, as it ideally should not appear endogenously (3), and should be closely tailored to the experimental setup. Often, genes with special optical properties are chosen, as we will see further below.

3.1.1 *Promoters in reporter constructs*

Comparing a reporter construct to a piece of computational code, a promoter acts like an “if” condition: it determines if the downstream reporter gene is expressed. As such, the choice of promoter is connected to the question of *what is investigated*.

One method of obtaining such promoters is to use existing promoter regions that are involved in the process of interest, which is thought to approximate the native gene regulation (4). Examples for this are the PTCH1_WT (5) with a length of 1.3kb. To identically copy a promoter is often challenging. For example, transcriptional regulation in mammals is typically governed by core, proximal, and distal promoter sequences,

whose genomic distance can be considerable, often ruling out a complete replication of these structures for experimental approaches (6).

As an alternative, promoters can also be designed. Normally, such synthetic promoters consist of a so-called minimal promoter, to which several repeats of relevant transcription factor (TF) or enhancer binding sites are added (7). Frequently used minimal promoters often show considerable expression strength on their own and possess characteristics that simplify experimental work, such as a short overall sequence. They include viral promoter elements, such as the simian virus SV40 promoter, mammalian promoter sequences such as the murine 3-phosphoglycerate kinase promoter (PGK), or engineered sequences (8, 9).

Synthetic promoters thus offer a parsimonious approach to identify the action of specific TFs when used in a reporter construct. Also, the usage of multiple TF binding sites gives rise to comparatively sensitive systems. To give examples, the synthetic promoter of the Wnt pathway reporter construct TOPFlash consists of a TATA-Box as minimal promoter, with seven TCF/LEF binding sites, totalling around 170 base pairs (10). 4xwtCBF1Luc, a synthetic Notch pathway reporter construct, incorporates a promoter consisting of four CBF1-binding sites and the basal simian virus-SV40-promoter, and has a total size of around 350 base pairs (11).

In a study, the synthetic 12GLI-RETKO-luc reporter construct, consisting of twelve GLI-binding sites and a basal thymidine kinase promoter, encompassing 500 base pairs, while the PTCH1 promoter fragment, which included two GLI-binding sites, contains about 4.3 kilobase pairs (12). The performance of the synthetic promoter far exceeded that of the native promoter fragment in this publication. Additionally, small reporter gene sizes are preferable for some approaches, such as lentivirus generation, as we will see further below.

For some applications, such as the permanent labelling of a subtype of cells for *in vivo* imaging, a continuous expression of the reporter gene may be desired. So-called constitutive promoters, such as the promoters of the immediate-early cytomegalovirus (CMV) or the human elongation factor 1α-subunit (EF1α), are often utilized. Varying in their expression strength, silencing profile and base pair length, they also need to be chosen carefully (13).

3.1.2 *Bioluminescent and fluorescent protein reporter genes*

After choosing the process to be investigated by selecting a promoter, the choice of the reporter gene is related to the question *how a process is investigated*. The expressed protein will be the measured entity, and its properties and kinetics heavily influence the experimental methodology. The first reporter genes were mostly metabolic agents, facilitating enzymatic reactions that did not exist in the target cells. The research on the *Escherichia coli* lac operon gave rise to modified β-galactosidases, which can be considered to be the earliest reporter genes (14). Before today's systems, chloramphenicol acetyltransferase (CAT) was widely employed. For its evaluation, chromatography, or extraction procedures needed to be applied (3). Harnessing the bioluminescence of the firefly *Photinus pyralis* by isolating its luciferase advanced the field considerably, enabling for example luminescence-based high-throughput methods (15, 16).

Luciferases are enzymes which release a photon upon catalysing the oxidation of their substrate, generally called luciferins. As of now, several luciferases can be employed as reporter genes, varying in e.g. their needed substrates, kinetics, wavelength of emitted photons, and cellular localizations. Firefly luciferase (FLuc) uses D-luciferin, is ATP dependent, and displays a lasting glow kinetic in most assays when CoASH is added (17, 18). Several luciferases originate from marine organisms, as bioluminescence is wide-spread in oceanic ecosystems. There, it serves as rapid long-distance directional communication system, especially for small and/or deep-sea organisms (19). The crustacean *Gaussia princeps*' Gaussia luciferase (GLuc) requires the substrate coelenterazine, which is the most frequently luciferin used in marine organisms. GLuc is ATP independent, and emits a more blue-shifted light, as do many marine luciferases of deep sea organisms. Also, GLuc is secreted by cells, and displays a rapid flash-kinetic (18). Natural luciferases have also been engineered to possess enhanced characteristics. For example, NanoLuc (NLuc), a modified version of the sea shrimp *Oplophorus gracilirostris'* luciferase, shows exceptional brightness, uses furimazine as substrate, is blue-shifted, and requires no ATP. In contrast to GLuc, is shows glow kinetics (20). These different properties of luciferases allow parallel usage in one assay, so-called multiplexing.

Bioluminescent assays have a negligible background and thus a higher signal-to-noise ratio, a higher dynamic range, and are employed for *in vivo* imaging and reporter gene assay screens, for example in drug discovery (21).

The palette of reporter genes was further considerably expanded with the discovery of green fluorescent protein (GFP) as fluorescent tag of the jellyfish *Aequorea victoria* (22). Today, a multitude of fluorophores exist, spanning from blue to far red emission, modified to enable diverse experimental techniques, and research is ongoing intensely (23). When choosing fluorophores, autofluorescence of the entity investigated has to be considered (24), which is generally negligible for luciferases. As especially the water and lipids in tissues absorb less light in the so-called “optical window” between 650 nm-950 nm, far-red fluorophores such as iRFP720 can also be utilized for *in vivo* imaging (23, 25). The simultaneous use of several fluorescent proteins is possible, but care has to be taken to successfully combine the excitation and emission profiles. In flow cytometry, the method of spectral compensation is routinely used, but not without pitfalls (26), as will be discussed in detail further below. Fluorophores remain a standard tool for microscopy and flow cytometry, especially for subcellular and molecular investigations (27).

Taken together, the choice of the reporter gene generally depends on the experimental method employed for signal readout. Combinations of reporter genes to track several biological processes at once are possible by utilizing different promoters and reporter genes, and special care has to be taken to combine reporter genes that can be experimentally well distinguished.

3.1.3 *Reporter systems for assessing protein-protein-interactions: BRET and FRET*

The special properties of bioluminescent and fluorescent proteins can also be used to investigate protein-protein interactions, for example in protein complexes or receptor-ligand interactions. Such systems can be based on Resonance Energy Transfer (RET), normally requiring a two-component system. In short, a donor molecule emits photons in an emission wavelength which overlaps with the excitation wavelength of a second molecule, the acceptor (28). For this to happen, the two molecules need to be in close

proximity, generally considered to be 10-100 Å, and protein orientation needs to be suitable to facilitate proton transfer (29, 30).

Bioluminescence-initiated RET (BRET) has been observed since the 1970's in deep sea organisms, such as the cnidarian *Renilla reniformis* (31). In this naturally occurring system, the *Renilla* luciferase (RLuc) emits blue light, by which in turn the *Renilla* GFP is excited, giving off green light. In experimental molecular biology, RLuc is still used for BRET, and yellow fluorescent protein (YFP) is still widely used as acceptor (32).

In fluorescence resonance energy transfer (FRET), two fluorophores are utilized. The first, more blue-shifted fluorophore is excited by external monochromatic light. Similar to BRET, this first molecule then gives off photons, which are able to excite a second fluorophore (28).

What are the advantages of BRET and FRET? In FRET, the donor molecule needs to be excited with monochromatic light to emit photons, often complicating the evaluation of the donor and acceptor light signals (28). In contrast, the donor molecule generates photons by an enzymatic reaction in BRET; eliminating this challenge. Additionally, the monochromatic light used for excitation is potentially able to also excite the acceptor molecule directly, if wavelengths are not chosen carefully. Exogenous illumination of the specimen under investigation is also connected to the induction of autofluorescence, adding additional noise to the signal output. Still, for single-cell analysis, FRET has been the preferred approach, as experimental methods were not sensitive enough to detect luciferases in such circumstances. Novel systems are addressing this issue, for example using the bright NLuc as donor molecule (33, 34).

3.1.4 *Reporter assay normalization*

Signal normalization is a crucial part of many reporter systems. Especially in transfection assays, where cells are temporarily imbued with a reporter cassette, the total signal is e.g. influenced by the transfection efficiency, the number of cells

transfected, and the transgene expression. This can lead to considerable signal fluctuation between experiments if not controlled for, and complicates data evaluation.

Several methods exist for signal normalization. The first method, a so-called vector normalization, is based on co-transfection. In early reporter assays, the combination of CAT as the reporter gene, and a co-transfected constitutive ß-galactosidase was for example utilized (3). Two different luciferases can be similarly employed (35). It is assumed that the ratio of expression of the constitutive transgene to the reporter gene should stay proportionally the same. Thus, if e.g. the transfection efficiency lowers, the absolute drop in constitutive transgene signal can be used to normalize the value of the reporter gene. Vector normalization is in theory able to control for all variables given above: transgene expression, transfection efficiency, and the number of transfected cells. Alternatively, reporter gene activity can also be normalized to the amount of viable cells, or surrogate markers, such as total protein content (36). Here, transfection efficiency and transgene expression are not controlled for. While it can be expected that the choice of the normalization method will influence experimental results, direct comparisons are lacking in the scientific literature.

3.1.5 *Construction and delivery of reporter systems*

In the previous sections, different reporter systems were discussed. If one has decided for a system, how is this subsequently delivered to the target cells or organisms? Conventionally, in a first step called cloning, the reporter construct of choice is normally integrated into a plasmid, circular DNA of historically bacterial origin. This plasmid then encodes for the individual components of the reporter system. In a second step, these plasmids are then delivered to the target by different means, often using viral or non-viral gene delivery vehicles.

3.1.5.1 Advanced reporter systems: LeGO and MuLE

In the last decades, molecular biology has transgressed from single-gene plasmid reporters to increasingly complex tools. The easy generation of multi-cassette reporters,

as well as chance-driven multicolour marking strategies, have opened up new routes of scientific inquiry.

The idea of using different colours for labelling of individual cells and their daughter cells was progressed greatly by the LeGO system (37, 38). Here, modified third-generation lentiviruses with constitutive promoters and different fluorophores are designed. When labelling cells, lentiviruses encoding for different colours are added in non-saturating conditions. As such, some labelled cells only incorporate one colour transgene, while others incorporate several, or none at all. As the integration of the transgene is stable, the daughter cells of the labelled cell keep their maternal colour. As thus, this system enables cell marking and tracking. Initially thought to serve gene network studies, and thus termed Lentivirus Gene Ontology (LeGO), it has been successfully utilized to show clonal descent of cell populations. This method has, for example, been used for single-cell tracking in the brain (39), and disease states such as liver tumours (40). In a recent publication focussing on tumour heterogeneity, using six fluorescent proteins, up to 41 discrete cell clones could be distinguished and tracked (41). With the LeGO methodology as basis, which facilitates a constitutive labelling of cells in different colours, it should be similarly be possible to construct a system with conditional fluorophores. Here, depending on the chosen promoters, the detectable colour of a cell should enable deducing intracellular states.

While a combination of different lentiviruses can be used to integrate several reporters in one cell, it is also possible to construct one plasmid containing several reporters. For such rather complex reporter constructs containing several expression cassettes, restriction enzyme-based cloning can be impractical. As alternative, site-specific recombination tools, such as the Multiple Lentiviral Expression (MuLE) system, can be utilized (42). The MuLE (multiple lentiviral expression) system, in turn, is based on the MultiSite Gateway technology, which has its roots in the recombination system of the bacteriophage λ (43).The core of these methods are so-called *att* sites, 7-base pair core sequences that have the ability to recombine with specific other *att* sites. For example, *attB1* recombines only with *attP1* sites, but not with *attP2* sites. As such, recombination specificity can be accomplished, even when processing several plasmids at once in one reaction.

For this, plasmids containing the individual reporter cassettes, called entry vectors, are designed. These reporter sequences are flanked both up- and downstream by *att* sites. In a recombination step, these plasmids are combined with the lentiviral destination vector, which contains fitting recombination sites. This leads to the integration of all entry vector cassettes into the same lentiviral plasmid. In the MuLE-system, up to four individual entry vectors can be integrated into one destination vector. With the resulting expression vector, lentiviruses containing the genetic information for several included reporter genes can be produced, which can be subsequently used for gene delivery into the target cells. Using the MuLE system, several conditional reporter cassettes can be introduced into the same cell, enabling complex combinatorial approaches.

3.2 Part Two: Developmental pathways in cancer research

In cancer, healthy endogenous cellular mechanisms are often abused to benefit the survival and growth of the transformed cells. Cellular modules that are frequently modified in various cancers are signalling pathways, especially developmental pathways such as Wnt, Hedgehog and Notch (44). These three pathways have been highlighted as key players in cancer stem cells (CSC), a suspected subpopulation of cancer cells that shows stem cell-like characteristics, such as the ability to divide, and a relatively undifferentiated state (45). As CSC seem to play an important part in metastasis formation and tumour recurrence after treatment, great efforts are taken to identify and therapeutically target them, including leveraging their role in these three pathways in the search of novel therapies (46, 47).

3.2.1 *The Wnt pathway*

In line with its importance in many human cancers, the first Wnt gene *Wnt1* was identified as a proto-oncogene in murine virally induced breast tumours (48). Its role in animal organismal patterning is indicated by the fact that eleven of the twelve conserved Wnt subfamilies are already present in the Cnidarian *Nematostella vectensis* (49). Not being present in single-celled organisms, it is assumed that the Wnt gene family could have played an evolutionarily crucial part in the emergence of animal multicellularity.

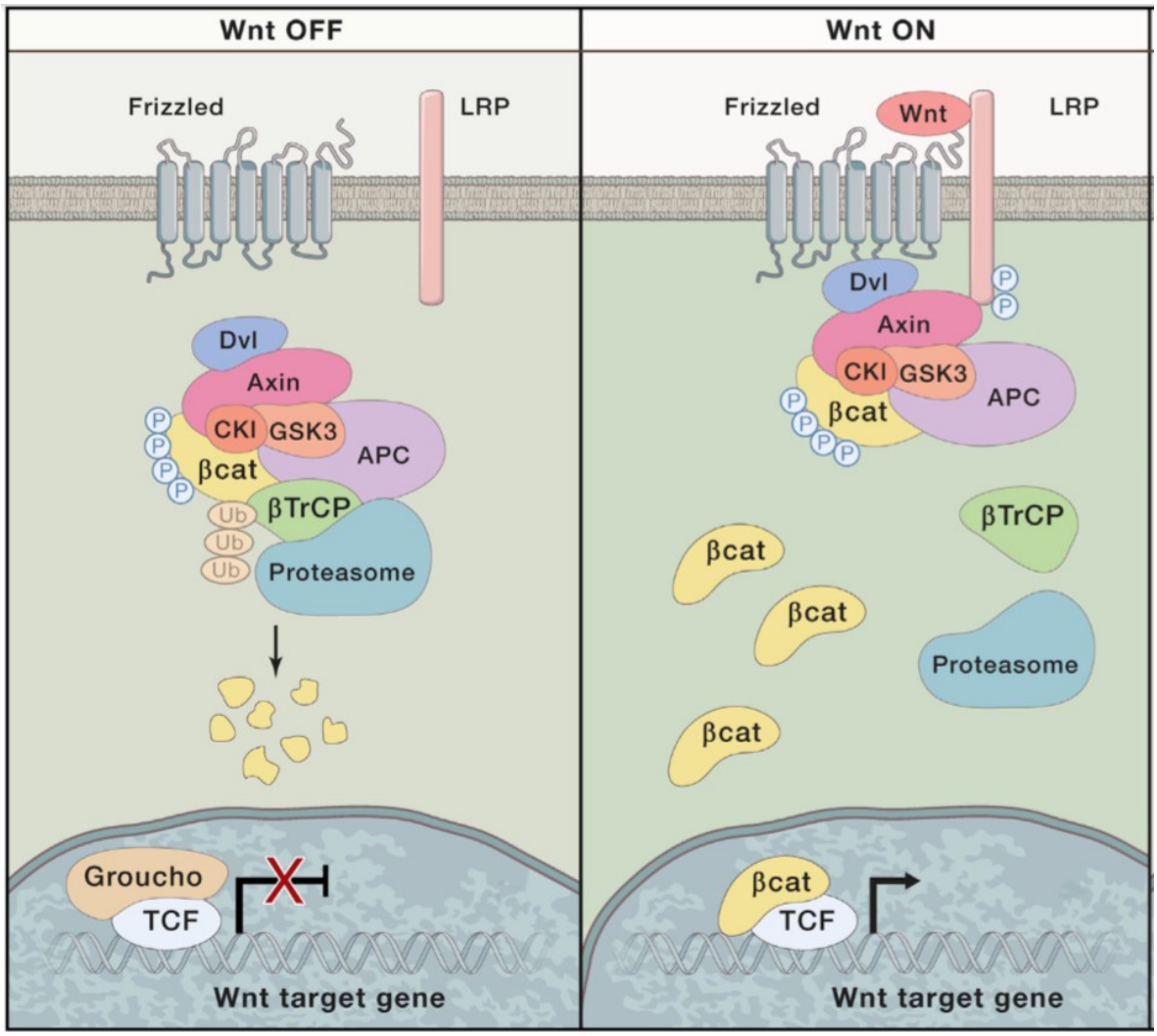


Figure 1: The canonical Wnt pathway. *Adapted from Nüsse and Clevers, 2017 (48).*

Chemically, the proteins of the Wnt family are glycoproteins with numerous, evolutionarily conserved cysteines. The Wnt proteins are covalently bound to lipid molecules, having importance for their bioactivity and complicating their isolation (50). Wnt proteins are secreted paracrine factors, meaning that they diffuse over small distances, and thus acts mostly locally (51). In the 1990's, the importance for certain colon cancer types was discovered (52). Today, it is recognized not only as a key signalling pathway in embryonal development, but also for its role in adult stem cells, as well as cancer aetiology and CSC (53). At the heart of the canonical Wnt signalling pathway is the transcription factor β-catenin (Fig. 1). If Wnt signalling is off, β-catenin is phosphorylated by the destruction complex, a multi-protein complex, leading to its degradation by proteasomes. In Wnt producing cells, the protein Porcupine in the endoplasmatic reticulum processes Wnt by palmitoylation, thus leading to Wnt maturation. Upon secretion, Wnt in vertebrates binds to heterodimeric receptor complexes consisting of Frizzled (Fz) and the LRP5/6 protein. It has been shown that palmitoleic acid lipid interacts closely with the Fz receptor (84). Upon binding of Wnt to the receptor complex, LRP5/6 is phosphorylated by the kinases GSK3 and CK1. This enables binding of a part of the destruction complex to the heterodimeric receptor.: axin interacts with LRP5/6, and Dishevelled (Dvl) with Fz. As a consequence, the destruction complex is disbanded, and β-catenin is no longer destroyed. β-catenin accumulates in the nucleus, where it interacts with TCF or LEF proteins to modulate gene expression. In the last years, modified versions of the canonical pathway have been proposed, in which active Wnt signalling does not inhibit phosphorylation of β-catenin, but rather leads to the inactivation of the proteasome (48). Other Wnt pathways exist, with the non-canonical pathway being pivotal for cytoskeletal regulation, and the Wnt/Ca^{2+} cascade being central for intracellular calcium homeostasis. Due to the relevance of this pathway for cancer therapy, there is a high interest in drug discovery of compounds that act on the Wnt pathway (21).

3.2.2 *The Hedgehog pathway*

Similar to Wnt, Hedgehog (HH) proteins play vital roles in pattern formation of neighbouring cells (54). In mammals, three HH proteins exist: Sonic, Indian and Desert HH. They are responsible for diverse developmental mechanisms, ranging from limb and notochord organization to bone and cartilage development, as well as germ cell development. Its role in stem cells, and CSC, make it a highly attractive target for cancer drug development (55-57). The HH protein is processed by autoproteolysis, and modified twice by lipidation, with cholesterol and palmitoleic acid lipid, during its maturation. Similarly to the Wnt protein, the palmitoleic acid lipid is again crucial for proper biological function (58). In vertebrates, HH proteins are secreted by the transmembrane protein Dispatched in concert with the glycoprotein SCUBE2 (54). The cellular localization of the HH signalling components in the target cell is strongly associated with microtubules (Fig. 2). In the off state, phosphorylation of the transcription factors of the glioma-associated oncogene (GLI) family by the kinases casein kinase 1 (CKI), glycogen synthase kinase 3β (GSK3β) and protein kinase A (PKA) takes place at the cilial base. As a result, the GLI proteins then undergo proteolytic cleavage, inducing repression of downstream pathway signalling.

Additionally, non-activated Patched receptor (PTCH) leads to the repression of the protein Smoothened (SMO) by mechanisms that are not fully elucidated yet. Upon HH pathway activation, secreted HH binds to PTCH. As a result, SMO repression is released, and SMO is transported to the cell membrane in the vicinity of a cilium. In short, this leads to the GLI proteins bypassing the proteases, and to their subsequent arrival in the nucleus, where they activate HH target genes by e.g. acting on GLI-binding sites (59).

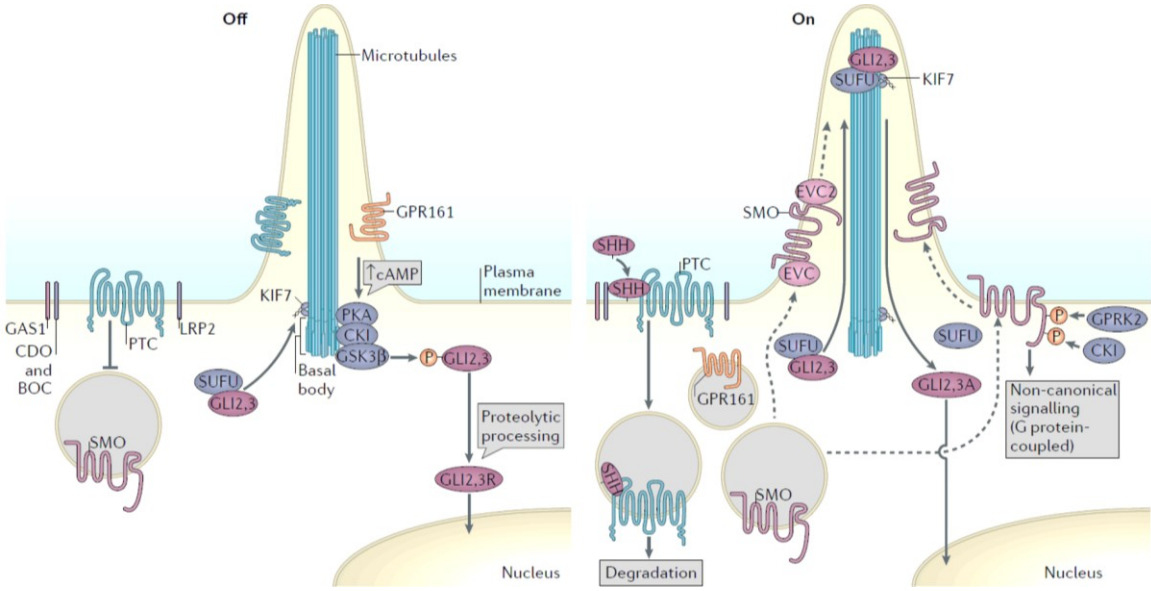


Figure 2: The Hedgehog pathway. *Adapted from Briscoe and Thérond, 2013 (54).*

3.2.3 *The Notch pathway*

In contrast to the previously described signalling pathways, the Notch pathway is known to rely mostly on direct cell-to-cell contact (60). Interestingly, while the Notch signalling cascade is relatively straightforward and does not include protease-based signal amplification, the consequences of Notch signalling are highly cell context dependent. This pathway can for example lead to cell death or cell proliferation, or the differentiation of cells into various cell types. Similarly to the Wnt and HH pathways, Notch is also implicated in stem cell maintenance (61), oncogenic as well as tumour-suppressive mechanisms (62), and CSC (63), making it again a target of high interest for cancer drug discovery.

The central mechanism in Notch signal transduction is proteolysis of the Notch receptor, releasing a moiety called the Notch Intracellular Domain (NICD), which can directly act as a transcription factor (Fig. 3). In contrast to the already mentioned pathways, Notch signal transduction is not mediated by secreted proteins, but by receptor interactions of the signalling cell and receiving cell. At the signalling cell, the receptors Jagged, Serrate or Delta are present. Upon direct binding of these receptors by

the Notch receptor on the adjacent receiver cell, the Notch receptor partly unfolds, enabling processing by the proteases ADAM and β-secretase, releasing the NICD. The NICD then travels to the nucleus, where downstream signalling in mammals is initiated by binding to the transcription factor Epstein Barr virus C-promoter binding factor 1 (CBF-1). The Notch pathway is tightly linked to inducing epigenetic modifications, such as histone acetylation (64, 65). Interestingly, mechanical forces seem to play a crucial role in Notch signalling, being able to directly trigger Notch proteolysis (66).

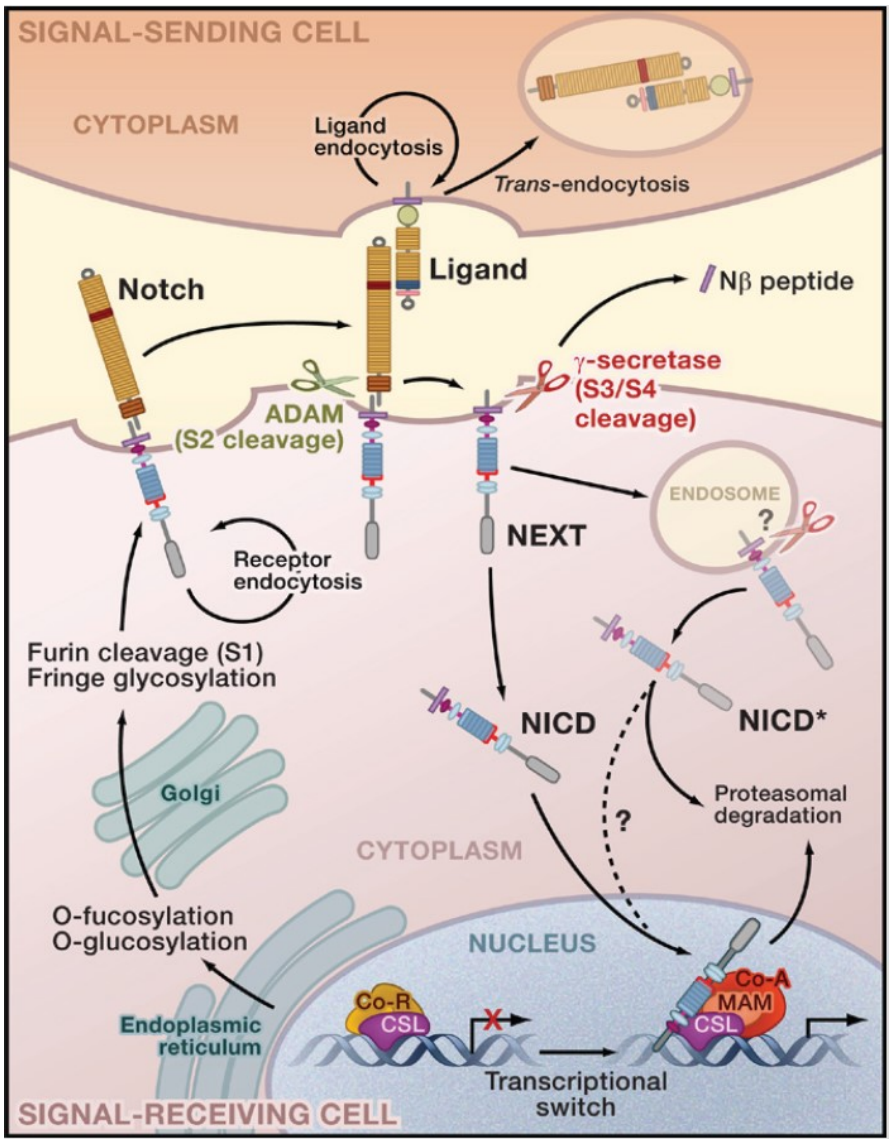


Figure 3: The Notch pathway. *Adapted from Kopan and Ilagan, 2009 (60).*

3.3 Part Three: Optical and imaging techniques - from single cell to multimodal *in vivo* methods

Imaging methods have emerged as vital tool in molecular biology. In this work, the focus will be on fluorophores and luciferases. We relied heavily on single-cell measurements by flow cytometry, as well as screening approaches. One focus of our work was the design of suitable multi-colour reporter gene constructs for both fluorophores and luciferases, which will also be discussed in this section. As advanced *in vivo* technique, the combination of several imaging modalities enables the discovery and tracking of malignant cells and therapeutic transfection in the mouse.

3.3.1 *High-throughput single cell investigation: flow cytometry*

In traditional flow cytometry, the visual properties of single cells can be investigated. At its core, a flow cytometer consists of fluidics, through which cells from a sample are guided, and in which they are illuminated by at least one laser. As a result, the scattered light or fluorophore emission of the cell under scrutiny is received by sensors, and this in turn conveys information about the properties of the cell. Modern flow cytometers can feature up to five lasers, and can detect a maximum of 14 parameters (67). A tremendous advantage of this technique is the throughput: up to 10,000 cells per second can be investigated (68). Flow cytometry can not only be used for single cells, but also for cell lysates and biological liquids (69, 70).

This method is possible with unstained cells, but dedicated dyes and antibodies augment the features that can be investigated. In an unstained cell, the incoming laser light is scattered. By this, the size and granularity of the cell can be determined, as well as the number of cells by counting the events that pass through the laser. The usage of lasers also facilitates usage of fluorescent dyes. Here, the laser light is not only scattered, but excites the fluorophore, resulting in light emission at a different wavelength, which

can be picked up by dedicated filters that detect fixed wavelength bands. With fluorescent dyes, features such as DNA or protein content can be explored. Additionally, flow cytometry has benefitted greatly from the design of specialized fluorescently labelled antibodies. These antibodies are tailored to the entity to be investigated, for example a cell surface receptor. If the receptor is present on the cell, the antibody will attach to it in a preceding experimental step. In flow cytometry, the fluorophore on the bound antibody emits a signal which can then be detected. At present, numerous antibody-fluorophore-combinations exist, enabling the isolation of previously elusive cell types. This ability is especially cherished in the area of immunology, where cell subtypes can be differentiated by the usage of various cell surface markers, in a process termed multiparameter flow cytometry (71).

Multiparameter flow cytometry requires precautions. For one, the fluorophore excitation and emission wavelength is, in contrast to the laser light which operates at fixed nanometer values, spread over a spectrum. Instead of the targeted excitation by lasers, this can lead to cross-excitation between fluorophores. As an example, mTurquoise2 can be excited with light ranging from 350-480nm, with its highest sensitivity between 420-450nm. Its emission is from 460-600nm, with a peak at 470-520nm (72). Given this information, it is intuitive that two fluorophores can also excite each other when their emission/excitation spectra overlap. Secondly, if a fluorophore has a broad emission spectrum that is picked up by several filters, signal spillover can occur. In the case of very bright fluorophores, it is possible that this signal spillover obstructs detection of another, less bright fluorophore.

As such, it is of importance to negate or compensate such signal spillover in multicolour experiments. This can be facilitated by two means: First, fluorophores with compatible spectra should be chosen. Secondly, signal spillover that is present can be managed by a process called compensation. In compensation, spectral overlap is mathematically calculated out (26). While some instruments can have internal compensation mechanisms, post-processing via dedicated flow cytometry analysis programs is also possible. In short, the emission strength of each used fluorophore upon excitation in the different filters is determined. This matrix can then be used to subtract the fluorophore emission signal in the “off-target” filters accordingly. While manual

compensation is discouraged in the literature, which includes the drawing of gates and thresholds, it is still standard in programs such as FlowJo (26), leading to possible negative impacts on compensated results and data interpretation.

In our work, we chose to combine four fluorophores: mTurquoise2, eGFP, tdTomato and iRFP720 to visualize activity of the developmental pathways Wnt, HH and Notch (Fig. 4).

3.3.2 *Luciferase multicolour combinations*

For luciferases, combinations are also possible. Often, for signal normalization purposes, an additional, constitutively expressed luciferase is added to transfection assays as described in section 1.1.4. Simultaneous detection of two luciferases has also been described (73). In our work, aimed at visualizing the activity of three developmental pathways, and wanted to also develop a luciferase-based reporter construct for this.

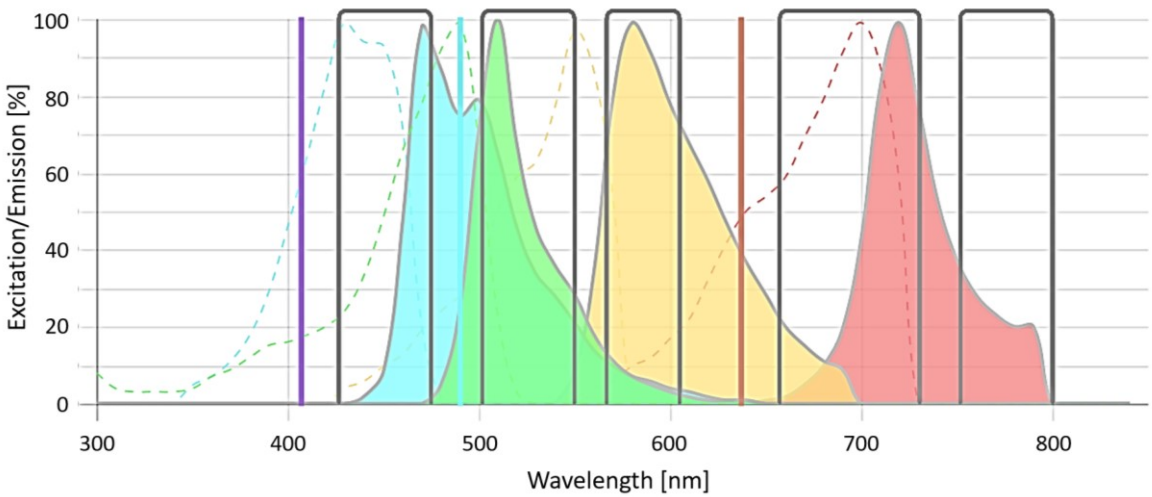


Figure 4: Selected fluorophores for the pathway reporter constructs*. Excitation (dashed lines) and emission spectra (continuous lines) of mTurquoise2 (turquoise), eGFP (green), tdTomato (yellow) and iRFP720 (red). The lasers (405nm, 488nm, 635nm) and filters (V1 [450/50nm], V2/B1 [525/50nm], B2 [585/40nm], B3/R1 [655-730nm], B4/R2 [750nm LP]) of the flow cytometer used are also indicated. Adapted from (74).*

In contrast to fluorophores, where single cell measurement is the goal, we decided to utilize a standard well plate format in which either the supernatant (extracellular luciferases) or the cell lysate (intracellular luciferase) is measured. As thus, the signal intensity is not investigated per cell, but per well, in line with drug development screening approaches (16). Special scrutiny rests on the cross-reactivity of the luciferases and the substrates. Cross-reactivity between GLuc and NLuc and their respective substrates has been described (75). As such, we decided to restrict measurement of GLuc and NLuc to different compartments, and also set the aim to be vigilant towards potential signal spillover. In our work regarding developmental pathway reporter design, we chose FLuc, GLuc and NLuc as luficerases (Tab. 1).

Luciferase	**Substrate**	**Location**
Firefly luciferase (FLuc)	Luciferin	Intracellular
Gaussia luciferase (GLuc)	Coelenterazine	Extracellular
NanoLuc (NLuc)	Furimazine	Intracellular

Table 1: Selected luciferases for the pathway reporter constructs.

3.3.3 *Multimodal in vivo imaging techniques*

Especially in animal experiments, it can be seen as ethical necessity to gain as much insight from one experimental animal as possible. In multimodal imaging, different visualization techniques such as for example magnet resonance imaging (MRI), bioluminescence imaging (BLI) and fluorescence imaging (FLI) are combined to maximize data output from one animal. Most often, an overlay of the resulting data is the aim. Multimodal imaging is also an emerging technique in cancer therapy, where e.g. a combination MRI and computer tomography variants can be used to more specifically determine the tumour phenotype (76). In mice, multimodal imaging enables the tracking

of cells, such as luciferase-labelled immune cells and their association with fluorescently labelled colon cancer cells (77). Also, the transfection potential of novel gene delivery methods can be assessed *in vivo*, using for example MRI, FLI and optical images (78).

Gene delivery to the lungs, especially targeting diseases such as cystic fibrosis, is an of now experimental mode of application (79). While different methods exist, aerosolization of PEI is advantageous compared with intravenous injections or instillations (80-82). In our work, we used multimodal imaging to investigate the *in vivo* transfection potential of intratracheally administered polyplexes, carrying the information for a luminescent reporter, in a breast cancer metastasis model featuring fluorescent cells. Different imaging modalities such as CT, MRI, fluorescence and bioluminescent imaging methods were used to investigate the effectiveness of gene delivery.

3.4 Part Four: Gene delivery

In 1928, before the clarification of the molecular basis of inheritance, the first seminal study identifying gene delivery was published by Frederick Griffith, now famously called "Griffith's Experiment" (83). He observed that virulent strains of pneumococci, which were heat-inactivated and thus apathogenic, could transfer their disease-inducing property to non-virulent strains when injected together subcutaneously into mice. Further investigations into the nature of this "transforming principle" within the next twenty years led to the experimental discovery that deoxyribonucleic acids, and not proteins, are the carriers of genetic information (84). As such, gene delivery has played a crucial part in uncovering one of the most significant findings in recent history.

Nowadays, gene delivery is applied broadly in laboratory contexts, and attempts to harness its power in the clinics are accelerating. While DNA can directly be applied for gene delivery ("naked DNA"), it suffers from several disadvantages. Its half-life, due to the nucleases encountered in the body, is quite limited, and because of the lack of adequate transport into the nucleus, the gene transfer remains comparatively ineffective (85, 86). Nonetheless, naked DNA remains a method featured prominently in current clinical trials, also due to its high safety profile (87).

To ameliorate these shortcomings, other approaches utilize vehicles for gene delivery. They can be classified as either viral or non-viral approaches. Differences exist regarding their mechanism, effectiveness of gene delivery, their safety profile, and method of application. In this work, we use two methods of gene delivery, third generation lentiviruses and linear polyethylenimine (LPEI). We rely on gene transfer of reporter constructs, which we assess with current imaging techniques.

3.4.1 *Lentiviruses*

The gene delivery properties of viruses are central to their function as pathogens. For example, lentiviruses are able to also stably integrate their genetic payload into non-dividing cells, and into the less risk-associated genomic locations of transcription units instead of, as gammaretroviruses, regulatory regions (88). For clinical as well as research settings, utmost care is taken to design lentiviruses that enable safe handling. One aspect of this the production of lentiviruses. This procedure utilizes a producer cell line to which plasmids, circular DNA of historically bacterial origin, encoding for the individual components of the lentivirus, are added. Similarly to a manual, the plasmid genetic information is read by the producer cells, and viral particles are produced. To minimize the dangers of accidentally producing virus with the possibility to replicate, or otherwise damage the target host, modifications to these plasmids have been made over time.

In a seminal paper by Naldini *et al.*, the first system, so-called first generation plasmids for lentivirus production, was generated. It is based on HIV-1 (89). Here, the genetic information required for a functional virus was split up on three plasmids: the transfer plasmid contains the provirus, and as such the genetic payload that is to be delivered. The other plasmids facilitate generation of the required viral structures and components, as well as packaging. Already, the genetic information of the virus was heavily modified: for example, the native viral envelope gene, which determines which cells can be targeted by the virus, was defective. Normally, HIV targets $CD4^+$ cells, leading to the infection of various immune cells (90). Instead, a third plasmid codes for a new

functional envelope, for example the G protein of the vesicular stomatitis virus (VSV-G), enabling the produced virus to infect many different cell types. Also, several functionalities that would have led to the addition of other genomic information into the virus were abolished. For functional virus to be generated, all three plasmids needed to be transfected into the same packaging cell. The resulting virus is replication-deficient, due to the deletion of key sequences from the packaging plasmid.

In the second generation system, additional viral sequences were removed, as they were found out to be non-essential for lentivirus generation (91). It thus further prevented unwanted reconstitution of replicating virus. Interestingly, the choice of producer cell line was relevant to this achievement, as HEK293T cells were found to produce virus even without the deleted *vif* and *vpu* sequences. HEK293T cells are a standard for lentivirus production to this day. Other proteins were dispensable because of the choice of VSV-G as envelope, which is still commonly used (92). The deletion of these sequences also reduced the pathogenicity of the constructs.

A year later, the system was further improved to give rise to third generation plasmids (93), a system that is at the moment the standard in many laboratories. The viral LTR in the transfer plasmid was chimerized to include a strong regulatory unit, abolishing the need for *tat*, which was consequently deleted. By this, only three of the nine HIV-1 proteins remained in this system. Biosafety was further enhanced by separating the genetic information of the packaging plasmid on two separate plasmids, leading to a total of four plasmids required for successful production of the virus. With the deletion of all non-essential genes, pathogenicity is largely prevented. Additionally, a modification of the LTR makes it unlikely that, upon transduction, full-length RNA of the vector can be generated, as well as reducing a possible unwanted enhancer effects on nearby endogenous genes after integration. A fourth-generation system has been introduced recently, in which the transfer plasmid design is further rationalized, reducing viral sequences that are transduced, and simplifying the design of longer transgene cassettes (94).

Different methods exist for the transfection of the producer cell line with these plasmids, having in common that non-viral gene delivery methods are employed.

Lentivirus production itself takes several days. Virus is present in the supernatant, and can be either directly used, or purified, and can then be applied to the target cells (95). In a next step, the lentiviral machinery, together with recruited cellular factors of the host cell, effectively mediate stable integration of the genomic payload, and thus a successful transduction in the target cells (88).

In the publication introducing the second generation lentivirus system, it is optimistically mentioned that the design of a stable producer cell line should be feasible, eliminating the need to transiently transfect a producer cell line. The need to transfect is a problem, especially for clinical applications, as the quality of the transfection and the resulting virus do change from batch to batch of transfected producer cell lines. In turn, this complicates the rigorous standardization required to approve new treatments (92). In search for a stable producer cell line, it became apparent that specific viral proteins, such as VSV-G, exert cytotoxicity that hinder such efforts (96). Current approaches follow different strategies, from inducible genes, to partly incorporating non-toxic viral proteins or generating less toxic protein variants, but each suffers from drawbacks, and research is ongoing (97, 98).

After transduction of the target cells, an additional election of stably transduced cells is often made, for example by utilizing an introduced selection marker such as antibiotic resistance, or a fluorophore that can be sorted for (99). Selection pressure should be maintained, or the stability of the transduction checked, as silencing of the transgene is reported to occur over time (100).

Taken together, gene transfer with lentiviruses results in a stable integration of the transgene into the host's genome. Being very efficient, the duration from virus production to successful transduction of the target cells requires approximately two weeks.

3.4.2 *LPEI*

While, as described above, naked DNA is used directly for gene transfer, nanocarriers are utilized to improve this process. Nanocarriers show some advantages in contrast to naked DNA, such as shielding of the DNA from endonucleases (101). The main carriers used are lipids in the form of liposomes or liposomal agents, which work by coating the DNA in spherical lipid bilayers (102), and cationic polymers, in which the negatively-charged DNA aggregates around a polymer. Typically, plasmid DNA (pDNA) is added to these vehicles and interacts with them, and the resulting complexes are used directly for non-viral gene delivery. This is a stark contrast to virus production for viral gene delivery, where e.g. the genomic payload needs to be modified to fit the proper viral syntax. The non-gene delivery formulations are taken up by the cells, and dissociate in the cytoplasm, releasing the genomic payload. The pDNA is then bound by a multitude of cellular proteins, and transcription can take place (103).

Non-viral gene delivery of DNA does normally not lead to integration in the genome of the receiving cells, and is thus transient as the plasmids are lost due to cell division. As the genomic payload needs to be located in the nucleus to be transcribed, non-viral transfection agents are especially effective when applied to dividing cells. In these, the nuclear envelope is temporarily disbanded, allowing easier access of the transfected DNA into the nascent nucleus (104). In non-dividing cells, the cellular proteins bound to the genomic payload can transport the DNA directly into the nucleus. It is estimated that only a relatively low percentage of DNA used for non-viral gene delivery actually reaches its nuclear destination (103). New approaches that use sophisticated genetic systems, such as the Sleeping Beauty transposase, can enable stable integration (105), but are not widespread as of now.

A frequently used cationic polymer of gene transfer is polyethylenimine (PEI) (106). In contrast to lipid-based agents, PEI can be easily functionalized chemically, for example to increase its stability (107), or to target it to specific cells populations (108). PEI is superior to liposomes in some applications, such as when applying it as aerosol in the lung (109). Interestingly, PEI-DNA polyplexes have been observed to partly stay intact within the nucleus, and it has been speculated that this decreases transfection efficiency (110).

For PEI, two main configurations exist: branched and linear PEI (LPEI). LPEI is superior regarding its increased transfection profile, and shows decreased cytotoxicity (111, 112). For production of the nanocarriers, the positively charged PEI is rapidly mixed with the negatively charged nucleotides, for example pDNA. This process, in the context of this work, is referred to as flash pipetting. The mixture ratio of PEI to DNA is expressed as the N/P ratio, denominating the ratio of nitrogen containing amine groups in the PEI, to phosphates in the nucleotide used (113). N/P ratios range usually between two and ten (114). The PEI-DNA complexes obtained by mixing are called polyplexes. The transfection ability of polyplexes depends heavily on the net charge: the more positive the polyplex, (and as such, the higher the relative amount of PEI, and the higher the resulting N/P ratio), the easier the interaction with the cell membrane. Unfortunately, electric charge also correlates with cytotoxicity, which is thought to be mediated by membrane destabilization (111). And as such, a compromise between cytotoxicity and transfection efficiency has to be determined carefully for experiments.

4 Publications

2.1 Luminescent and Fluorescent Triple Reporter Plasmid Constructs for Wnt, Hedgehog and Notch Pathway

Julia Maier, Haider Sami, Alexander Taschauer, Martina Anton, and Manfred Ogris. *PLOS ONE,* under review.

Aims:

Development of single and combined luminescent and fluorescent reporter plasmids for visualizing the activity for the Wnt, Hedgehog and Notch Pathway.

1. Evaluation of available pathway-sensitive pathway reporter constructs for the Wnt, Hedgehog and Notch pathway
2. Cloning of each a combinable set of luciferase- or fluorescence-based reporter plasmids for the three pathways
3. Comparison of original and newly designed reporter constructs with respect to signal fold increase upon induction with plasmid-based activators
4. Generation of MuLE-backbone based three-pathway reporter constructs suitable for lentivirus production, utilizing the generated luminescent and fluorescent reporter plasmids
5. Comparison of the generated single and three pathway reporter plasmids
6. Verification of the suitability on the generated reporter plasmids in an assay utilizing chemical compounds interfering with the Wnt, Hedgehog and Notch pathways.

Hypotheses:

1. Generation and usage of combinable single and three pathway constructs is feasible.
2. Application of plasmid-based and/or chemical activation are suitable to demonstrate the performance of the generated single and three pathway constructs.

Contributions:

J.M. planned the project, performed the experiments, evaluated the data, and co-wrote the manuscript (first authorship).

PLOS ONE

Luminescent and fluorescent triple reporter plasmid constructs for Wnt, Hedgehog and Notch pathway

--Manuscript Draft--

Manuscript Number:	
Article Type:	Research Article
Full Title:	Luminescent and fluorescent triple reporter plasmid constructs for Wnt, Hedgehog and Notch pathway
Short Title:	Luminescent and fluorescent triple pathway reporters
Corresponding Author:	Manfred Ogris Universitat Wien Wien, AUSTRIA
Keywords:	reporter gene; plasmid; luciferase; fluorescent protein; signalling pathway; wnt; notch; hedgehog; gateway system; firefly luciferase; gaussia luciferase; nanoluc; mTurquoise2; tdTomato; EGFP; iRFP720; multi-gene plasmid; drug screening
Abstract:	Tracking the activity of signalling pathways is a fundamental method for basic science, as well as in cancer- and pharmaceutical research. The developmental pathways Wnt, Hedgehog and Notch are frequently deregulated in cancers and represent a valuable target for the discovery of novel anticancer compounds. Here we present reporter systems for tracking activity of these pathways by using specific promoter elements driving the expression of either sensitive luciferases, or fluorescent proteins. A high level of sensitivity was obtained using the luciferase reporter genes for firefly (FLuc), secreted Gaussia (GLuc) and synthetic NanoLuc (NLuc). As fluorescent reporter proteins, mTurqouise2, tdTomato and iRFP720 were chosen. Specificity of pathway activity was validated by co-transfection with pathway activating genes, showing significant response to induction. In addition, multi-gene plasmids were cloned, allowing the detection of all three pathways by one vector. First studies with synthetic compounds confirmed the applicability of the system for future drug screening approaches.
Order of Authors:	Julia Maier
	Haider Sami
	Alexander Taschauer
	Martina Anton
	Manfred Ogris
Opposed Reviewers:	
Additional Information:	
Question	**Response**
Financial Disclosure Enter a financial disclosure statement that describes the sources of funding for the work included in this submission. Review the submission guidelines for detailed requirements. View published research articles from *PLOS ONE* for specific examples. This statement is required for submission and **will appear in the published article** if	This work was supported by the uni:docs stipend of the University of Vienna to JM. Open access funding was provided by the University of Vienna. The funders had no role in study design, data collection and analysis, decision to publish, or preparation of the manuscript.

Powered by Editorial Manager® and ProduXion Manager® from Aries Systems Corporation

the submission is accepted. Please make sure it is accurate. **Unfunded studies** Enter: *The author(s) received no specific funding for this work.* **Funded studies** Enter a statement with the following details: • Initials of the authors who received each award • Grant numbers awarded to each author • The full name of each funder • URL of each funder website • Did the sponsors or funders play any role in the study design, data collection and analysis, decision to publish, or preparation of the manuscript? • **NO** - Include this sentence at the end of your statement: *The funders had no role in study design, data collection and analysis, decision to publish, or preparation of the manuscript.* • **YES** - Specify the role(s) played. * typeset	
Competing Interests Use the instructions below to enter a competing interest statement for this submission. On behalf of all authors, disclose any competing interests that could be perceived to bias this work—acknowledging all financial support and any other relevant financial or non-financial competing interests. This statement **will appear in the published article** if the submission is accepted. Please make sure it is accurate. View published research articles from *PLOS ONE* for specific examples.	The authors have declared that no competing interests exist.

Powered by Editorial Manager® and ProduXion Manager® from Aries Systems Corporation

NO authors have competing interests Enter: *The authors have declared that no competing interests exist.* **Authors with competing interests** Enter competing interest details beginning with this statement: *I have read the journal's policy and the authors of this manuscript have the following competing interests: [insert competing interests here]* * typeset	
Ethics Statement Enter an ethics statement for this submission. This statement is required if the study involved: • Human participants • Human specimens or tissue • Vertebrate animals or cephalopods • Vertebrate embryos or tissues • Field research Write "N/A" if the submission does not require an ethics statement. General guidance is provided below. Consult the submission guidelines for detailed instructions. **Make sure that all information entered here is included in the Methods section of the manuscript.**	N/A

Powered by Editorial Manager® and ProduXion Manager® from Aries Systems Corporation

Format for specific study types **Human Subject Research (involving human participants and/or tissue)** • Give the name of the institutional review board or ethics committee that approved the study • Include the approval number and/or a statement indicating approval of this research • Indicate the form of consent obtained (written/oral) or the reason that consent was not obtained (e.g. the data were analyzed anonymously) **Animal Research (involving vertebrate animals, embryos or tissues)** • Provide the name of the Institutional Animal Care and Use Committee (IACUC) or other relevant ethics board that reviewed the study protocol, and indicate whether they approved this research or granted a formal waiver of ethical approval • Include an approval number if one was obtained • If the study involved *non-human primates*, add *additional details* about animal welfare and steps taken to ameliorate suffering • If anesthesia, euthanasia, or any kind of animal sacrifice is part of the study, include briefly which substances and/or methods were applied **Field Research** Include the following details if this study involves the collection of plant, animal, or other materials from a natural setting: • Field permit number • Name of the institution or relevant body that granted permission	
Data Availability Authors are required to make all data underlying the findings described fully available, without restriction, and from the time of publication. PLOS allows rare exceptions to address legal and ethical concerns. See the PLOS Data Policy and FAQ for detailed information.	Yes - all data are fully available without restriction

Powered by Editorial Manager® and ProduXion Manager® from Aries Systems Corporation

A Data Availability Statement describing where the data can be found is required at submission. Your answers to this question constitute the Data Availability Statement and **will be published in the article**, if accepted. **Important:** Stating 'data available on request from the author' is not sufficient. If your data are only available upon request, select 'No' for the first question and explain your exceptional situation in the text box. Do the authors confirm that all data underlying the findings described in their manuscript are fully available without restriction?	
Describe where the data may be found in full sentences. If you are copying our sample text, replace any instances of XXX with the appropriate details. • If the data are **held or will be held in a public repository**, include URLs, accession numbers or DOIs. If this information will only be available after acceptance, indicate this by ticking the box below. For example: *All XXX files are available from the XXX database (accession number(s) XXX, XXX.*). • If the data are all contained **within the manuscript and/or Supporting Information files**, enter the following: *All relevant data are within the manuscript and its Supporting Information files.* • If neither of these applies but you are able to provide **details of access elsewhere**, with or without limitations, please do so. For example: *Data cannot be shared publicly because of [XXX]. Data are available from the XXX Institutional Data Access / Ethics Committee (contact via XXX) for researchers who meet the criteria for access to confidential data.* *The data underlying the results presented in the study are available from (include the name of the third party*	All relevant data are within the manuscript and its Supporting Information files. All plasmid maps and sequence information have either been uploaded or are available at addgene.org

Powered by Editorial Manager® and ProduXion Manager® from Aries Systems Corporation

and contact information or URL). • This text is appropriate if the data are owned by a third party and authors do not have permission to share the data. * typeset	
Additional data availability information:	

Powered by Editorial Manager® and ProduXion Manager® from Aries Systems Corporation

Cover Letter

universität wien

Fakultät für Lebenswissenschaften

Univ.Prof. Dr. Manfred Ogris
Department für Pharmazeutische Chemie
Althanstraße 14
A-1090 Wien
m.ogris@univie.ac.at
T +43 (1) 4277-55551
F +43 (1) 4277-95 51

http://klinischepharmazie.univie.ac.at/mmctresearch/

To the editor

PLOS one

Dear Editor,

We would like to submit our manuscript Maier et al entitled **, Luminescent and fluorescent triple reporter plasmid constructs for Wnt, Hedgehog and Notch pathway'** to PLOS ONE as a research article. Here we present the development and evaluation of a plasmid based reporter system, which allows to simultaneously monitor the activity of three key signalling pathways, namely Wnt, Hedgehog and Notch in mammalian cells. Pathway specific promoter elements drive the expression of either fluorescent proteins or luciferases. We thoroughly monitored the specificity of the reporters by using cell lines without intrinsic pathway activity and validated activation by co-transfection with plasmids encoding for the respective activating proteins. Care was taken that luciferases (Firefly, Gaussia and NanoLuc) or fluorescent proteins (mTurquoise2, tdTomato and iRFP720) can be measured simultaneously. We also generated plasmids with all three pathway reporter cassettes in one (named 3P-Luc and 3P-Fluor). This multi-gene approach ensures comparability between the individual pathway activities, as it levels our variations due to different transfection activities of individual plasmids or positioning effects when using integrating

vectors. Both 3P-Fluo and 3P-Luc are designed as lentiviral entry plasmids and include selection markers, which allows convenient generation of lentivirus for stable labelling and selection of cells. We think that this technology will be very helpful for drug screening approaches *in vitro*, but also preclinical drug development in animal models. We would be very pleased if our manuscript would be in principle suitable for publication in PLOS ONE.

Yours sincerely

Manfred Ogris

Professor for Pharmaceutical Sciences, University of Vienna

Manuscript

Click here to access/download;Manuscript;Maier et al POne.docx

Luminescent and fluorescent triple reporter plasmid constructs for Wnt, Hedgehog and Notch pathway

Julia Maier[1], Haider Sami[1], Alexander Taschauer[1], Martina Anton[2], Manfred Ogris[1]*

[1] Laboratory of MacroMolecular Cancer Therapeutics (MMCT), Center of Pharmaceutical Sciences, Department of Pharmaceutical Chemistry, University of Vienna, Althanstrasse 14, A-1090 Vienna, Austria

[2] Institutes of Molecular Immunology and Experimental Oncology, Klinikum rechts der Isar, Technische Universität München, Munich, Germany.

*Corresponding author

Email: m.ogris@univie.ac.at

Short title: Luminescent and fluorescent triple pathway reporters

Abstract

Tracking the activity of signalling pathways is a fundamental method for basic science, as well as in cancer- and pharmaceutical research. The developmental pathways Wnt, Hedgehog and Notch are frequently deregulated in cancers and represent a valuable target for the discovery of novel anticancer compounds. Here we present reporter systems for tracking activity of these pathways by using specific promoter elements driving the expression of either sensitive luciferases, or fluorescent proteins. A high level of sensitivity was obtained using the luciferase reporter genes for firefly (FLuc), secreted *Gaussia* (GLuc) and synthetic NanoLuc (NLuc). As fluorescent reporter proteins, mTurqouise2, tdTomato and iRFP720 were chosen. Specificity of pathway activity was validated by co-transfection with pathway activating genes, showing significant response to induction. In addition, multi-gene plasmids were cloned, allowing the detection of all three pathways by one vector. First studies with synthetic compounds confirmed the applicability of the system for future drug screening approaches.

Introduction

Dysregulation of developmental pathways plays a pivotal role in cancer (1) . Up-regulation of Wnt, for example, correlates with dismal prognosis in a broad range of solid cancers, leading to development of several Wnt inhibitors and their evaluation within advanced clinical studies (2). More broadly, targeting the Wnt, Hedgehog (Hh) and Notch pathway has been described as a successful approach in cancer therapy (3). It is speculated that such an approach might also be effective against therapy-resistant cancer cell sub-populations, such as cancer initiating cells, which are known to show deregulation of these three pathways (4). In the search of novel treatment options, compound screening libraries are nowadays often employed. These allow the selection of suitable molecular structures from millions of compounds using appropriate *in silico* models (5). Nevertheless, initial virtual screening results need to be validated and further screened in biological systems. For this purpose, reporter genes expressed under the control of pathway specific response elements are often employed. Regulation of pathways mostly depends on the activity of transcription factors binding to promoter elements. Hence, several natively occurring (6), but also synthetic promoter elements have been designed to drive expression of reporter genes (7). To give an example, the canonical Wnt pathway is activated after binding of Wnt signal proteins (e.g. Wnt3a) to its receptor frizzled and the LPR co-receptors (8). Factors downstream of LPR inactivate the β-catenin destruction complex. The stabilised β-catenin accumulates and translocates to the nucleus, where it forms an active complex with LEF (lymphoid enhancer factor) and TCF (T-cell factor) leading to a transcriptional switch. Hence, the most commonly used Wnt reporter is a synthetic promoter element with multiple TCF/LEF binding sites (9). Similarly, the Sonic Hedgehog pathway is initiated by binding of SHH protein to its receptor Patched (PTCH), which releases the PTCH inhibition of Smoothened (Smo). Smo in turn activates Gli transcription factors, which after promoter binding initiate expression of hedgehog target genes. Here, the most prominent reporter is based on multiple GLI binding sites (10). In case of Notch pathway, after ligand binding the Notch receptor sheds its intracellular domain (NICD), which translocates to the nucleus and associates with DNA binding proteins like CBF and activates Notch related gene expression. Hence, CBF promoters can be used for Notch reporter expression purposes (11).

For reporter systems, all of the aforementioned promoter elements have been mostly used in conjunction with firefly luciferase, which usually requires the lysis of cells or analysis of the supernatant. With luciferases, a very high signal to noise ratio is obtained, and they can be utilised both in cell culture, but also *in vivo* (12). On the other hand, fluorescent reporter proteins covering the whole range from UV, visible light and near infrared (13) enable activity measurements in individual cells by flow cytometry or, using fluorescence microscopy, also in tissues, but with a considerably lower signal to noise ratio when compared with luciferase assays. For many applications in developmental- and cancer biology, multi-reporter gene constructs would be desirable, allowing the simultaneous analysis of interconnected pathways. Also for Wnt, Hh and Notch it is supposed that their interplay is crucial, especially in therapy-resistant subsets of cancer cells, and drug discovery is ongoing (3). With the technical advances in developing diode pumped lasers, several easy to use flow cytometers have been developed being equipped with three or more laser allowing multiplex analysis (14). The excitation wavelengths usually range from near UV (405 nm, violet laser), blue (488 nm) to dark red (638 nm), allowing simultaneous detection of several distinct fluorescent proteins (15). For luciferases, multiplexing is possible when combining enzymes requiring different substrates. An established approach is normalization of firefly luciferase activity (FLuc, substrate luciferin) by co-transfection with *Renilla* luciferase (*RLuc*, substrate colenterazine) (12). Signal separation is achieved harnessing the differences in enzyme kinetics, where *RLuc* exhibits a flash kinetic, and FLuc a glow type kinetic. An alternative coelenterazine driven, ATP independent luciferase is derived from *Gaussia princeps* (GLuc), offering a significantly higher signal (16). GLuc is secreted in its native form, allowing also physical separation form cytoplasmic FLuc. More recently, NanoLuc (NLuc), derived from *Oplophorus gracilirostris*, has been introduced (17). This extremely bright, ATP independent luciferase with glow type luminescence requires the imidazopyrazinone based substrate furimazine. Hence, luciferase reporter can be combined differing in substrate requirements, cellular trafficking (secreted vs cytoplasmic) and enzyme kinetics (18). Towards the goal of tracking multiple pathways simultaneously, transient and stable co-transfection with several luciferase reporter based plasmids is feasible, however position effects occur when expression cassettes integrate at different genomic sites (19). To avoid such effects and allow a direct comparison of different promoter elements, use of insulator elements is one

89 option. Alternatively, plasmids with multiple expression cassettes can be generated with new cloning
90 techniques, such as the MultiSite Gateway cloning technology, simplifying the development of such
91 complex multi-gene vectors (20). However, it is critical to compare the performance of reporters within
92 multiple expression cassettes to their single-expression counterparts, so as to assess their applicability.
93 Here, we present the development of single and multi-gene vector constructs for Wnt, Hh and Notch
94 reporter constructs with either luciferases or fluorophores as reporter genes. Their specificity and
95 performance in transfection assays was evaluated and several compounds known to interfere with the
96 distinct pathway tested.

97 Material and methods

98 Cells

99 HeLa (#CCL2, ATCC, Manassas, US) and 293T (#CRL-3216, ATCC) cells were cultured in
100 DMEM/4.5g/L glucose (#D5671, Sigma-Aldrich, Darmstadt, Germany) with 10% heat inactivated fetal
101 bovine serum (FBS, #S181H, Biowest, Nuaillé, France), 2% L-Glutamin (#G7513, Sigma-Aldrich) and
102 1% Penicillin/Streptomycin (#P0781, Sigma-Aldrich) at 37°C, 5% CO_2 and saturated humidity. L Wnt-
103 3A cells (#CRL-2647, ATCC) were maintained under the same conditions, with 0.4mg/ml G-418
104 (#G418-RO, Sigma Aldrich) supplemented in the medium. Conditioned medium (CM) for activation
105 of the Wnt pathway was produced as described (21).

106

107 Plasmids

108 The 12GLI-RETKO-luc reporter was a gift from Peter Zaphiropoulos (GLI-RET) (22), CBF:H2B-
109 Venus from Anna-Katerina Hadjantonakis (CBF-Ven, Addgene plasmid #44211) (23), CBFRE (mt)
110 EGFP from Nicholas Gaiano (Cmu-eG, Addgene plasmid #26870) (24), EF.hICN1.CMV.GFP from
111 Linzhao Cheng (Addgene plasmid #17623) (25), hGli1 flag3x from Martin Fernandez-Zapico (phGli1,
112 Addgene plasmid #84922), human beta-catenin pcDNA3 from Eric Fearon (pβ-cat, Addgene plasmid
113 #16828) (26), M50 Super 8x TOPFlash (TOPFlash, Addgene plasmid #12456) and M51 Super 8x

FOPFlash (FOPFlash, Addgene plasmid #12457) were gifts from Randall Moon (27). pAd-Wnt3a was a gift from Tong-Chuan He (pWnt3a, Addgene plasmid #12518) (28) and pCAGGS-NICD from Nicholas Gaiano (pNICD, Addgene plasmid #26891) (29). pCMV-Gluc, a secreted variant, was acquired from New England Biolabs (NEB, # N8081S, Frankfurt am Main, Germany). The plasmid pEGFPLuc was acquired from Clontech (Mountain View, USA). pGL3b hPtch1 prom wt (PT wt) and pGL3-PTCH (mutated GLI binding sites, PT mut) were gifts from Fritz Aberger (30). pLUT7 HA-Gli1 was a gift from Michael Ruppert (pHA-Gli1, Addgene plasmid #62970) (10), pLV-beta-catenin deltaN90 from Bob Weinberg (pβ-catΔ90, Addgene plasmid #36985) (31), pmTurquoise2-NES from Dorus Gadella (Addgene plasmid#36206) (32). Promoterless pNL1.1 (#N1001) was obtained from Promega (Mannheim, Germany). pUC19 was included in the One Shot TOP10 set (#C404003) from Thermo Fisher Scientific (Schwerte, Germany). All remaining plasmids are content of the Multiple Lentiviral Expression System Kit, which was a gift from Ian Frew (Addgene kit #1000000060) (20). All plasmid maps, as well as in silico cloning, was performed using SnapGene (v3.1.4, GSL Biotech LLC, Chicago, USA).

Cloning

Primers were synthesized by Microsynth (Microsynth Austria GmbH, Vienna, Austria). All restriction enzymes were fast-digest variants from ThermoFisher Scientific. For preparative PCR, Q5 high-fidelity DNA polymerase (NEB, #M0492S) was used. Digests and PCR products were routinely gel purified in 0.7%-1.5% agarose gels (#443666A, VWR, Vienna, Austria) in sodium borate buffer at 80V. For gel extractions, a commercial kit (#K0692, ThermoFisher Scientific) was used as per the manual. Ligations were performed with T4 DNA ligase from ThermoFisher Scientific (#EL0011) or Blunt/TA ligase from NEB (#M0367S). For LR reactions, LR clonase plus from ThermoFisher Scientific (#12538120) was used as per the manual. Plasmids from LR reactions were transformed into chemically competent *E.coli* One Shot Mach1 (#C862003, ThermoFisher Scientific) as per manufacturer's instructions. All other plasmids were propagated either in *E.coli* 10-beta (#C3019I, NEB) or DH5α after heat shock transformation. All bacteria were expanded in LB medium with

appropriate antibiotics, and plasmids isolated with commercial miniprep or maxiprep kits (ThermoFisher Scientific, #K0503 and #K0492). All plasmids were characterized and validated by analytical restriction digests, and additional sequencing (Microsynth), if required.

Luciferase reporter cloning

pMuLE_ENTR_TOP-NLuc1.1_L5-L4 (TOP-NLuc, for Wnt pathway): pMuLE_ENTR_MCS_L5-L4 was digested with KpnI and BamHI (pMuLE backbone, 2600 bp), M50 Super 8x TOPFlash with KpnI and Hind III (TOP promoter, 214bp), and pNL1.1 with HindIII and BamHI (NLuc cDNA, 822 bp). The three target fragments were ligated together to yield the final plasmid.

pMuLE_ENTR_12GLI-FLuc_R4-R3 (GLI-FLuc, for Hh pathway): A PCR of 12GLI-RETKO-luc was performed (forward primer: gaggagctctatacactccgctatcgc, reverse primer: tacactagtcagcagatgaacactgac). The resulting fragment was cut by SacI and SpeI (12GLI-Fluc expression cassette, 4000 bp), and cloned into a SacI/SpeI digested pMuLE_ENTR_MCS_R4-R3 (pMuLE backbone, 2800 bp).

pMuLE_ENTR_CBF-GLuc_L3-L2 (CBF-GLuc, for Notch pathway): pMuLE_ENTR_MCS_L3-L2 was cut with EcoRI and XhoI (pMuLe backbone, 2600 bp). A segment of CBF:H2B-Venus was PCR amplified (forward primer: aatgaattcgtattaccgccatgc, reverse primer: ccttagtcaccgccttct) and digested with EcoRI and HindIII (CBF promoter, 416 bp). pCMV-Gluc was cut with HindIII and XhoI (GLuc cDNA, 596 bp). The three pieces were ligated to yield the final plasmid.

pMuLE_EXPR_CMV-eGFP_TOP-NLuc1.1_GLI-FLuc_CBF-GLuc (3 pathway-luciferases, 3P-Luc, for Wnt, Hh and Notch pathways): An LR reaction of pMuLE_Lenti_Dest_Neo, pMuLE_ENTR_CMV-eGFP_L1-R5, and the three abovementioned ENTR luciferase reporter plasmids was performed.

Fluorophore reporter cloning

pMuLE_ENTR_TOP-iRFP_L5-L4 (TOP-iRFP, for Wnt pathway): pMuLE_ENTR_MCS_L5-L4 was cut with KpnI and SpeI (pMuLE backbone, 2600 bp). A PCR of M50 Super 8x TOPFlash was

Auxilliary plasmids

EF.hICN1 (phICN1): For easy usage in flow cytometry, the CMV.GFP of the plasmid EF.hICN1.CMV.GFP was removed by digestion with EcoRI (9.2kb fragment), after which it was ligated. pUC19 and pDest were used as control or stuffer plasmids in transfections.

3P plasmid system

A set of plasmids generated in this work, including maps and sequences, can be found at Addgene (see data in S1 Table), while maps and the *in silico* generated sequence for CBF-GLuc (S1A Fig, S1 File) and 3P-Luc (S1B Fig, S2 File) are in the supplementary information.

Transfections

If not mentioned otherwise, 293T cells were used. Cells were seeded in white 96-well plates (Greiner Bio-One, #655098) for luciferase reporter assays or in transparent well plates (Greiner Bio-One, #655160) for fluorophore reporter assays. Twenty-four hours after seeding , cells were transfected using linear polyethylenimine (LPEI) in principle as described (33). Growth media was exchanged for 100 µl serum-free DMEM high glucose. Polyplexes were generated after mixing all relevant plasmids at a final plasmid concentration of at least 20 µg/ml in HBS buffer at N/P 9, and further diluted with HBS after particle formation when required. If not described otherwise, 100 µl DMEM high glucose with 1% FBS 2% L-Glutamine were added four hours after transfection, and cells further incubated. If not stated otherwise, the evaluation of the pathways was performed 24h after transfection for the Wnt pathway, and 48h after transfection for Hh and Notch pathways.

Luciferase reporter assays

For single pathway reporters, transfections were carried out as follows: If not stated otherwise, for FLuc and NLuc containing reporter plasmids 50ng per well were used. For normalization, 10ng pCMV-Gluc were added. For GLuc containing reporter plasmids, 50ng per well plus 50ng CMV driven pEGFP-Luc was taken. Additionally, 25ng pUC19 or the respective inducer plasmid were added. Care was taken not to detach cells when aspirating liquid, as this can negatively influence the signal

normalization. All luminescence measurements were performed with an infinite M200Pro plate reader (Tecan, Grödig, Austria).

For GLuc activity measurements, 20 µl supernatant was transferred to a new white 96-well plate, 50 µl coelenterazine buffer (20µM coelenterazine in PBS supplemented with 5mM NaCl, pH 7.2 as per Tannous et al, ref (34)) added per well and the signal acquired for 10 seconds after a wait time of 2 seconds. For NLuc measurements, 160 µl medium were, removed leaving 40 µl in the well. Then, 40 µl of Nano-Glo reagent (Promega, #N1110) was added, incubated for 3 min at RT and signal acquired for 10 seconds. For FLuc measurements, supernatant was completely aspirated. Cells were lysed in 30 µl 1x Passive Lysis Buffer (Promega, #E194A) and shaken for 30min at 500RPM at RT on an Eppendorf ThermoMixer C. For the measurement, 100 µl of luciferase assay reagent (35) were injected and the signal acquired for 10 seconds after a lag time of 2 seconds.

For the 3P-Luc based experiments and their comparison with individual plasmids, cells were co-transfected with 50 ng reporter plasmid plus 25 ng of respective inducer plasmid or pUC19. Luciferase activities were measured as described above. All luciferase activities were normalised to total cell viability using the CellTiter Fluor kit (Promega #G6081). For this, supernatant was completely aspirated and, if required, GLuc measured as described above. 100 µl of PBS and 20 µl 5x CellTiter-Fluor reagent was added, and plates incubated up to 2.5h at cell culture conditions. The complete supernatant was then transferred to a black 96-well plate (Greiner Bio-One, #655209) and fluorescence measured as by manufacturers recommendation. Afterwards, the cells were utilised for FLuc or NLuc measurements.

Signal normalization was carried out as follows: First, from each reporter and normalizer value, background was subtracted. Per well, RLUs from reporter were divided by RLUs (or fluorescence units) from the normalisation method. For better graphical representation, the result was multiplied to give values of similar magnitude, using the same factor within one parameter comparison. For single reporter experiments, CMV-driven luciferases were used to normalize RLU values per well.

Fluorophore reporter assays

400ng of the reporter plasmid and 400ng pUC19 or the respective inducer were co-transfected per well. For the measurement, cells were washed once with PBS, detached with Versene (#15040-33, ThermoFisher Scientific), and the cell suspension transferred into a PCR plate (Nerbe, #04-083-0150, nerbe plus GmbH, Winsen, Germany). Cells were measured on a Macs-Quant Analyzer 10 flow cytometer (Miltenyi BiotecGmbH, Bergisch Gladbach, Germany) equipped with solid state laser emitting at 488 nm (FSC, SCC, B1-B3), 405 nm (V1 and V2) and 638 nm (R1 and R2). Plates were actively cooled for the whole measurement to 4°C using an Inheco CPAC cooling unit (INHECO, Planegg, Germany). Analysis of flow cytometry data was done with FlowJo 10.1r5 (FlowJo LLC, Ashland OR, USA). All signals were acquired in area (A) and height (H) mode. As a gating strategy, the main cell population was gated first in FSC-A versus (vs.) SSC-A, and single cells were further selected in FSC-A vs. FSC-H. mTurquoise2 was gated in V1-A vs. V2-A (V1: 450/50 nm bandpass (BP), V2: 525/50nm BP), tdTomato in B1-A (525/50 nm BP) vs. B3-A (655-730 nm BP), and iRFP in R1-A (655-730 nm BP) vs R2-A (750nm logpass (LP)). For analysis of 3P-Fluc, compensation matrices were generated in FlowJo by separately analyzing CMV-driven variants of all four colours. The appropriate matrix was then applied to the measured values of 3P-Fluor before analysis.

Small molecule evaluation

The following small molecules were evaluated for induction or reduction of pathway activity. Wnt: CHIR99021(#SML1046) (36), LY2090314 (#SML1438) (36), niclosamide (N3510) (37), LGK-974 (#S7143) (36); Hh: SAG dihydrochloride (SAG, #SML1314) (38), sonidegib (#S2151) (39), vismodegib (#S1082) (40); Notch: suberohydroxamic acid (SBHA, #390585) (41), DAPT (#S2215) (42), Dibenzazepine (DBZ, #S2711) (43), valproic acid sodium salt (VPA, #P4543) (44). All reagents were purchased from Selleckchem (Munich, Germany) or Sigma Aldrich. VPA and SAG were dissolved in ultrapure water (Arium pro, Sartorius AG, Göttingen, Germany), and the remaining compounds in DMSO (#D5879, Sigma-Aldrich).

Transfections and evaluations were performed as described above, with the following changes: For induction of the Wnt-pathway in the respective wells, 100 µl CM (1:1) was added to the wells four hours after transfection. Treatments were also added four hours after transfection, at a final concentration of 10µM. An equal amount of appropriate solvent (water or DMSO) was added to the solvent control conditions.

Statistical analysis

If not mentioned otherwise, all experiments were at least performed twice, with each condition at least in triplicate. Statistical analysis was performed using GraphPad Prism, version 7.02 (GraphPad Software La Jolla, USA). For fold induction analysis, results from identical experiments were pooled. Statistical analysis consisted of an unpaired t-test, columns show mean values, and error bars denominate standard deviation.

Results

Performance of single luciferase pathway reporters

The Wnt-pathway sensitive TOP promoter was used to drive NLuc expression (Fig 1A). Several plasmids were first evaluated regarding their ability to induce the Wnt pathway, with pWnt3a performing best (Fig S2A) and was thus selected for further experiment. The sensitivity of TOP-NLuc to Wnt-pathway induction (by co-transfection with pAd-Wnt3A) was compared with the established Wnt reporter TOPFlash (Fig 1B-C). The normalized RLUs of TOPFlash and TOP-NLuc were comparable in side-by side experiments with similar signal induction of approximately 100-fold (Fig 1B). The control plasmid FOPFlash, having mutant TCF/LEF binding sites, did not show a significant signal increase upon induction, as expected.

Fig 1. Evaluation of Wnt, Hh and Notch luciferase single reporters via luminescence readout. (A) The Wnt promoter TOP was combined with NLuc. (D) The Hh promoter GLI-RET was backbone switched to obtain GLI-FLuc. (G) For the Notch (Not) reporter construct, the CBF promoter was combined with GLuc. All

289 transfections were carried out in 293T cells. B, E, H: Luminescence measurement of cells transfected with the
290 indicated plasmid and co-transfected with either pUC19 control or the indicated inducer plasmid. C, F, I: fold
291 increase in signal for the indicated plasmid upon co-transfection with pUC19 control versus inducer plasmid (C:
292 pWnt3a; F: phGli1; I: phICN1). In B, E and H results are show from a representative experiment; C, F and I are
293 the average of 2-5 independent experiments. (**P≤0.01, ****P≤0.0001, ns=not significant, t-test, n=4).
294 Normalised RLUs were multiplied with 10 (CBF-GLuc), 100 (TOP-NLuc) or 1000 (FOPFlash, TOPFlash, GLI-
295 RET and GLI-FLuc).

296

297 As luminescence-based Hh reporter, GLI-FLuc was generated (Fig 1D). For induction, several
298 plasmid-based inducers were evaluated (pUC19 and pDest were used as control plasmids), with phGli1
299 offering the most consistent results (Fig S2B). The original reporter GLI-RET and the new GLI-FLuc
300 showed similar performance, both in terms of expression strength (Fig 1E) and fold increase in signal
301 after induction with phGli1 (Fig 1F).

302 The plasmid CBF-GLuc was cloned for tracking Notch activity (Fig 1G). Two different Notch-
303 inducing plasmids, phICN1 and pNICD, were evaluated (Fig S2C) and phICN1 was chosen for further
304 experiments. Although increase in normalized RLUs and fold increase upon induction of CBF-GLuc
305 were considerably lower compared to TOP-NLuc and GLI-FLuc, results were statistically significant,
306 and consistent over several experiments (Fig 1H, G). In contrast to the plasmids described above, a
307 direct comparison of CBF-GLuc with CBF-based luciferase reporter was not feasible, as the original
308 version is a fluorophore-based reporter.

309 Taken together, the newly developed pathway-sensitive luciferase based reporters perform equally
310 well to their original counterparts where applicable, and all show statistically significant responsiveness
311 as well as robust fold-increase when induced with appropriate pathway activators.

312 Performance of single fluorophore pathway reporters

313 In a next step, fluorophore reporter genes were generated to evaluate specificity and signal dynamics.
314 With the Wnt-construct TOP-iRFP (Fig 2A), baseline iRFP signal in 293T cells resulted in <0.04%

315 iRFP$^+$ cells, which increased significantly to a mean of 0.85% positive cells upon induction with
316 pWnt3a (Fig 2B). This corresponds to a signal increase of around 30-fold (Fig 2C).

317 ***Fig 2. Evaluation of Wnt, Hh and Notch fluorescent single reporters via flow cytometry.*** (A) The Wnt
318 promoter TOP was combined with iRFP. (D) The Hh sensitive promoter PTCH1 was joined with mTurquoise2
319 (mT2). (G) For the Notch (Not) reporter construct, the CBF promoter was combined with tdTomato (tdT).
320 Transfection were carried out either in 293T cells (B, C, E, F) or HeLa (H, I). B, E, H: Fluorescence measurement
321 of cells transfected with the indicated plasmid and co-transfected with either pUC19 control (white bars) or the
322 indicated inducer plasmid (grey bars). C, F, I: fold increase in signal for the indicated plasmid upon co-transfection
323 with pUC19 control versus inducer plasmid (C: pWnt3a; F: phGli1; I: phICN1). In B, E and H results are shown
324 from a representative experiment; C, F and I are the average of 3-6 independent experiments. (**P≤0.01,
325 ****P≤0.0001, ns=not significant, t-test, n≥4).

326 For the Hh reporter construct, the promoter PT was chosen (Fig 2D). The fluorophore reporter
327 construct PT-mT2 resulted in approx. 3.5 % mTurquoise2$^+$ cells upon induction with phGli1,
328 corresponding to an increase of 2.6-fold when compared to control (pUC19) transfected cells (Fig 2E-
329 F). In addition, original and mutant binding versions of the promoter driving FLuc were compared (Fig
330 S3). Also here, signal increase was significantly higher when compared to mutant control.

331 As a Notch reporter protein, tdTomato was used and evaluated in HeLa cells (Fig 2G-I), as 293T
332 cells did not show any signal increase upon induction with CBF-fluorophore construct (Fig S4). In case
333 of HeLa cells, CBF-tdTomato showed a highly significant, 11.5-fold signal increase upon induction.
334 This was in contrast to the original plasmid reporter CBF-Ven, which in our hands only achieved a non-
335 significant increase in the number of positive cells (1.2-fold, compared to 0.9 fold using the mutant
336 binding site plasmid version Cmu-eG). Of note, CBF-tdT exhibited a baseline signal several times lower
337 than that of both the original and mutant plasmid reporter versions CBF-Ven and Cmu-eG (Fig 2H).

338 Taken together, all fluorophore-reporter constructs showed significant signal increases upon
339 induction, and satisfactory fold increases.

Development of multicistronic pathway reporters

Based on the modified Gateway cloning system described by Albers and colleagues (20), polycistronic plasmid vectors were designed and cloned utilising the Multiple Lentiviral Expression System Kit. The luciferase reporter 3P-Luc contained Wnt-NLuc, Hh-FLuc (using GLI-FLuc), and Notch-Gluc (using CBF-Gluc) expression cassettes, and in addition a PGK promoter driven Neomycin resistance for selection purposes and a CMV driven EGFP expression cassette for future sorting (for map see Fig S1B, scheme see Fig 3A). The yield of the resulting large plasmid (15,489 bp) was in the range of 4.8 µg per ml culture volume. The single luciferase reporter plasmids were compared side-by-side with 3P-Luc (Fig 3B-E). For all three pathways, induction was significant using the 3P-Luc plasmid. For the Wnt (Fig 3C) and Hh pathways (Fig 3D), signal induction was less pronounced when compared to the single reporters. Interestingly, Notch single reporter induction was not significant in these assays (Fig 3B).

Fig 3. Evaluation of triple pathway reporter constructs. (A) The three single luciferase reporter gene plasmids for the Wnt, Hh and Notch pathways were joined by a gateway approach to yield 3P-Luc. (F) 3P-Fluor was generated from the three pathway reporter plasmids with indicated fluorophore reporters. Experiments in B, C, D, E, H and I were carried out in 293T cells. In panel G, 293T cell were used for pWnt3a and phGli1 and corresponding pUC19 control transfections, Hela were used in panel G for phICN1 and corresponding pUC19 control and in panel J. (B): Luminescence measurement of cells transfected with the indicated plasmid and co-transfected with either pUC19 control or the indicated inducer plasmid. Normalised RLUs were multiplied with 0.1 (Wnt-pathway experiments), 1 (Hh-pathway experiments) or 0.01 (Notch-pathway experiments). C-E: Quantification of fold increases for Wnt (C), Hh (D) and Notch (E). (G) Evaluation of compensated 3P-Fluor with a compensation matrix applied. Cells were transfected with 3P-Fluor and co-transfected with either pUC19 control or the indicated inducer plasmid. H-J: Quantification of fold increases of fluorescence positive cells for Wnt (H), Hh (I) and Notch (J). In B and G results are shown from a representative experiment; C, D, E, H, I and J are the average of 3-4 independent experiments. (**P≤0.01, ***P≤0.001, ****P≤0.0001, n.s.=not significant, t-test, n≥3)

The fluorescence reporter 3P-Fluor (Fig 3F) consisted of Wnt-iRFP, Hh-mT2 (using PT-mT2), and Notch-tdT. Using CMV-driven fluorophore variants for iRFP, mTurquoise2, tdTomato and eGFP, a compensation matrix was generated to minimise signal overspill between the individual colours. The

matrices used showed a considerable interplay of mTurquoise2, eGFP and tdTomato (for 293 T see Table S2, for HeLa see Table S3). Analyzing the compensated data, a robust increase of iRFP$^+$ cells after induction of the Wnt pathway was observed, with a mean 6.1-fold increase (Fig 3G, H). In contrast to this, the data for the Hh (Fig 3G, I) and Notch pathway (Fig 3G, J) show neither a significant increase of fluorophore-positive cells upon induction, nor a fold-increase. Here, the detection of a clear-cut mTurquoise2$^+$ or tdTomato$^+$ subpopulation was not possible despite the application of compensation (Fig S5).

Small molecule evaluation

In an initial experimental series, several published small molecules were evaluated regarding their capability to induce or reduce the activity of single luciferase pathway reporters (Fig 4). 293T cells were transiently co-transfected with reporter and normalizing plasmid, and inducer plasmids where indicated. All compounds were tested at 10µM and added 4 hours after transfection. Activity was measured after 24 (Wnt) and 48 h (Hh, Notch), respectively. While CHIR99021 showed a significant TOP-NLuc induction, the activation seen with LY2090314 was not significant (Fig 4A). Niclosamide significantly decreased TOP-NLuc activity, while LGK-974 did not change the signal compared to solvent control.

Fig 4. Small molecule evaluation with the novel reporters. 293T cells were transfected with the indicated reporter plasmid and treated with the listed compounds (10 µM). (A) TOP-NLuc; (B) GLI-FLuc, (C) CBF-Gluc. White bars: uninduced conditions, grey bars: induction with conditioned medium (A: CM, contains Wnt3a) or by co-transfection (B: phGli1, C: phICN1). CHIR=CHIR99021, LGK=LGK-974, LY=LY2090314, Niclo=niclosamide, Soni=sonidegib, Vismo=vismodegib. (**P≤0.01, ***P≤0.001, ****P≤0.0001, n.s.=not significant, t-test, n=4) Normalised RLUs were multiplied with 100 (TOP-NLuc, GLI-FLuc and CBF-GLuc).

After transfection with the Hh reporter GLI-FLuc, SAG did not induce the Hh pathway, and in fact gave lower FLuc signals that the solvent control (Fig 4B). In cells co-transfected with phGli1, only vismodegib significantly decreased Hh signalling.

(11). The lower performance observed in our experiments could not be fully elucidated, but it could be due to the normalization method used.

We assumed that due to the signal amplifying effects of luciferase enzymes (46), the signal increase would be considerably reduced when pairing the same promoters with fluorophores. Bauer and colleagues directly compared TOP-GFP and TOP-Luc adding Wnt3a protein, estimating a >100-fold increase in both cases, although apparently saturating amounts of protein were added (47). In another approach, a bidirectional NF-κB-responsive reporter was cloned simultaneously driving expression of FLuc and EGFP (48) . Upon stimulation with TNFa, luciferase activity increased several hundred fold, whereas the number of EGFP positive cells increase from 0.3 to 35% (although not considering the absolute EGFP expression per cell). From this, one could consider that luciferase based vectors offer a higher dynamic range, but fluorophore-based vectors are not necessarily less sensitive in terms of induction. In our experiments, the fold increase upon induction using fluorescent proteins decreased only to around one third (TOP and CBF promoter) and half (PT promoter), respectively. Still, it should be kept in mind that the half-life of reporter proteins largely differ, e.g. with 3h for cytoplasmic firefly luciferase (49) and >24h for EGFP (50). To improve the dynamics of the readout, destabilised protein versions of the reporter proteins can be utilised (49, 50), although this could come with an overall decreased sensitivity. We also observed a dependence on the type of fluorophore used: although the original version CBF:H2B-Venus did not show significant signal increase upon induction, our CBF-tdTomato construct performed at considerably lower baseline with >10-fold induction (Fig 2I), which is clearly above than the luciferase version CBF-GLuc (Fig 1I).

In a next step, we generated triple pathway reporter plasmids with our constructs, which were then also evaluated. We used the approach described by Albers et al., based on Gateway cloning (20). As backbone for the Gateway cloning approach, a lentiviral transfer plasmid was chosen, offering the possibility for transient transfection, but also the generation of stably transduced cell lines using a lentivirus. An additional CMV-EGFP cassette was added to enable sorting of transfected or transduced cells with FACS, as well as a neomycin cassette, adding an additional choice for cell selection (Fig S1B). For 3P-Luc, all luciferase activities had to be normalised to total cell viability, as normalization

with CMV-driven luciferases was not possible, due to the genes already used as pathway reporters. The single reporters were included in these experiments, also to investigate differences due to the normalization method. With single reporters, we saw that the choice of normalization method (CMV-driven luciferases in Fig, 1, CellTiterFluor in Fig 3B-E) had significant influence on the calculated induction level. TOP-NLuc showed >100-fold induction in Fig 1C and >700-fold induction in Fig 3C. With GLI-FLuc, the difference was less pronounced (200-fold in Fig 1F vs 70-fold in Fig 3D). The reaction of the single Notch reporter is remarkable, as it failed to reach a significant increase upon induction in Fig 3B, but had a highly significant response in Fig 1H, where we used another normalization approach. We thus assume that the alternative normalization method based on total cell viability instead of our usual co-transfection with CMV-driven luciferases, had an appreciable impact on the results. Investigation of the most appropriate normalization method would in itself be a separate study. Side-by-side comparison of induction levels between single reporter and 3P-Luc revealed remarkably lower levels for Wnt and Hh in 3P-Luc (700- vs 2.7-fold for Wnt, 70- vs 9-fold for Hh). Surprisingly, the Notch reporter performed better in the 3P-Luc construct (8-fold). The differences between single- and multiple pathway reporter are intriguing and can be explained in several ways. For example, all promoters, also our synthetic constructs, require the binding of transcriptions factors (TF) for activation. At least two effects can explain reduced activity of promoter elements within multicistronic vectors. Firstly, promoters interacting with similar TF will compete for these proteins (51). Hence, it appears reasonable that single plasmids in an episomal status would be less prone to TF limitation when compared to several promoters in close vicinity in one plasmid. Secondly, steric hindrance can be an obstacle for TF binding (52), which makes it necessary to include spacer elements within TF binding sites in synthetic promoter elements. Such an effect is also possible in our case, even when different TF bind to the distinct promoter elements. However, in light of the aforementioned explanation, the increased activation of the Notch reporter on the 3P-Luc plasmid still appears contradictory.

With the ambitious aim of enabling pathway activity research on the live single cell level, we generated a fluorophore based triple reporter named 3P-Fluor. While the Wnt reporter iRFP was clearly

inducible (6-fold increase in number of positive cells, compared to 30-fold with the single reporter), we were unable to detect a clear population of mTurquoise2^{+} and tdTomato^{+} cells, at induced as well as at control conditions. The reduction in iRFP signal, compared to the single pathway reporter plasmid, can be explained as for 3P-Luc. We assume that the strong absolute signal intensity of eGFP made compensation of existing, but faint mTurquoise and tdTomato signal impracticable, as our compensation matrices show the large overspill of eGFP in these channels. In case of tdTomato, the fluorophore was excited at 488 nm with only approximately 25% efficiency. This and the overall lower promoter strength when compared to CMV caused potentially too much signal overspill. The same can be assumed for mTurquoise2: while the 405 nm diode laser excites the fluorophore with approx. 50% efficiency, it also excited eGFP with approx. 17% (all spectra information obtained from https://www.fpbase.org/spectra/). Using flow cytometers with better-suited excitation wavelengths and emission filters would be one option. Alternatively, the CMV-EGFP cassette can be either eliminated and selection of transfected/transduced cells be carried out using neomycin. As another approach, either a weaker, constitutive active promoter or a destabilised EGFP version, e.g. D2EGFP (50), could be employed. Regarding the Hh promoter used, the presented data indicates that the 12GLI promoter outperforms the PTCH1 promoter. In a follow-up construct, we aim to implement a new 12GLI-mTurquoise2 reporter.

Lastly, we evaluated several small molecule to demonstrate the suitability of our single pathway reporters for such an approach. CHIR99021 and LY2090314 both inhibit GSK3 (36) and hence induced the Wnt reporter TOP-NLuc, albeit LY2090314 only non-significantly due to presumably potential toxicity of the compound (53). LGK-974, a porcupine inhibitor, blocks Wnt secretion (36). In accordance with literature, no effect of this compound was observed as Wnt pathway activation was facilitated externally by direct Wnt3a expression. Niclosamide did decrease the Wnt signal, as it induces DVL2 downregulation and LRP6 degradation (37).

The SMO-activating compound SAG did not induce our Hh-reporter, but as it was used at lower concentrations and measured within shorter timeframes, our setup might need optimization (38). Sonidegib is a SMO antagonist (39), and as such does not interfere with our Gli-based pathway

induction, explaining why we see no decrease in Hh pathway activity. Interestingly, vismodegib has a similar mode of action, but also inhibits the expression of Gli1/2 (40), supporting the inhibitory effect we saw in our assay.

VPA is a histone deacetylase, leading to the activation of Notch1, which in turn induces Notch signalling via CBF1 (44). We saw no Notch pathway activation in our setup, which can be due to the cell line used (54). SBHA, which operates in a similar fashion (41), also failed to induce Notch signalling. The Notch pathway inhibitor DAPT blocks γ-secretase activity (42), and did not inhibit the Notch pathway in our assay. As we transfected cells to produce the Notch intracellular domain directly, thus bypassing the γ-secretase step, our findings are in line with the literature. DBZ, one of the most potent Notch inhibitors, affects the intracellular domain (43), which is in accordance with the reduced activity of our Notch reporter.

For further studies, we have produced VSV-G pseudotyped lentiviral vectors with 3P-Luc and 3P-Fluor constructs as transfer plasmids. Cells stably transduced with these multi-reporter lentiviral vectors will be utilized for broader screening approaches.

Taken together, we report successful generation and evaluation of a multi-gene, luciferase-based three pathway reporter. Additionally, a functioning fluorescence based 3P-Fluor construct has the potential to enable in vitro screening approaches as well as in vivo applications using preclinical imaging. The fluorescence based reporter will need further optimization, but offers possibilities for studying the interplay of Wnt, Hh and Notch pathway and their response to treatment approaches on a single cell level.

Acknowledgements

We would like to mention the contributions of Katarina Peric, Islam Abd El Rahman, Nawid Shayganfar, and Susanne Wiederkum to this work. Additionally, we would like to thank Laura Patricia Brandt, Ian Frew, Anna-Katerina Hadjantonakis and Peter Zaphiropoulos for their advice. Open access funding was provided by University of Vienna.

References

1. Nwabo Kamdje AH, Takam Kamga P, Tagne Simo R, Vecchio L, Seke Etet PF, Muller JM, et al. Developmental pathways associated with cancer metastasis: Notch, Wnt, and Hedgehog. Cancer Biol Med. 2017;14(2):109-20.

2. Krishnamurthy N, Kurzrock R. Targeting the Wnt/beta-catenin pathway in cancer: Update on effectors and inhibitors. Cancer Treat Rev. 2018;62:50-60.

3. Takebe N, Miele L, Harris PJ, Jeong W, Bando H, Kahn M, et al. Targeting Notch, Hedgehog, and Wnt pathways in cancer stem cells: clinical update. Nature reviews Clinical oncology. 2015;12(8):445-64.

4. Batlle E, Clevers H. Cancer stem cells revisited. Nature medicine. 2017;23(10):1124.

5. Sacan A, Ekins S, Kortagere S. Applications and limitations of in silico models in drug discovery. Bioinformatics and Drug Discovery: Springer; 2012. p. 87-124.

6. Schmalhofer O, Spaderna S, Brabletz T. Native promoter reporters validate transcriptional targets. Methods Mol Biol. 2008;468:111-28.

7. Engstrom MD, Pfleger BF. Transcription control engineering and applications in synthetic biology. Synth Syst Biotechnol. 2017;2(3):176-91.

8. Zhan T, Rindtorff N, Boutros M. Wnt signaling in cancer. Oncogene. 2017;36(11):1461-73.

9. Barolo S. Transgenic Wnt/TCF pathway reporters: all you need is Lef? Oncogene. 2006;25(57):7505-11.

10. Deng W, Vanderbilt DB, Lin CC, Martin KH, Brundage KM, Ruppert JM. SOX9 inhibits beta-TrCP-mediated protein degradation to promote nuclear GLI1 expression and cancer stem cell properties. J Cell Sci. 2015;128(6):1123-38.

11. Hsieh J, Henkel T, Salmon P, Robey E, Peterson MG, Hayward SD. Truncated mammalian Notch1 activates CBF1/RBPJk-repressed genes by a mechanism resembling that of Epstein-Barr virus EBNA2. Molecular and cellular biology. 1996;16(3):952-9.

12. Tung JK, Berglund K, Gutekunst C-A, Hochgeschwender U, Gross RE. Bioluminescence imaging in live cells and animals. Neurophotonics. 2016;3(2):025001.

552 13. Thorn K. Genetically encoded fluorescent tags. Mol Biol Cell. 2017;28(7):848-57.
553 14. Telford WG. Overview of Lasers for Flow Cytometry. Methods Mol Biol. 2018;1678:447-79.
554 15. Telford WG, Shcherbakova DM, Buschke D, Hawley TS, Verkhusha VV. Multiparametric
555 flow cytometry using near-infrared fluorescent proteins engineered from bacterial phytochromes. PLoS
556 One. 2015;10(3):e0122342.
557 16. Tannous BA, Kim DE, Fernandez JL, Weissleder R, Breakefield XO. Codon-optimized
558 Gaussia luciferase cDNA for mammalian gene expression in culture and in vivo. Mol Ther.
559 2005;11(3):435-43.
560 17. Hall MP, Unch J, Binkowski BF, Valley MP, Butler BL, Wood MG, et al. Engineered luciferase
561 reporter from a deep sea shrimp utilizing a novel imidazopyrazinone substrate. ACS Chem Biol.
562 2012;7(11):1848-57.
563 18. Didiot M-C, Serafini S, Pfeifer MJ, King FJ, Parker CN. Multiplexed reporter gene assays:
564 monitoring the cell viability and the compound kinetics on luciferase activity. Journal of biomolecular
565 screening. 2011;16(7):786-93.
566 19. Akhtar W, de Jong J, Pindyurin AV, Pagie L, Meuleman W, de Ridder J, et al. Chromatin
567 position effects assayed by thousands of reporters integrated in parallel. Cell. 2013;154(4):914-27.
568 20. Albers J, Danzer C, Rechsteiner M, Lehmann H, Brandt LP, Hejhal T, et al. A versatile modular
569 vector system for rapid combinatorial mammalian genetics. The Journal of clinical investigation.
570 2015;125(4):1603.
571 21. ATCC. Protocol for Wnt-3A Conditioned Medium 2016 [Available from:
572 https://www.lgcstandards-atcc.org/Products/All/CRL-2647.aspx?geo_country=at#culturemethod.
573 22. Kogerman P, Grimm T, Kogerman L, Krause D, Undén AB, Sandstedt B, et al. Mammalian
574 suppressor-of-fused modulates nuclear–cytoplasmic shuttling of Gli-1. Nature cell biology.
575 1999;1(5):312.
576 23. Nowotschin S, Xenopoulos P, Schrode N, Hadjantonakis A-K. A bright single-cell resolution
577 live imaging reporter of Notch signaling in the mouse. BMC developmental biology. 2013;13(1):15.
578 24. Mizutani K-i, Yoon K, Dang L, Tokunaga A, Gaiano N. Differential Notch signalling
579 distinguishes neural stem cells from intermediate progenitors. Nature. 2007;449(7160):351.

580 25. Yu X, Alder JK, Chun JH, Friedman AD, Heimfeld S, Cheng L, et al. HES1 inhibits cycling of
581 hematopoietic progenitor cells via DNA binding. Stem Cells. 2006;24(4):876-88.
582 26. Kolligs FT, Hu G, Dang CV, Fearon ER. Neoplastic transformation of RK3E by mutant β-
583 catenin requires deregulation of Tcf/Lef transcription but not activation of c-myc expression. Molecular
584 and cellular biology. 1999;19(8):5696-706.
585 27. Veeman MT, Slusarski DC, Kaykas A, Louie SH, Moon RT. Zebrafish prickle, a modulator of
586 noncanonical Wnt/Fz signaling, regulates gastrulation movements. Current Biology. 2003;13(8):680-5.
587 28. Luo Q, Kang Q, Si W, Jiang W, Park JK, Peng Y, et al. Connective tissue growth factor (CTGF)
588 is regulated by Wnt and bone morphogenetic proteins signaling in osteoblast differentiation of
589 mesenchymal stem cells. Journal of Biological Chemistry. 2004;279(53):55958-68.
590 29. Dang L, Yoon K, Wang M, Gaiano N. Notch3 signaling promotes radial glial/progenitor
591 character in the mammalian telencephalon. Developmental neuroscience. 2006;28(1-2):58-69.
592 30. Winklmayr M, Schmid C, Laner-Plamberger S, Kaser A, Aberger F, Eichberger T, et al. Non-
593 consensus GLI binding sites in Hedgehog target gene regulation. BMC molecular biology.
594 2010;11(1):2.
595 31. Guo W, Keckesova Z, Donaher JL, Shibue T, Tischler V, Reinhardt F, et al. Slug and Sox9
596 cooperatively determine the mammary stem cell state. Cell. 2012;148(5):1015-28.
597 32. Goedhart J, von Stetten D, Noirclerc-Savoye M, Lelimousin M, Joosen L, Hink MA, et al.
598 Structure-guided evolution of cyan fluorescent proteins towards a quantum yield of 93%. Nat Commun.
599 2012;3:751.
600 33. Taschauer A, Geyer A, Gehrig S, Maier J, Sami H, Ogris M. Up-scaled synthesis and
601 characterization of nonviral gene delivery particles for transient in vitro and in vivo transgene
602 expression. Human gene therapy methods. 2016;27(3):87-97.
603 34. Tannous BA. Gaussia luciferase reporter assay for monitoring biological processes in culture
604 and in vivo. Nature protocols. 2009;4(4):582.
605 35. Mueller K, Ogris M, Sami H. Firefly luciferase based reporter gene assay for investigating
606 nanoparticle mediated nucleic acid delivery. Methods Mol Biol. 2013;948:in press.

607 36. Nusse R, Clevers H. Wnt/β-catenin signaling, disease, and emerging therapeutic modalities.
608 Cell. 2017;169(6):985-99.
609 37. Ahmed K, Shaw HV, Koval A, Katanaev VL. A second WNT for old drugs: drug repositioning
610 against WNT-dependent cancers. Cancers. 2016;8(7):66.
611 38. Di Magno L, Basile A, Coni S, Manni S, Sdruscia G, D'Amico D, et al. The energy sensor
612 AMPK regulates Hedgehog signaling in human cells through a unique Gli1 metabolic checkpoint.
613 Oncotarget. 2016;7(8):9538.
614 39. Jain S, Song R, Xie J. Sonidegib: mechanism of action, pharmacology, and clinical utility for
615 advanced basal cell carcinomas. OncoTargets and therapy. 2017;10:1645.
616 40. Singh BN, Fu J, Srivastava RK, Shankar S. Hedgehog signaling antagonist GDC-0449
617 (Vismodegib) inhibits pancreatic cancer stem cell characteristics: molecular mechanisms. PloS one.
618 2011;6(11):e27306.
619 41. Ning L, Greenblatt DY, Kunnimalaiyaan M, Chen H. Suberoyl bis-hydroxamic acid activates
620 Notch-1 signaling and induces apoptosis in medullary thyroid carcinoma cells. The Oncologist.
621 2008;13(2):98-104.
622 42. Geling A, Steiner H, Willem M, Bally-Cuif L, Haass C. A γ-secretase inhibitor blocks Notch
623 signaling in vivo and causes a severe neurogenic phenotype in zebrafish. EMBO reports. 2002;3(7):688-
624 94.
625 43. Milano J, McKay J, Dagenais C, Foster-Brown L, Pognan F, Gadient R, et al. Modulation of
626 notch processing by gamma-secretase inhibitors causes intestinal goblet cell metaplasia and induction
627 of genes known to specify gut secretory lineage differentiation. Toxicol Sci. 2004;82(1):341-58.
628 44. Greenblatt DY, Vaccaro AM, Jaskula-Sztul R, Ning L, Haymart M, Kunnimalaiyaan M, et al.
629 Valproic acid activates notch-1 signaling and regulates the neuroendocrine phenotype in carcinoid
630 cancer cells. The oncologist. 2007;12(8):942-51.
631 45. Hernandez-Garcia CM, Finer JJ. Identification and validation of promoters and cis-acting
632 regulatory elements. Plant Sci. 2014;217-218:109-19.
633 46. Roda A, Guardigli M, Michelini E, Mirasoli M. Bioluminescence in analytical chemistry and
634 in vivo imaging. TrAC Trends in Analytical Chemistry. 2009;28(3):307-22.

635 47. Bauer M, Benard J, Gaasterland T, Willert K, Cappellen D. WNT5A encodes two isoforms
636 with distinct functions in cancers. PLoS One. 2013;8(11):e80526.
637 48. Kuri P, Ellwanger K, Kufer TA, Leptin M, Bajoghli B. A high-sensitivity bi-directional reporter
638 to monitor NF-kappaB activity in cell culture and zebrafish in real time. J Cell Sci. 2017;130(3):648-
639 57.
640 49. Leclerc GM, Boockfor FR, Faught WJ, Frawley LS. Development of a destabilized firefly
641 luciferase enzyme for measurement of gene expression. Biotechniques. 2000;29(3):590-1, 4-6, 8
642 passim.
643 50. Rios AC, Denans N, Marcelle C. Real-time observation of Wnt beta-catenin signaling in the
644 chick embryo. Dev Dyn. 2010;239(1):346-53.
645 51. Karreth FA, Tay Y, Pandolfi PP. Target competition: transcription factors enter the limelight.
646 Genome Biol. 2014;15(4):114.
647 52. Rushton PJ. What Have We Learned About Synthetic Promoter Construction? Methods Mol
648 Biol. 2016;1482:1-13.
649 53. Kunnimalaiyaan S, Schwartz VK, Jackson IA, Gamblin TC, Kunnimalaiyaan M.
650 Antiproliferative and apoptotic effect of LY2090314, a GSK-3 inhibitor, in neuroblastoma in vitro.
651 BMC cancer. 2018;18(1):560.
652 54. Pinchot SN, Jaskula-Sztul R, Ning L, Peters NR, Cook MR, Kunnimalaiyaan M, et al.
653 Identification and validation of Notch pathway activating compounds through a novel high-throughput
654 screening method. Cancer. 2011;117(7):1386-98.

655

Figure 1

Click here to access/download;Figure;Fig1.tiff

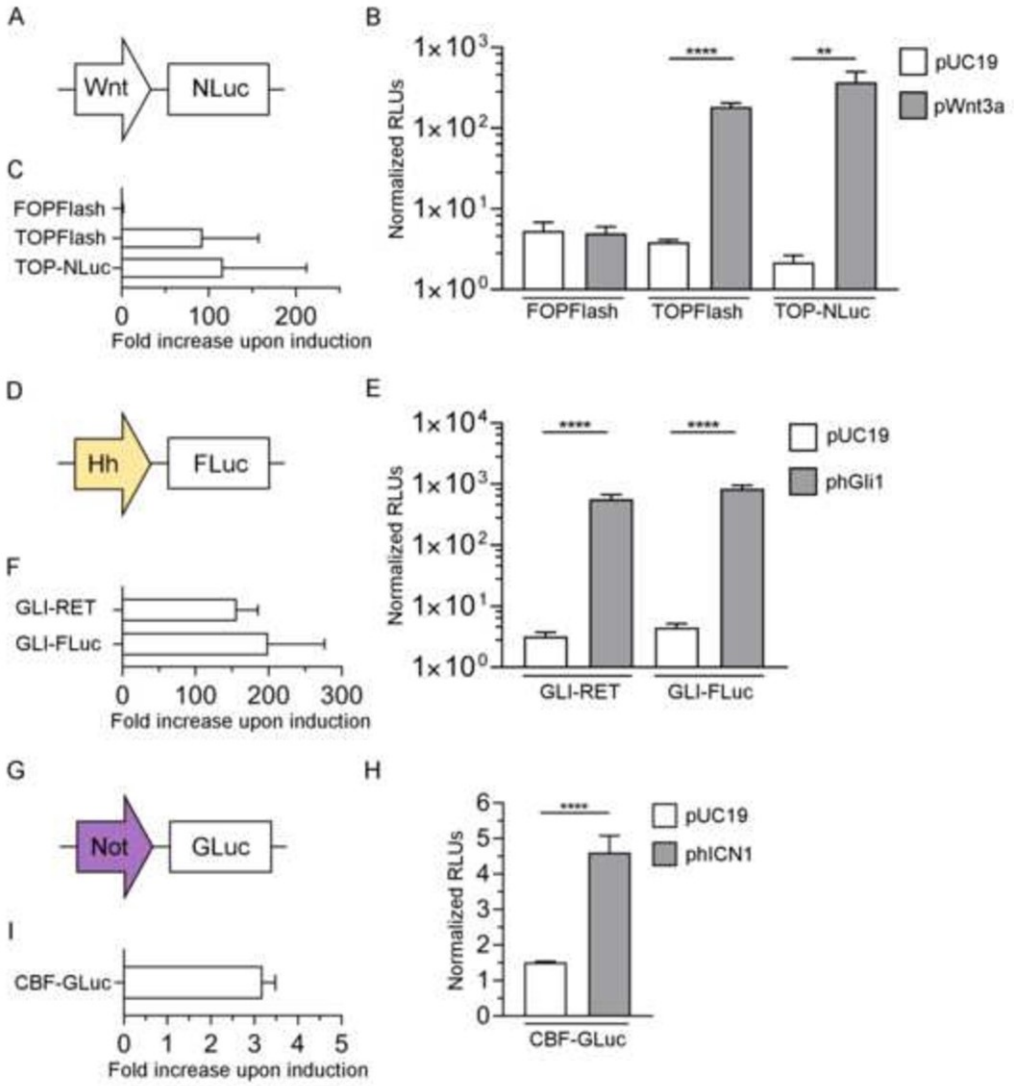


Figure 2

Click here to access/download;Figure;Fig2.tiff

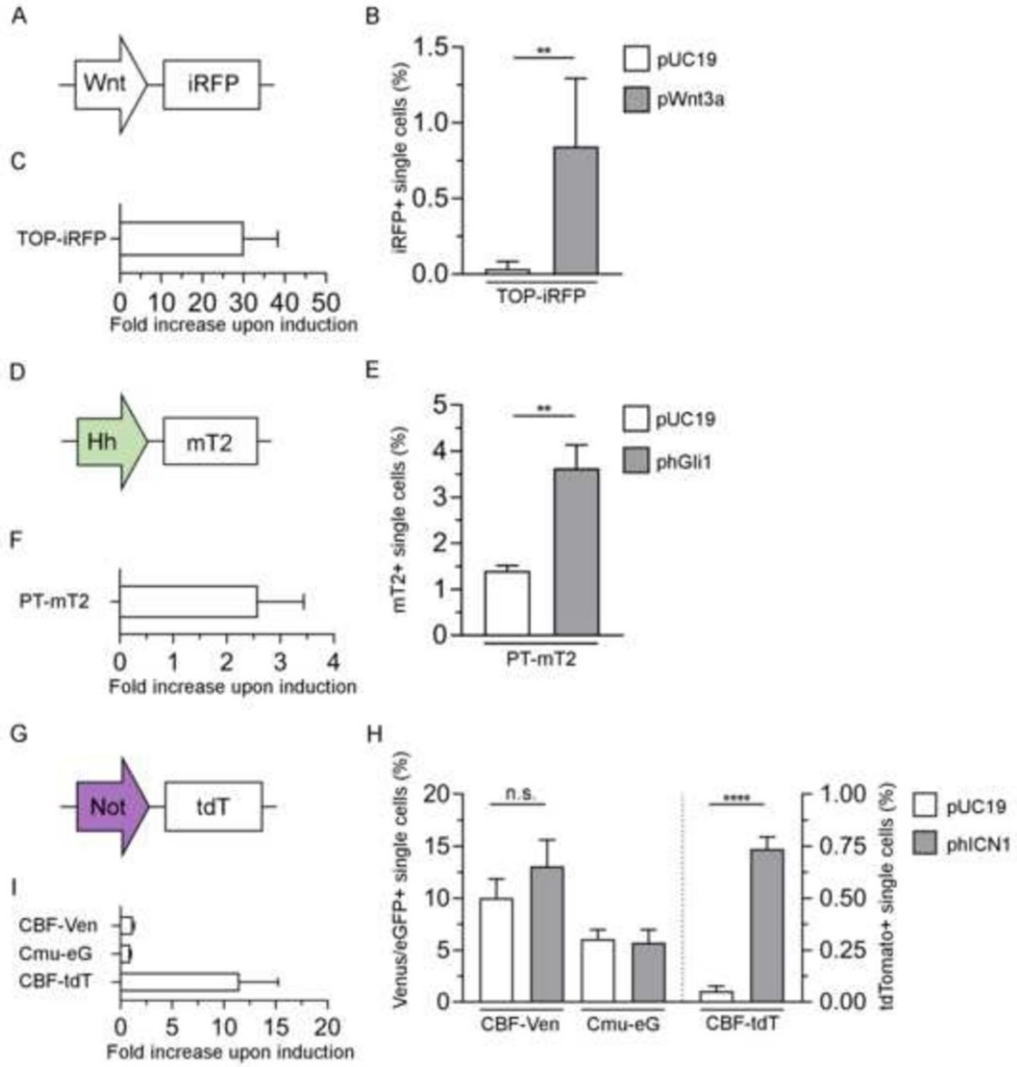


Figure 3

Click here to access/download;Figure;Fig3.tiff

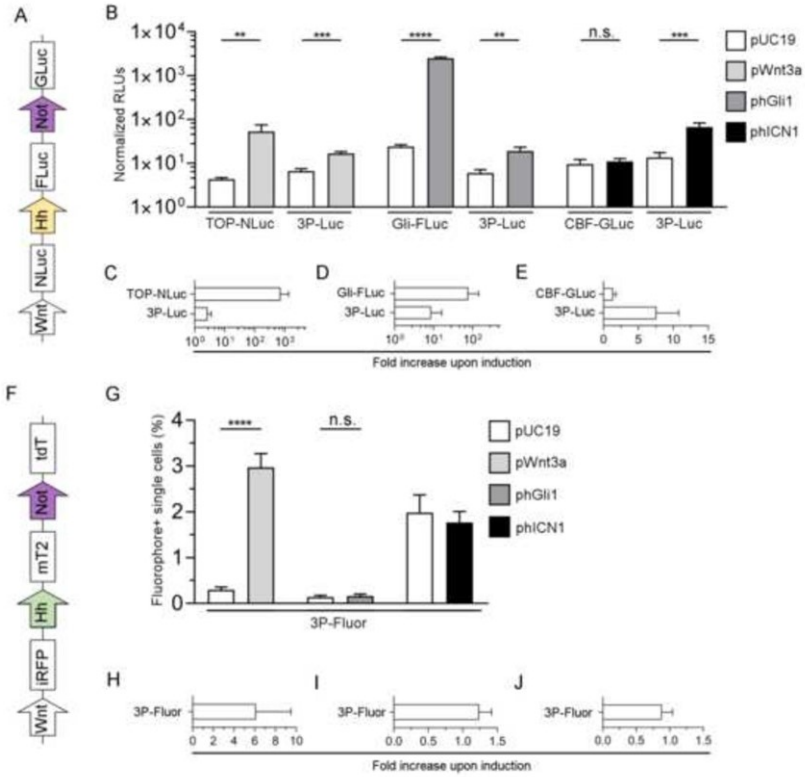
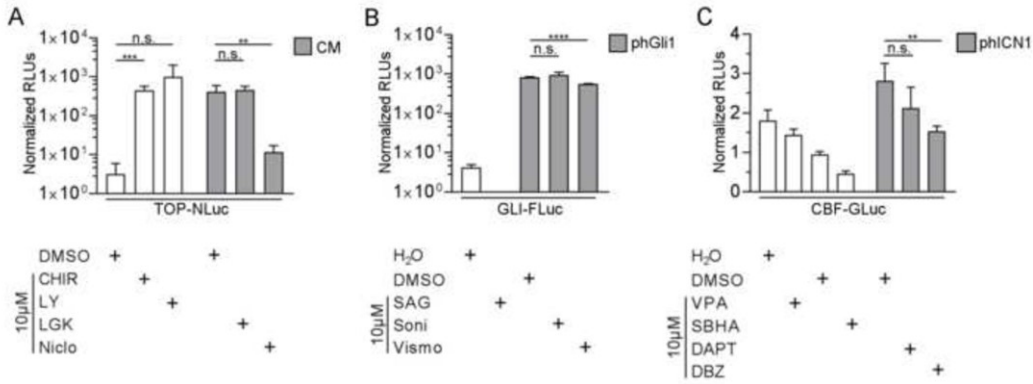


Figure 4

Click here to access/download;Figure;Fig4.tiff



Supporting Information - Compressed/ZIP File Archive



2.2 Multimodal Fluorescence and Bioluminescence Imaging Reveals Transfection Potential of Intratracheally Administered Polyplexes for Breast Cancer Lung Metastases

Antonia Geyer, Alexander Taschauer, Fatih Alioglu, Martina Anton, **Julia Maier**, Elisabeth Drothler, Manuela Simlinger, Sümeyye Yavuz, Haider Sami, and Manfred Ogris. *Human Gene Therapy*, 2017. 28(12):1202-13.

Aims:

Development of single and combined luminescent and fluorescent reporter plasmids for visualizing the activity for the Wnt, Hedgehog and Notch Pathway.

3. Evaluation of smallest iRFP720 signal with significant signal by *in vivo* FLI
4. Signal intensity and gene expression of intratracheally microsprayed LPEI-pDNA (FLuc) by BLI
5. Analysis of the signal and morphological overlap of multimodal imaging with BLI, FLI and MRI

Hypotheses:

6. Tumour growth *in vivo* can be adequately assessed by iRFP720 FLI imaging, including tumour burden, allowing disease tracking before conventional signs of sickness are detectable
7. Intratracheally microsprayed LPEI-pDNA is suitable for transfection of lung tissue
8. Multimodal imaging reveals morphological information, and enables tracking of co-localized FLuc-transfected iRFP720^{+} cells

Contributions:

J.M. was involved in experimental design and experimental work (cell transductions, transduced cell sorting), and co-authored.

Multimodal Fluorescence and Bioluminescence Imaging Reveals Transfection Potential of Intratracheally Administered Polyplexes for Breast Cancer Lung Metastases

Antonia Geyer,[1,†] Alexander Taschauer,[1,†] Fatih Alioglu,[1] Martina Anton,[2] Julia Maier,[1] Elisabeth Drothler,[1] Manuela Simlinger,[1] Sümeyye Yavuz,[1] Haider Sami,[1,*] and Manfred Ogris[1,*]

[1]*Laboratory of MacroMolecular Cancer Therapeutics (MMCT), Center of Pharmaceutical Sciences, Department of Pharmaceutical Chemistry, University of Vienna, Vienna, Austria;* [2]*Institutes of Molecular Immunology and Experimental Oncology, Klinikum rechts der Isar, Technische Universität München, Munich, Germany.*
[†]*These authors contributed equally to this work.*

Downloaded by Vienna University Library from www.liebertpub.com at 08/06/18. For personal use only.

Local delivery of anticancer agents or gene therapeutics to lung tumors can circumvent side effects or accumulation in non-target organs, but accessibility via the alveolar side of the blood–air barrier remains challenging. Polyplexes based on plasmid and linear polyethylenimine (LPEI) transfect healthy lung tissue when applied intravenously (i.v.) in the mouse, but direct delivery into the lungs results in low transfection of lung tissue. Nevertheless, LPEI could offer the potential to transfect lung tumors selectively, if accessible from the alveolar side. This study combined near infrared fluorescent protein 720 (*iRFP720*) and firefly luciferase as reporter genes for detection of tumor lesions and transfection efficiency of LPEI polyplexes, after intratracheal microspraying in mice bearing 4T1 triple negative breast cancer lung metastases. Simultaneous flow cytometric analysis of iRFP720 and enhanced green fluorescent protein expression *in vitro* demonstrated the potential to combine these reporter genes within transfection studies. Polyplex biophysics was characterized by single nanoparticle tracking analysis (NTA) to monitor physical integrity after microspraying *in vitro*. 4T1 cells were transduced with *iRFP720*-encoding lentivirus and evaluated by flow cytometry for stable iRFP720 expression. Growth of 4T1-iRFP720 cells was monitored in Balb/c mice by tomographic near infrared imaging, tissue and tumor morphology by computed tomography and magnetic resonance imaging. In 4T1-iRFP720 tumor-bearing mice, intratracheal administration of luciferase-encoding plasmid DNA by LPEI polyplexes resulted in successful tumor transfection, as revealed by bioluminescence imaging.

Keywords: plasmid DNA, linear polyethylenimine, intratracheal lung delivery, near infrared imaging, bioluminescence imaging, breast cancer

INTRODUCTION

LINEAR POLYETHYLENIMINE (LPEI), albeit having its drawbacks of being a non-biodegradable polymer, still has the advantage of being one of the most efficient transfection reagents, both *in vitro* and *in vivo*. Several clinical trials have already been conducted, and all of them have concentrated on localized delivery, for example for the treatment of superficial bladder cancer (https://clinicaltrials.gov/ct2/show/NCT00595088), but LPEI is also suitable for local gene therapy of the lungs.[1] Pulmonary delivery of macromolecules such as nucleic acids and nanoparticulate formulations is challenging because of the biological barriers such as distribution into the deep lung, overcoming the mucus layer,[2] and rapid clearance from the lungs.[3] The presence of lung tumors, either primary ones or lung metastases arising from breast, colon, and other cancers, changes lung morphology, and such tumors are in principle accessible from the apical site, for example by inhalation or instillation of drug carriers.[4] For PEI-based gene carriers, it was demonstrated that

*Correspondence: Dr. Haider Sami and Prof. Manfred Ogris, Laboratory of MacroMolecular Cancer Therapeutics (MMCT), Center of Pharmaceutical Sciences, Department of Pharmaceutical Chemistry, University of Vienna, Althanstrasse 14, A-1090 Vienna, Austria. E-mail: haider.sami@univie.ac.at; m.ogris@univie.ac.at

© 2017 by Mary Ann Liebert, Inc.
DOI: 10.1089/hum.2017.137

Downloaded by Vienna University Library from www.liebertpub.com at 08/06/18. For personal use only.

lung tumors can be transfected when applied as an aerosol,[5] although this also depends on the tumor type and potential restricted access.[6] In order to optimize application routes and delivery agents, optical *in vivo* imaging can help to identify bottlenecks, with respect to both nucleic acid delivery and transgene expression. To this end, near infrared (NIR) fluorescent dyes have been used directly attached to either the nucleic acid or to the carrier system to monitor the biodistribution and potential redistribution dynamics.[3,7–9] When using suitable imaging systems, both biodistribution and transgene expression can be monitored by using bioluminescence imaging (BLI) to track luciferase reporter gene expression.[7] On the other hand, simultaneous tracking of both tumor growth and transfection requires multiple imaging modalities. BLI of tumor cells, stably transduced with luciferase reporter, is one of the most sensitive methods, allowing the detection of <100 luciferase positive cells.[10] To allow three-dimensional (3D) imaging of the BLI signal, a method based on wavelength-dependent absorption of luciferase emitted light was developed, which together with the reconstruction of a virtual surface enables tomographic analysis.[11] In combination with morphological imaging, for example computed tomography (CT) and suitable CT contrast agents, this method enables precise allocation of tumor nodules to organ structures (Gehrig *et al*., in preparation). As an alternative to luciferase labeling, fluorescent reporter gene products can also be used. However, *in vivo* tissue absorption poses challenges for their usage. For instance, fluorescent proteins emitting in the green–yellow–orange part of the spectrum are most suited for labeling of only superficial tumors, for example subcutaneously (s.c.) implanted tumors.[12] More recently, the Verkhusha lab developed a protein series, termed iRFPs, with strong far-red and NIR-shifted excitation and emission maxima.[13] Due to their efficient tissue penetration, fluorescence imaging tomography (FLIT) for 3D-signal reconstruction is feasible.

The present study combines NIR fluorescent protein *iRFP720* and firefly luciferase–based reporter genes for detection of tumor lesions and monitoring *in vivo* transfection efficiency of LPEI polyplexes (after microspray-based intratracheal administration), respectively. Influence of microspraying on size and *in vitro* transfection efficiency of LPEI polyplexes was investigated by nanoparticle tracking analysis and luciferase reporter gene assay, respectively. LPEI polyplexes were intratracheally administered in mice bearing lung metastases of syngeneic 4T1 breast cancer cells, and their transfection profile was investigated by BLI in combination with fluorescence imaging–based visualization of 4T1-iRFP720 tumors.

MATERIALS AND METHODS

Transfection and transduction reagents

The CpG-free plasmid *pCpG-hCMV-EF1α-LucSH* expresses luciferase-bleomycin fusion protein under the control of the human elongation factor alpha promoter.[8] The iRFP720-encoding plasmid *piRFP720-N1* was a gift from Vladislav Verkhusha (Addgene plasmid # 45461). *pEGFP-N1* was bought from Clontech (now TaKaRa Bio USA, Inc., Mountain View, CA). Plasmids were expanded using either *Escherichia coli* DH5α (pEGFP-N1 based) or GT115 (pCpG based), as described elsewhere,[8] and purified using commercial kits (GeneJET Plasmid Maxiprep Kit; Thermo Fisher Scientific, Schwerte, Germany; and NucleoBond® PC 10,000; Macherey-Nagel, Dueren, Germany). LPEI (10 kDa) was synthesized and used as described earlier.[14] The VSV-G pseudotyped, self-inactivating lentivirus expresses *iRFP720* under the control of the constitutively active phosphoglycerol (PGK) promoter. The *iRFP720* cDNA was excised from *piRFP720-N1* by XbaI and inserted into pHIV-7 carrying the PGK promoter. Lentiviral vector production was performed in 293T cells, as described earlier.[15]

Cell culture and transductions

4T1 murine triple negative breast cancer cells (CRL-2539) and human lung adenocarcinoma A549 cells (CRM-CCL-185) were obtained from ATCC (LGC Standards GmbH, Wesel, Germany) and cultured in RPMI1640 (supplemented with 10% fetal bovine serum, L-glutamine, and antibiotics). 4T1 cells were lentivirally transduced with polybrene, as described earlier,[15] and sorted for iRFP720 expression on a FACS Aria III (BD Biosciences, San Jose, CA) using 633 nm excitation and a 780/60 bandpass emission filter to obtain 4T1-iRFP720 cells. 4T1-Luc cells were bought from PerkinElmer (Waltham, MA).

Polyplex synthesis

All polyplex solutions were prepared by flash pipetting based on the protocol by Rödl *et al*.[16] For *in vitro* transfection experiments, polyplexes were prepared at different N/P ratios (six or nine) at pDNA concentration of 20 μg/mL (for transfection experiment with *piRFP720-N1* and *pEGFP-N1*) or 267 μg/mL (for microspraying of polyplexes *in vitro*) in HEPES-buffered glucose (HBG buffer; 20 mM HEPES, 5% [w/V] glucose, pH 7.4, sterile filtered). Polyplexes for *in vivo* application were generated at a N/P of 9 at a final pDNA concentration of 267 μg/mL in HBG buffer.

Downloaded by Vienna University Library from www.liebertpub.com at 08/06/18. For personal use only.

In vitro transfections with piRFP720-N1 and pEGFP-N1

A549 cells (10,000 cells/well) were seeded in 200 μL of medium onto a 96-well plate. After 24 h, the medium was replaced with 80 μL of RPMI1640 (without supplements) and 20 μL of of polyplex solution (containing 400 ng of *piRFP720-N1*, or 400 ng of *pEGFP-N1*, or a mixture of 200 ng of *piRFP720-N1* and 200 ng of *pEGFP-N1* complexed at a N/P of 9) was added per well. After 4 h of treatment with polyplexes, 100 μL of complete medium was added. For flow cytometric analysis, cells were detached after 24 h total transfection time using 30 μL of TrypLE (Thermo Fisher Scientific) and then re-suspended in 130 μL of phosphate-buffered saline (PBS; Dulbecco's PBS; Sigma–Aldrich, Darmstadt, Germany). DAPI (2-[4-amidinophenyl]-6-indolecarbamidine dihydrochloride; Sigma–Aldrich) was used for distinguishing between live and dead cells at a final concentration of 1 μg/mL. One hundred microliters of each cell suspension was analyzed using a MacsQuant Analyzer 10 flow cytometer (Miltenyi Biotec GmbH, Bergisch Gladbach, Germany). During flow cytometry analysis, cells were permanently cooled at 4°C using a Inheco CPAC unit (INHECO, Planegg, Germany). DAPI was excited with 405 nm, and emission was detected with a 450/50 nm band pass filter. Enhanced green fluorescent protein (EGFP) was excited with 488 nm and detected with a 525/50 nm band pass filter. iRFP720 was excited with 635 nm and detected with a 655–730 nm band pass filter. For evaluating expression levels of EGFP and iRFP720, dead cells were excluded.

Microspraying of polyplexes *in vitro*: biophysical characterization and cell transfection

After polyplex preparation, 75 μL of polyplex solution (generated at N/P ratios of 6 and 9) was microsprayed into 1.5 mL centrifuge tubes using a MicroSprayer®/Syringe Assembly (MSA-250-M; Penn-Century, Inc., Wyndmoor, PA). For evaluating the influence of microspraying on nanoparticle properties, microsprayed and non-microsprayed polyplexes were investigated for *in vitro* transfection efficiency in 4T1 and A549 cells by firefly luciferase assay and for size by nanoparticle tracking analysis (NTA; NanoSight NS500, Malvern, United Kingdom). Size evaluation of microsprayed and non-microsprayed polyplexes was done by NTA using a procedure described earlier.[14]

Within *in vitro* transfection assay (based on firefly luciferase reporter gene), A549 and 4T1 cells (10,000 cells/well) were seeded onto a 96-well plate. After 24 h, the medium was replaced with RPMI1640 (without supplements), and 10 μL of polyplex solution (containing 200 ng of *pCpG-hCMV-EF1α-LucSH*, at N/Ps of 6 and 9) was added per well. After 4 h of treatment with polyplexes, 100 μL of RPMI1640 (with supplements) was added. After 24 h of addition of polyplexes, supernatant was removed, and cells were lysed using 30 μL of passive lysis buffer (Promega, Mannheim, Germany). For evaluating luciferase expression, 100 μL of homemade D-luciferin solution (based on sodium salt of luciferin; Promega) was added to 10 μL of cell lysate using the Tecan Infinite M200Pro equipped with auto-injectors, and luminescence (integration time: 10,000 ms; waiting time: 2 s) was measured; 1 nanogram of recombinant luciferase protein corresponds to 10^6 light units. Relative light unit values were normalized based on total protein amount per well. Protein quantification was done for rest of the cell lysate using a BCA assay kit (Pierce; Thermo Fisher Scientific) following the manufacturer's instructions.

Tumor models, intratracheal application

Mice (Balb/cJRj, female; purchased from Janvier Labs, Le Genest-Saint-Isle, France) were housed in individually ventilated cages (Type 2L; Tecniplast, Hohenpeißenberg, Germany) under specified pathogen-free conditions and allowed to acclimatize for at least 10 days prior to experiments. Autoclaved water and food (standard rodent diet; SSniff, Soest, Germany) were provided *ad libitum*. Low fluorescent diet (AIN-76A; Brogaarden Korn & Foder ApS, Lynge, Denmark) was used for at least 7 days prior to the experiments. All procedures were approved by local ethics committee and are in accordance with the Austrian law for the protection of animals and the EU directive 2010/63/EU for animal experiments.

For 4T1-Luc tumor model generation, 4T1-Luc cells were harvested with TrypLE (Thermo Fisher Scientific), washed, and re-suspended in PBS; 10^5 cells (counted by MacsQuant Analyzer 10 flow cytometer) in 100 μL of PBS were injected into the lateral tail vein of mice ($n=3$). For 4T1-iRFP720 tumor model generation, 4T1-iRFP720 cells were harvested with TrypLE, washed, and re-suspended in PBS; 10^5 cells (counted by MacsQuant Analyzer 10 flow cytometer) in 100 μL of PBS were injected into the lateral tail vein of mice ($n=4$). For tumor model characterization by FLI, mice were imaged on days 5, 7, and 10 post implantation by epifluorescence imaging and on day 14 post implantation by FLIT, as described below.

For intratracheal application of polyplexes, 75 μL of polyplex solution (a N/P 9 of in HBG, containing 20 μg of plasmid) was applied using the MicroSprayer®/Syringe Assembly (MSA-250-M; Penn-Century, Inc.), as recently described.[3] On day 8 post

implantation of 4T1-iRFP720 cells, LPEI polyplexes (at N/P of 9) were intratracheally administered ($n=3$). In brief, ketamin/xylazin (80 mg/kg and 5 mg/kg, respectively) anesthetized mice were placed on an intubation platform made in-house and intubated with a 18G 1″ catheter (BBraun, Melsungen, Germany). Polyplex solution was administered intratracheally right above the tracheal bifurcation, ensuring equal delivery into both lungs. Gooseneck light guides (white LED) were placed externally on the trachea (ventral side) so that the transmitted light ensured proper placement of the tube. On day 9 post implantation (24 h transfection), the mice were imaged first by FLI, followed by BLI and magnetic resonance imaging (MRI), as described below.

Downloaded by Vienna University Library from www.liebertpub.com at 08/06/18. For personal use only.

In vivo imaging

Optical imaging and CT was carried out on an IVIS Spectrum CT imaging system (PerkinElmer). Mice were shaved ventrally and dorsally to improve the signal quality for fluorescence and bioluminescence measurements. For FLIT imaging, mice received intraperitoneally 300 μl Scanlux (Iopamidol, Sanochemia, Vienna; 300 mg iodine/mL) in 5% glucose (w/v) at a ratio of 1:1.5. Fluorescence imaging was performed in epifluorescence mode, as described earlier,[3] with automated exposure time using the following excitation (Ex)/emission (Em) filter combination (excitation: 30 nm bandwidth; emission: 20 nm bandwidth): Ex: 640 nm with Em: 680 nm, 700 nm, 720 nm, 740 nm, 760 nm; and Ex: 675 nm with Em: 720 nm, 740 nm, 760 nm, 780 nm, 800 nm. All animals were imaged along with a control animal, and spectral unmixing was done for each image separately. For 3D measurement, mice were first scanned by CT in low resolution and afterwards measured for fluorescence emission in transillumination mode, according to the technique described previously.[3] Mice were anesthetized by 1.5–2% isoflurane in oxygen, placed ventral up on the grid plate, and fluorescence images were acquired at Ex: 675 nm (30 nm BW) and Em: 720 nm (20 nm BW). For BLI, luciferin (D-luciferin potassium salt VivoTrace™; Intrace Medical, Lausanne, Switzerland; dissolved in PBS at 30 mg/mL) was injected s.c. at a dose of 120 mg/kg. Bioluminescence signal was subsequently collected for 45 min at an exposure of 5 min in stage B to gain maximum signals after 20–40 min.

For MRI analysis, anesthetized animals were imaged by an Aspect Imaging™ M3 compact MRI system (AspectImaging, Shoham, Israel). T2 weighted images were acquired using a 50 mm × 30 mm body coil (time to repetition [TR]: 3,250 ms; time to echo [TE]: 63.47 ms; number of slices: 15; slice thickness: 1 mm; number of excitations: 7; slice orientation: coronal; center of slice position: 0; flip angle: 90°; scan time: 5 min 46 s). Analysis was performed by a veterinary clinical radiologist using VivoQuant™ (Invicro, Boston, MA).

Histology

After imaging, mice were sacrificed by an overdose of anesthesia and intubated. Ten percent formalin (4% formaldehyde in HBS, prepared using paraformaldehyde; Sigma–Aldrich) was instilled, as per a reported method.[17] Briefly, the intratracheal tube was connected to a bottle (filled with 10% formalin) at a height of 25 cm, and the lungs were instilled utilizing the pressure of the fluid over a time period of 5 min. The lungs were subsequently fixed in formalin for 22 h, dehydrated by gradient ethanol treatment (70%, 96%, and 100%), cleared by Xylene (Sigma–Aldrich), and embedded using Paraplast® (Sigma–Aldrich). After sectioning, the tissues were rehydrated in a descending ethanol row and stained using hematoxylin according to Harris (Carl Roth GmbH + Co. KG, Karlsruhe, Germany) and Eosin Y (Sigma–Aldrich; 3 min hematoxylin, 1 s acidified ethanol, 20 s NH_4OH, 10 min eosin) for morphological analysis.

Immunohistochemistry

Sections were boiled for at least 20 min in pH 8 EDTA-Tween buffer (1 mM of EDTA +0.05% Tween R 20 in PBS) in a water bath. EDTA-Tween buffer was prepared by mixing 1 mM of EDTA (Sigma–Aldrich) with 0.05% Tween® 20 (Sigma–Aldrich) in PBS, and the pH was adjusted to 8. The sections were allowed to cool for 30 min at room temperature, and endogenous peroxidase was blocked using 3% H_2O_2 (v/v) in PBS. Unspecific binding sites were blocked using normal rabbit serum (Vectastain ABC Kit; Vector Laboratories, Burlingame, CA) for 30 min. The polyclonal goat anti-firefly luciferase antibody (Abcam, Cambridge, United Kingdom) was diluted in 2% bovine serum albumin (Sigma–Aldrich) in PBS to a final concentration of 1 μg/mL, and the sections were treated overnight at 4°C. In parallel, control sections were incubated with an equivalent amount of buffer for secondary antibody control. After washing in PBS, the biotinylated rabbit anti-goat antibody (Vectastain ABC Kit; Vector Laboratories) was applied for 30 min and subsequently treated with ABC reagent of the same kit for 30 min. The sections were then treated with 0.5% Triton® X-100 (Sigma–Aldrich) in PBS followed by incubation in a 3,3-diaminobenzidine tetrahydrochloride (DAB; Sigma–Aldrich) substrate solution (10 tablets in 250 mL of PBS +1.25 mL of Triton® X-100) for 7 min. Counterstaining of the sections was done using hematoxylin.

Downloaded by Vienna University Library from www.liebertpub.com at 08/06/18. For personal use only.

RESULTS

The most NIR-shifted protein, namely iRFP720, with excitation/emission maxima of 710/760 nm, was selected for transfection studies. Within *in vitro* transfection studies, as can be seen in Fig. 1A and B, *iRFP720* plasmid showed similar expression profile when compared to *EGFP*-encoding plasmid. Both plasmids share the same backbone (N1) and promoter (CMV). There was no fluorescence overspill between the two fluorophores when using the 488 nm laser line for excitation and a 525–550 nm bandpass filter for EGFP, and 635 nm laser excitation and a 655–730 nm bandpass filter for iRFP720. Within co-transfection experiment (Fig. 1C), a high level of transgene expression for both *iRFP720* and *EGFP* reporter genes was observed, with good signal correlation. However, low EGFP-expressing cells were negative for iRFP720 expression. Further, the *iRFP720* cDNA was cloned into a pHIV7/SF-GFP-derived plasmid, replacing *EGFP* and the SF-promoter, and VSV-G pseudotyped self-inactivating (SIN) lentivirus was produced in HEK-293T cells. This lentivirus was used to transduce 4T1 cells stably. After cell sorting, 85–94% cells remained positive for iRFP720 expression (Supplementary Fig. S1; Supplementary Data are available online at www.liebertpub.com/hum).

Next, the influence of the microspraying process on biophysical properties (Fig. 2) and transfection efficiency of LPEI polyplexes (Fig. 3) was evaluated. With an increased N/P ratio (nine vs. six), particles appeared significantly smaller. After microspraying of polyplexes, both broadness of the size distribution and average size increased due to probable aggregation, thereby resulting in a decrease in particle concentration, as shown in Fig. 2A and B, respectively. Nevertheless, the fraction of particles up to 200 nm in size decreased only slightly (Fig. 2B). When comparing the *in vitro* transfection efficiency of native to microsprayed particles, A549 cells showed higher transfection than 4T1 cells with a N/P of 9, showing highest transfection efficiency in both cell types (Fig. 3). Microspraying of polyplexes affects transfection efficiency slightly in the case of A549 (at N/P of 9) and more significantly in the case of 4T1 cells for both treatment ratios (*i.e.*, at N/P of 6 and at N/P of 9).

Further on, the 4T1-iRFP720 disseminated tumor model (Fig. 4) was established, and it was compared to the already established 4T1-Luc model (Supplementary Fig. S2). iRFP720 fluorescence signal of 4T1-iRFP720 cell suspension was acquired with the imaging system, and optimal signal intensity was achieved with Ex 675/Em 720–740 nm as shown in Fig. 4A. In control experiments, the validity and high sensitivity of the 4T1-luc model could be confirmed. When 10^5 4T1-Luc cells were injected i.v. into Balb/c mice, a significant BLI signal (10-fold above background) was measured (Supplementary Fig. S2A), which further increased by three log units on day 8 after tumor cell injection (Supplementary Fig. S2A). Because of this high BLI signal, DLIT measurement and 3D signal reconstruction was possible. In the case of the 4T1-iRFP720 model, as expected, 4T1-iRFP720 cells resulted in a considerably lower signal/noise ratio when measured by epifluorescence imaging. Fluorescence signals clearly distinguishable from background appeared earliest at day 5 post injection (Supplementary Fig. S3), and required the application of the background unmixing technique.[3]

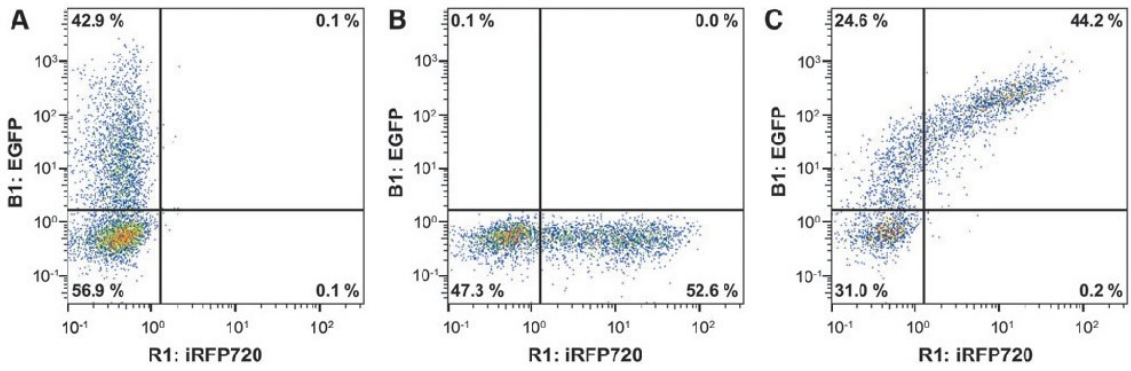


Figure 1. Combination of near infrared (NIR)-emitting *iRFP720* reporter gene with enhanced green fluorescent protein (*EGFP*) reporters for transient transfection studies. Cells were transfected with 400 ng of *pEGFP-N1* **(A)**, 400 ng of *piRFP720* **(B)**, or with a mixture of 200 ng of each plasmid **(C)** using linear polyethylenimine (LPEI), as described in the Materials and Methods. Live cells were gated after addition of 2-(4-amidinophenyl)-6-indolecarbamidine dihydrochloride (DAPI) and represented as density plots showing iRFP720 fluorescence on the *x*-axis and EGFP fluorescence on the *y*-axis.

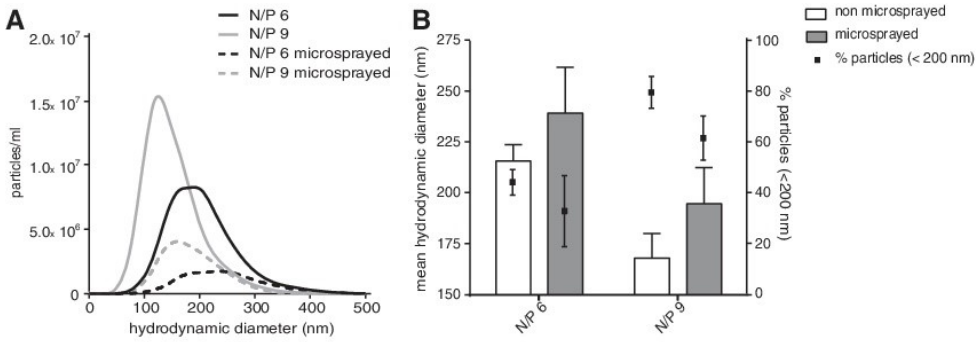


Figure 2. Influence of microspraying on biophysical properties of LPEI polyplexes. Polyplexes (N/P of 6 and N/P of 9) were generated in HEPES-buffered glucose (HBG) buffer at a final pDNA concentration of 267 μg/mL and underwent microspraying with a PennCentury microsprayer. They were then analyzed by nanoparticle tracking analysis (as described in the Materials and Methods) to plot particle size distribution **(A)**, and mean hydrodynamic diameter and percentage of particles within a range of up to 200 nm **(B)**. Data shown are representative of three different experiments.

Downloaded by Vienna University Library from www.liebertpub.com at 08/06/18. For personal use only.

With late-stage tumors (day 14 after injection), 3D signal analysis (FLIT) together with CT and contrast agent was feasible (4B). Distinct tumor areas could be identified in the lungs. Pathological evaluation of mouse lungs (21 days post tumor implantation) revealed macroscopic multiple pale nodules up to 2 mm in diameter (Fig. 4C). To examine the microanatomy of tumors and their invasion pattern, first the lung fixation technique was optimized to preserve the organ structure (Supplementary Fig. S4). Simply excising the lungs, followed by the standard fixation and embedding procedure, resulted in collapsed lung tissue without the possibility of studying bronchio-alveolar structure. Optimal structure conservation was achieved when instilling lungs of dead animals with formalin solution prior to formalin-fixed paraffin-embedded processing (Supplementary Fig. S4A and C). Hence, this fixation technology was also applied to tumor-bearing animals. 4T1-iRFP720 tumors exhibited a multifocal nodular-like appearance, with invasive parenchymal growth pattern and oligofocal single cell infiltrates (Fig. 4D and E), responsible for the macroscopic nodular structure. Notably, the tumor cells were located in the alveolar septs and could also be detected inside the alveolar space (Fig. 4E). Inside the compact tumor formations, the vascularization consisted only of capillaries, as larger vessels could not be detected.

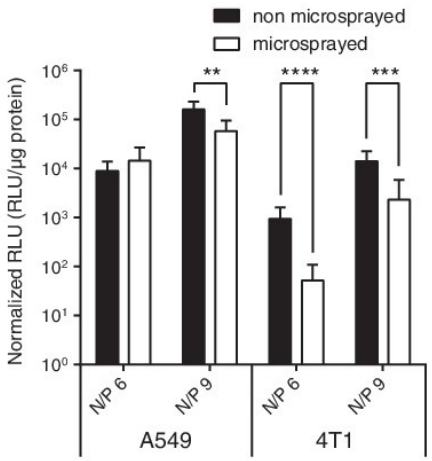


Figure 3. Influence of microspraying on *in vitro* transfection efficiency. A549 and 4T1 cells (10,000 cells/well) were treated with *pCpG-hCMV-EF1a*-LucSH-based polyplexes at a concentration of 200 ng of pDNA/well. The polyplex solution was tested before and after microspraying. Twenty-four hours later, luciferase expression was evaluated by luciferase assay protocol. Relative light unit (RLU) values were normalized based on total protein amount per well. Normalized RLU values are shown as mean values ($n=9$; error bars indicate standard deviation; *$p \leq 0.05$; **$p \leq 0.01$; ***$p \leq 0.001$; ****$p \leq 0.0001$; U test [Mann-Whitney]).

Furthermore, the transfection pattern of LPEI polyplexes in 4T1-iRFP720 tumor-bearing mice was investigated (Fig. 5). In all experiments, N/P 9 polyplexes were used due to their higher stability (Fig. 2) and reliability of *in vivo* transfection.[14] First, the tumor load and its spatial localization were evaluated using fluorescence imaging and spectral unmixing (Fig. 5A–C). Two animals showed highest signal intensities in the area of the right lung. In one animal, the overall signal intensity was less. However, the main signal was located in the left area of the lungs, with a less intense signal in the right lung (Fig. 5B). After spatially localizing the tumor via FLI signal, BLI imaging was performed on these animals to investigate the transfection pattern. Polyplex-treated animals exhibited significant BLI signals (Fig. 5D–F) when compared to control animals (data

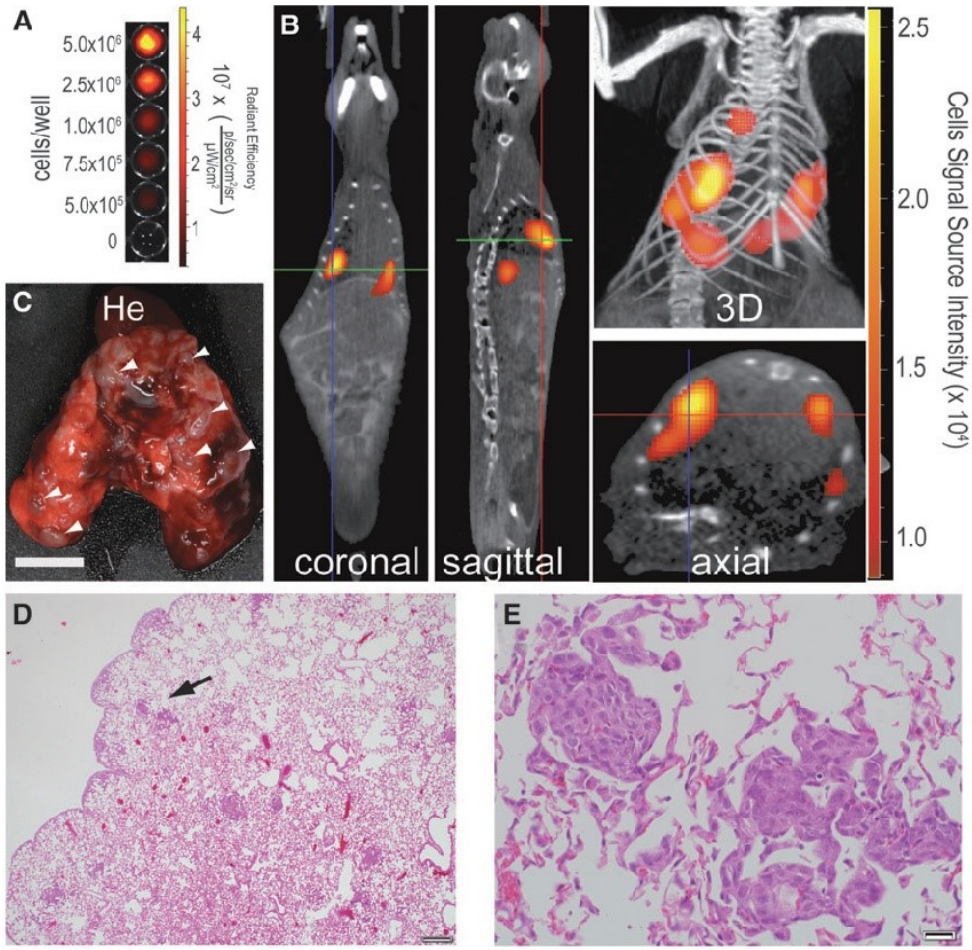


Figure 4. Characterization of 4T1-iRFP720 tumor model in Balb/c mice. **(A)** Epifluorescence imaging of 4T1-iRFP720 cell suspension (Ex 675 nm, Em 720 nm) on a 96-well plate, 5×10^5–5×10^6 cells/well. **(B)** Fluorescence imaging tomography (FLIT)/computed tomography (CT) analysis of 4T1-iRFP720 tumors 14 days after intravenous (i.v.) injection of 10^5 cells. Animals received iopamidol contrast agent i.v. prior to imaging. The CT picture (grayscale) is overlaid with the FLIT signal (color coded). Colored lines denote the position of the optical section in coronal (*red*), axial (*green*), or sagittal (*violet*) view. **(C)** Explanted lung/heart 21 days after tumor cell injection. He denotes heart. *White arrowheads* point at tumor nodules (pale appearance). Scale bar: 5 mm. **(D** and **E)** Instillation fixed, hematoxylin and eosin–stained tumor-infiltrated lungs 9 days after tumor cell injection. Scale bar: 200 μm **(D)** and 20 μm **(E)**. *Arrow* in **(D)** indicates the magnified area in **(E)**.

Downloaded by Vienna University Library from www.liebertpub.com at 08/06/18. For personal use only.

not shown). However, the BLI signals were low in signal intensity. Importantly, the localization of the BLI source not only matched the side of the FLI signal, but also partially overlapped with the fluorescence signals. Using MRI and histological analysis, tumor structures within the same localization could also be morphologically identified. Histological examination (Supplementary Fig. S5) revealed tumor nodules in all lobes. Interestingly, in the case of the animal with low FLI signal (Fig. 5B), no diffuse morphological alterations of the structure in MRI were seen, but a nodular structure of high echogenicity in the dorsal portion of the right caudal lobe, surrounded by finger-like structures of medium echogenicity, were observed only inside the left lung (Fig. 5H). The MRI of the control animal showed that all thoracic structures were of physiological appearance (i.e., no structures with high echogenicity; Fig. 5I). Histologically, tumors of this particular animal were also found in all lobes but with an area of presumably dystelectatic lung tissue inside the left lobe. For validation of LPEI polyplex-mediated luciferase gene delivery to 4T1-iRFP720 tumor, immunohistochemical staining for firefly luciferase protein of the tumor-bearing lungs was performed for both polyplex-transfected and untransfected mice (Supplementary Fig. S6). Immunohistochemical analysis revealed a pale but distinct homogenous

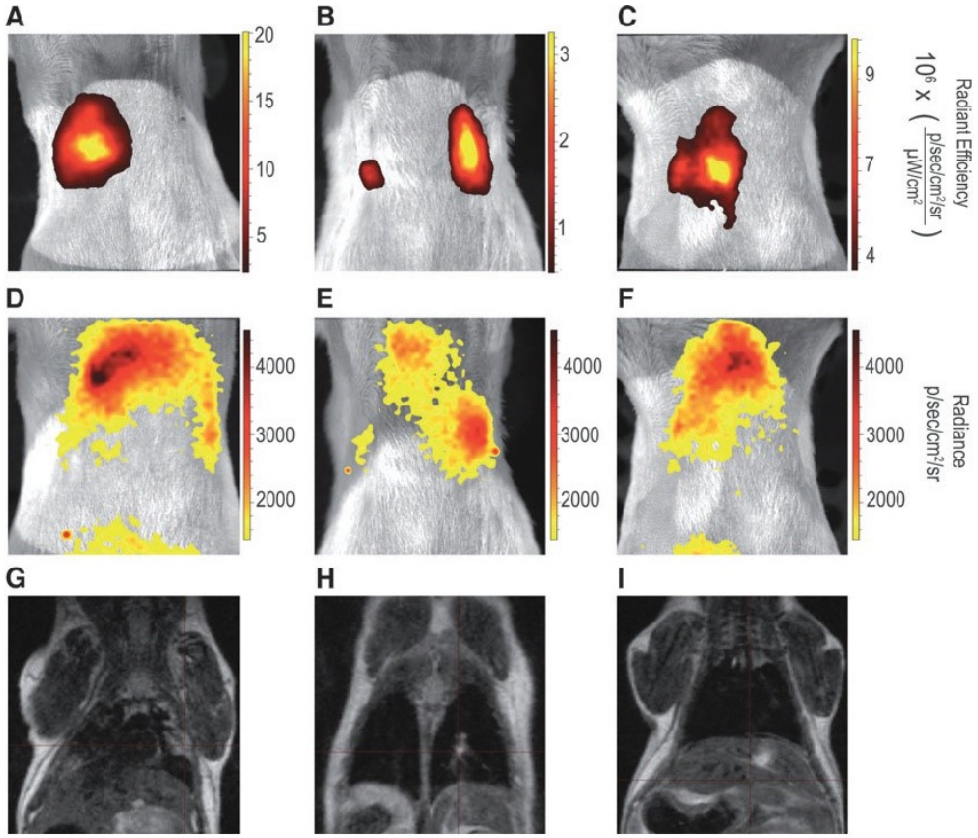


Figure 5. Transfection of 4T1-iRFP720 tumor after intratracheal instillation. Balb/c mice received 10^5 4T1-iRFP720 cells i.v. On day 8 after tumor cell injection, LPEI polyplexes (N/P 9) were applied intratracheally, and on day 9 (24 h transfection), mice were imaged by FLIT, bioluminescence imaging (BLI), and magnetic resonance imaging (MRI), as described in Materials and Methods. **(A–C)** 4T1-iRFP720 fluorescence signal (color coded, after spectral unmixing) is overlaid on a reflected light picture (B/W). **(D–F)** BLI signal (color coded) overlaid on a reflected light picture (B/W). **(G** and **H)** MRI picture (T2 weighted) of tumor-bearing animals. **(I)** MRI (T2) of healthy control animal. Note: data from the same animal shown in A, D, and G, in B, E, and H, and in C and F, respectively. $n=3$ for FLI/BLI imaging; $n=2$ for MRI imaging.

Downloaded by Vienna University Library from www.liebertpub.com at 08/06/18. For personal use only.

staining pattern similar to stably transfected control tumor (4T1-Luc)-bearing lungs expressing luciferase (data not shown), thereby indicating the presence of luciferase protein in polyplex-transfected tumor mice (Supplementary Fig. S6).

DISCUSSION

Tracking *in vivo* transgene expression with optical imaging via BLI of luciferase activity is a well-established method. Here, luciferases with a red-shifted emission spectrum offer optimal signal for deeper-seated signals, as there is an inverse correlation between tissue absorption and wavelength of the emitted light.[18] Also, for fluorescence imaging *in vivo*, the use of fluorophores emitting in the green to orange spectrum is precluded due to absorption at a lower wavelength (*e.g.*, by hemoglobin and skin melanin). An absorption minimum is possible within the so-called biological window, ranging from approximately 650 to 900 nm, enabling preclinical and clinical use of fluorophores emitting within this range.[19,20] The fluorescent spectrum of recombinant proteins has been considerably extended into the far red and NIR, with development of a whole series of NIR-shifted protein variants with high stability and quantum yield.[13] With iRFP720 being the most red-shifted variant, this reporter protein was utilized to label different cancer lines.

First, cells were co-transfected with *EGFP*-encoding plasmid with a similar backbone (N1 based). Separate excitation with 488 and 635 nm laser lines, respectively, did not give any spectral

Downloaded by Vienna University Library from www.liebertpub.com at 08/06/18. For personal use only.

overlap and hence need for signal compensation. In co-transfection, a good signal correlation was observed in cells with high levels of transgene expression. Notably, cells exhibiting low EGFP signals were negative for iRFP. This could be due to lower quantum yields of iRFP720 (in contrast to EGFP), as iRFP720 is excited only with approximately 50% efficiency when using the 635 nm laser. Nevertheless, the signal observed was specific and significant.

Next, a lentiviral vector was generated for efficient gene marking of 4T1 cells with *iRFP720*, and positive cells were selected by sorting. The 4T1 murine triple-negative breast cancer model syngeneic in Balb/c mice resembles several aspects of the human disease situation, such as receptor status and metastasis formation. Both orthotopically implanted tumors and direct i.v. injected tumor cells form intravascular tumors in the lungs,[21] and there is no significant difference in gene expression pattern between lung metastases derived from orthotopically implanted 4T1 cells when compared to lesions induced by i.v. injected cells.[22]

The study also directly compared the 4T1-iRFP720 cells to the commercialized 4T1-Luc cells in terms of growth kinetics and sensitivity of tumor detection (Supplementary Fig. S2). It is important to note that 4T1-luc cells grew considerably faster, with mice turning moribund already 6–7 days after injection of 10^5 cells (heavy breathing, weight loss >10%), with a notably higher sensitivity. In contrast, 4T1-iRFP720-injected mice remained clinically unaffected for 14–19 days post implantation, also when injecting 10^6 instead of 10^5 cells (data not shown).

To obtain detailed information on the tumor micromorphology, the lung fixation procedure had to be optimized, as shown in Supplementary Fig. S4. In the case of the lungs, the penetration of the diaphragm usually leads to lung collapse. Hence, *in situ* fixation by whole-body perfusion, instillation, and other methods can be applied.[17] Using formalin instillation fixation, based on a constant fluid pressure, very good preservation of alveolar structures was achieved. The histological studies revealed that 4T1-iRFP720 cells form small multifocal parenchymal nodular or nodular-like tumors, with single-cell infiltrates growing within the alveolar sept architecture, as well as occasional peribronchiolar colonialization with slight side preferences, when injected i.v. (Fig. 4D and Supplementary Fig. S5). This is in contrast to the pattern observed with 4T1-Luc, where i.v.-injected cells led to tumor infiltrated parenchyma without detectable isolated tumor nodules.[22] Interestingly, FLI imaging nevertheless showed a good sensitivity, as it was able to determine a significant tumor load.

These findings could not be entirely verified using morphological analysis with the MRI. In one mouse (Fig. 5G), diffuse infiltration of both sides of the lungs was observed, matching the histological findings (Supplementary Fig. S5A), whereas FLI only showed a signal in the right lung area. In contrast, the second mouse (Fig. 5B) showed FLI signals in both lungs, as also seen in histology, but with MRI (Fig. 5H), only a high echogenicity structure in the right lung was observed. Moreover, this structure could also be morphologically related to structures other than cancerous tissue. For that reason, it is important to consider that 2D imaging cannot be used for fine morphological analysis to determine the exact location of the signal, and in the case of one particularly high signal, smaller signals can appear invisible. Also, the second example shows that morphological *in vivo* imaging by MRI can be limited in terms of sensitivity.

It is important to note that epifluorescence in the case of deep-seated signals comes to a limit, and transfluorescence technique in 2D or FLIT would be advisable for a more accurate quantification, but this would also then be more time-consuming. Taken together, it is nevertheless important to consider the high value of FLI *in vivo* imaging of iRFP720 to monitor lung tumor load in mice in terms of relative signal quantification, and with that, animals could be signal-dependent treated before they become clinically affected or even moribund. Furthermore, in the case of sufficient fluorescence emission, FLIT imaging for absolute quantification and localization could also give additional information about the tumor load (Fig. 4B). As a consequence, refinement of animal procedures to improve the ethics of lung metastasis experiments could be achieved using this model. It is also possible that if all transduced cancerous cells express the fluorescence protein, tumor load–dependent treatment in a comparable tumor load could be gained. However, it is also important to note that the heterogeneity of iRFP720 expression within the whole tumor cannot be ruled out, as approximately 90% of 4T1-iRFP720 cells were fluorescent (Supplementary Fig. S1).

When analyzing the individual tumor nodules as well as nodular structures and their growth pattern along the alveolar septs and, with that, the interference with healthy, alveolar tissue, obviously tumor cells breached through the endothelium, basal membrane, and alveolar wall and reached the air side. Similar to the clinical situation, 4T1 cells from either orthotopically implanted tumors or i.v. injected ones form intravascular tumors, occluding vessels, and after prolonged growth invade the pa-

Downloaded by Vienna University Library from www.liebertpub.com at 08/06/18. For personal use only.

renchyma and reach the luminal side, as also observed in Fig. 4E.[21] This should make these tumors accessible for LPEI polyplexes when applied via the airways.

Accessibility is of key importance, as Hasenpusch *et al.* demonstrated that only lung tumors with access to the air side were accessible for aerosolized polyplexes.[6] In this case, only tumors that grew after intrabronchiolar cell application were transfected by polyplexes, whereas i.v.-applied cells (A549 human lung carcinoma xenografted in NSG-mice) exhibited a diffuse parenchymal infiltration pattern and could not be transfected by aerosolized polyplexes. In the case of optical imaging, sensitivity of detection was much lower for fluorescence imaging in comparison to bioluminescence. This is substantiated by the presence of a clear bioluminescence signal in the lung area (Supplementary Fig. S2) immediately after i.v. injection of 10^5 4T1-luc cells. On the other hand, with 4T1-iRFP a significant signal was only seen at the earliest at 5 days post implantation. However, the tumor growth rate was observed to be more aggressive in the luciferase-transfected tumor cells in comparison to 4T1-iRFP720 cells (Supplementary Figs. S2 and S3). Switching to a chlorophyll-free diet could reduce fluorescence from stomach and intestine, but the spectral unmixing procedure still had to be applied to improve detection of the lesion by 2D epi-fluorescence imaging.[3] Despite the spectral unmixing process, signals from the stomach were still detectable. This indicates the need to reduce background both by a reduced FL diet and also by the spectral unmixing procedure.

In a similar work by Shcherbakova and Verkhusha,[13] 3D tomographic imaging of deep-seated signals in the liver by FLIT was achieved using iRFP713 after transduction with *iRFP713*-encoding adenovirus. However, in the present study, FLIT was possible only in individual animals with high fluorescence signal and probably also high tumor load. Due to less sensitivity, 3D FLIT imaging with subsequent quantification based on a created database needs a critical threshold to gain a better signal-to-noise ratio. In the case of the presented mid-stage tumor load and a rather low expression rate of iRFP720 protein in 4T1-iRFP720 cells (data not shown), FLIT reconstruction was possible but not without excluding background from the stomach. Selecting and sorting of cells with even higher iRFP720 levels might help to increase the homogeneity of RFP expression within the whole tumor, but care has to be taken to avoid cytotoxic effects due to high reporter gene expression. In order to improve sensitivity, alternatives are also being considered, such as the use of luciferases with substrates other than luciferin and approaches based on bioluminescence resonance energy transfer.[23]

Consideration of biophysical properties of polyplexes is crucial for efficiency of transfection both *in vitro* and *in vivo*, and especially with respect to the influence of microspraying on size and transfection ability. NTA showed that N/P 9–based polyplexes had significantly higher percentage of particles up to 200 nm in size in comparison to N/P 6, which can be ascribed to the excess polymer, as also reported in other studies.[24,25] The microspraying process did not drastically change the fraction of particles up to 200 nm, which are important for transfection.[26] This is supported by the results of *in vitro* transfection of A549 cells, where there was only slight decrease in transfection efficiency (Fig. 3). However, in the case of 4T1 cells, detrimental effect of microspraying on transfection efficiency may be ascribed to their low transfectability, which can also be observed in comparison to A549 (Fig. 3). When compared to the very high bioluminescence signal observed with N/P 9 LPEI polyplexes in Balb/c mice,[14] transfection was very low when applying such polyplexes intratracheally (data not shown). This is in agreement with observations by Bragonzi *et al.*, where a 100-fold lower luciferase activity was seen with LPEI polyplexes when comparing intratracheal to i.v. application.[27]

Additional barriers for lung delivery include mucus in the larger airways, surfactant in the alveolae, and clearance by the phagocytic system in the lungs, especially for nanoparticles bearing a cationic charge such as polyplexes. Albeit mucus-producing breast cancers are known, that is, mucinous (colloidal) breast cancer,[28] triple-negative breast cancer is not known for exuberant mucus production. With IT delivery, BLI signals could be detected in the lung area, overlapping at least partially with the iRFP720 signal using FLI imaging. Notably, the side of the animal with BLI signal matched in all cases with the side having the fluorescence signals. However, the signal was very low, and an untreated animal was needed to verify the BLI signal. Importantly, immunohistochemical evaluation showed the same staining pattern as could be observed in stably transduced 4T1-luc-bearing tumor lungs showing a rather pale homogenous staining pattern. Nevertheless, background staining and unspecific binding especially for the healthy tissue cannot fully be excluded (Supplementary Fig. S6). To investigate potential transfection of healthy tissue and especially the bronchiolar epithelium, further studies need to be conducted.

With the data presented here, the study successfully utilized LPEI polyplexes to transfect lung lesions after intratracheal delivery. As transfection levels were still rather low, and transfection of healthy tissue cannot be completely excluded, further improvements for the LPEI polyplex part are conceivable. Imaging-based biodistribution studies of these polyplexes can also help in tracking the transfection process. For instance, some studies show liver accumulation of nucleic acids after lung delivery. This possibility of liver accumulation cannot be ruled out in the present study. To pursue tumor selective transgene expression further, the authors plan to apply targeting strategies on the transcriptional level using tumor-selective promoter elements,[29] de-targeting transgene expression on the transcriptional level utilizing microRNA binding domains,[30] or for selectivity of tumor cell uptake combined de-targeting with PEG and re-targeting with ligand binding peptides.[31,32]

ACKNOWLEDGMENTS

Parts of this work have received support from the EU/EFPIA Innovative Medicines Initiative Joint Undertaking COMPACT grant no. 115363. J.M. is supported by the uni:docs fellowship program for doctoral candidates of the University of Vienna. We are very grateful to Gerald Schmauss and Karin Aumayr (Research Institute for Molecular Pathology GmbH, Vienna, Austria) for sorting of iRFP720 transduced cells. We are grateful to Sebastian Gehrig for help and discussions regarding MRI analysis.

AUTHOR DISCLOSURE

No competing financial interests exist.

Downloaded by Vienna University Library from www.liebertpub.com at 08/06/18. For personal use only.

REFERENCES

1. McLachlan G, Davidson H, Holder E, et al. Preclinical evaluation of three non-viral gene transfer agents for cystic fibrosis after aerosol delivery to the ovine lung. Gene Ther 2011;18:996–1005.
2. Mastorakos P, da Silva AL, Chisholm J, et al. Highly compacted biodegradable DNA nanoparticles capable of overcoming the mucus barrier for inhaled lung gene therapy. Proc Natl Acad Sci U S A 2015;112:8720–8725.
3. Geyer A, Lorenzer C, Gehrig S, et al. Fluorescence- and computed tomography for assessing the biodistribution of siRNA after intratracheal application in mice. Int J Pharm 2017;525:359–366.
4. Kuzmov A and Minko T. Nanotechnology approaches for inhalation treatment of lung diseases. J Control Release 2015;219:500–518.
5. Densmore CL. The re-emergence of aerosol gene delivery: a viable approach to lung cancer therapy. Curr Cancer Drug Targets 2003;3:275–286.
6. Hasenpusch G, Pfeifer C, Aneja MK, et al. Aerosolized BC-819 inhibits primary but not secondary lung cancer growth. PLoS One 2011;6:e20760.
7. Zintchenko A, Susha AS, Concia M, et al. Drug nanocarriers labeled with near-infrared-emitting quantum dots (quantoplexes): imaging fast dynamics of distribution in living animals. Mol Ther 2009;17:1849–1856.
8. Navarro G, Maiwald G, Haase R, et al. Low generation PAMAM dendrimer and CpG free plasmids allow targeted and extended transgene expression in tumors after systemic delivery. J Control Release 2010;146:99–105.
9. Medarova Z, Pham W, Farrar C, et al. *In vivo* imaging of siRNA delivery and silencing in tumors. Nat Med 2007;13:372–377.
10. Rabinovich BA, Ye Y, Etto T, et al. Visualizing fewer than 10 mouse T cells with an enhanced firefly luciferase in immunocompetent mouse models of cancer. Proc Natl Acad Sci U S A 2008;105:14342–14346.
11. Kuo C, Coquoz O, Troy TL, et al. Three-dimensional reconstruction of *in vivo* bioluminescent sources based on multispectral imaging. J Biomed Opt 2007;12:024007.
12. Hong H, Yang Y, Cai W. Imaging gene expression in live cells and tissues. Cold Spring Harb Protoc 2011;2011:pdb top103.
13. Shcherbakova DM, Verkhusha VV. Near-infrared fluorescent proteins for multicolor *in vivo* imaging. Nat Methods 2013;10:751–754.
14. Taschauer A, Geyer A, Gehrig S, et al. Up-scaled synthesis and characterization of nonviral gene delivery particles for transient *in vitro* and *in vivo* transgene expression. Hum Gene Ther Methods 2016;27:87–97.
15. Su B, Cengizeroglu A, Farkasova K, et al. Systemic TNFalpha gene therapy synergizes with liposomal doxorubicine in the treatment of metastatic cancer. Mol Ther 2013;21:300–308.
16. Rodl W, Schaffert D, Wagner E, et al. Synthesis of polyethylenimine-based nanocarriers for systemic tumor targeting of nucleic acids. Methods Mol Biol 2013;948:105–120.
17. Braber S, Verheijden KA, Henricks PA, et al. A comparison of fixation methods on lung morphology in a murine model of emphysema. Am J Physiol Lung Cell Mol Physiol 2010;299:L843–851.
18. Mezzanotte L, van 't Root M, Karatas H, et al. *In vivo* molecular bioluminescence imaging: new tools and applications. Trends Biotechnol 2017;35:640–652.
19. Owens EA, Henary M, El Fakhri G, et al. Tissue-specific near-infrared fluorescence imaging. Acc Chem Res 2016;49:1731–1740.
20. Vahrmeijer AL, Hutteman M, van der Vorst JR, et al. Image-guided cancer surgery using near-infrared fluorescence. Nat Rev Clin Oncol 2013;10:507–518.
21. Wong CW, Song C, Grimes MM, et al. Intravascular location of breast cancer cells after spontaneous metastasis to the lung. Am J Pathol 2002;161:749–753.
22. Rashid OM, Nagahashi M, Ramachandran S, et al. Is tail vein injection a relevant breast cancer lung metastasis model? J Thorac Dis 2013;5:385–392.
23. Rumyantsev KA, Turoverov KK, Verkhusha VV. Near-infrared bioluminescent proteins for two-color multimodal imaging. Sci Rep 2016;6:36588.
24. Boeckle S, von Gersdorff K, van der Piepen S, et al. Purification of polyethylenimine polyplexes highlights the role of free polycations in gene transfer. J Gene Med 2004;6:1102–1111.
25. Fahrmeir J, Gunther M, Tietze N, et al. Electrophoretic purification of tumor-targeted polyethylenimine--based polyplexes reduces toxic side effects *in vivo*. J Control Release 2007;122:236–245.

26. von Gersdorff K, Sanders NN, Vandenbroucke R, et al. The internalization route resulting in successful gene expression depends on polyethylenimine both cell line and polyplex type. Mol Ther 2006;14:745–753.

27. Bragonzi A, Dina G, Villa A, et al. Biodistribution and transgene expression with nonviral cationic vector/DNA complexes in the lungs. Gene Ther 2000;7:1753–1760.

28. Dumitru A, Procop A, Iliesiu A, et al. Mucinous breast cancer: a review study of 5 year experience from a hospital-based series of cases. Maedica (Buchar) 2015;10:14–18.

29. Haase R, Magnusson T, Su B, et al. Generation of a tumor- and tissue-specific episomal non-viral vector system. BMC Biotechnol 2013;13:49.

30. Kopp F, Schnoedt M, Haase R, et al. De-targeting by miR-143 decreases unwanted transgene expression in non-tumorigenic cells. Gene Ther 2013;20:1104–1109.

31. Schafer A, Pahnke A, Schaffert D, et al. Disconnecting the yin and yang relation of epidermal growth factor receptor (EGFR)-mediated delivery: a fully synthetic, EGFR-targeted gene transfer system avoiding receptor activation. Hum Gene Ther 2011;22:1463–1473.

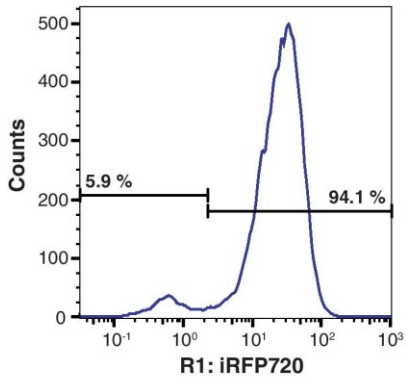
32. Klutz K, Schaffert D, Willhauck MJ, et al. Epidermal growth factor receptor-targeted (131)I-therapy of liver cancer following systemic delivery of the sodium iodide symporter gene. Mol Ther 2011;19:676–685.

Received for publication July 29, 2017;
accepted after revision September 3, 2017.

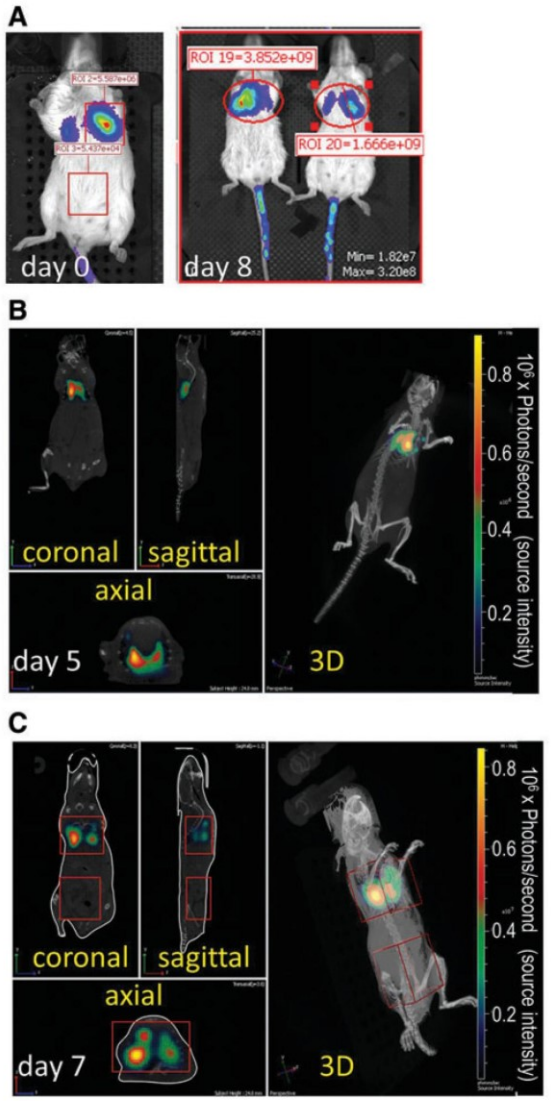
Published online: September 5, 2017.

Downloaded by Vienna University Library from www.liebertpub.com at 08/06/18. For personal use only.

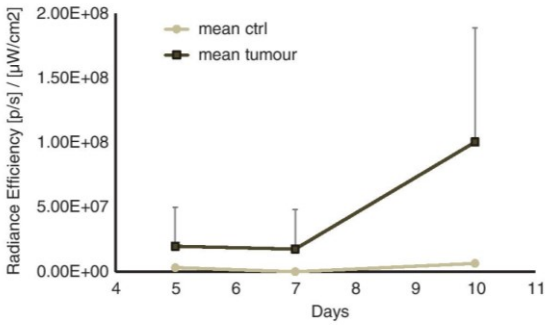
Supplementary Data



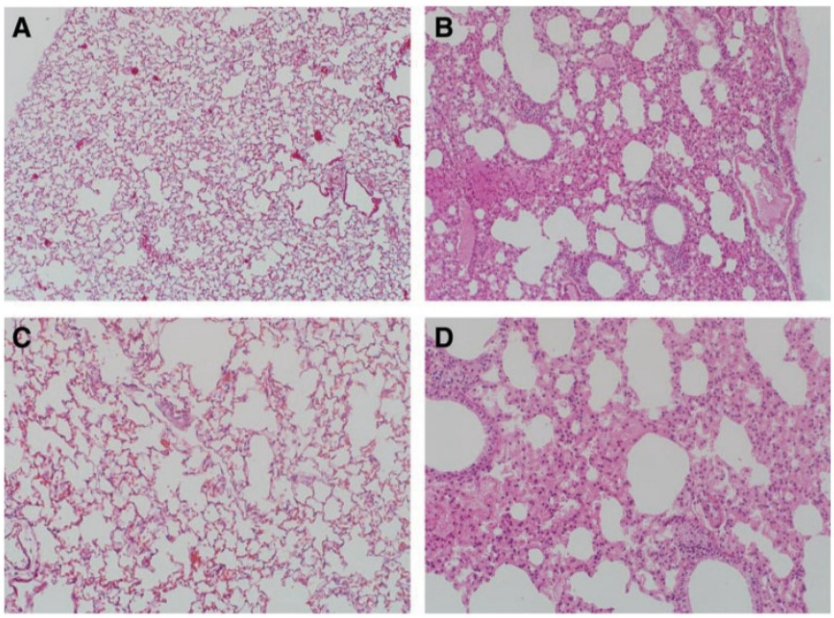
Supplementary Figure S1. Lentiviral-based transduction of 4T1 cells with iRFP720 gene under constitutive expression. iRFP720 expression of 4T1 cells as analyzed by flow cytometry.



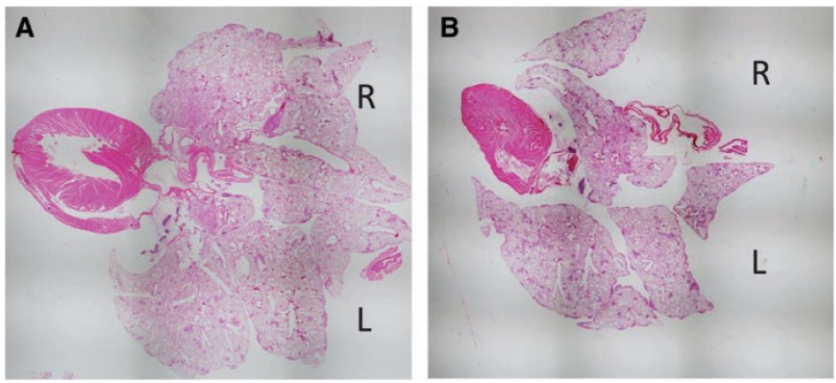
Supplementary Figure S2. BLI and DLIT measurements in the 4T1-Luc tumor model. Female Balb/c mice were injected with 1×10^5 4T1-Luc cells and imaged either immediately after injection, day 0 **(A),** after 5 days **(B)**, after 7 days **(C)**, or after 8 days (**A**, *right*) thereafter. Imaging was carried out after injection of Na-luciferin at a dose of 60 mg/kg intraperitoneally. **(A)** Color-coded BLI image overlaid in a reflected light picture (B/W). ROIs shown BLI signal in photons/s/ROI. **(B** and **C)** Color-coded DLIT signal overlaid on CT image (B/W). Coronal, sagittal, and axial section and maximum intensity projection 3D reconstructed model (3D) is shown.



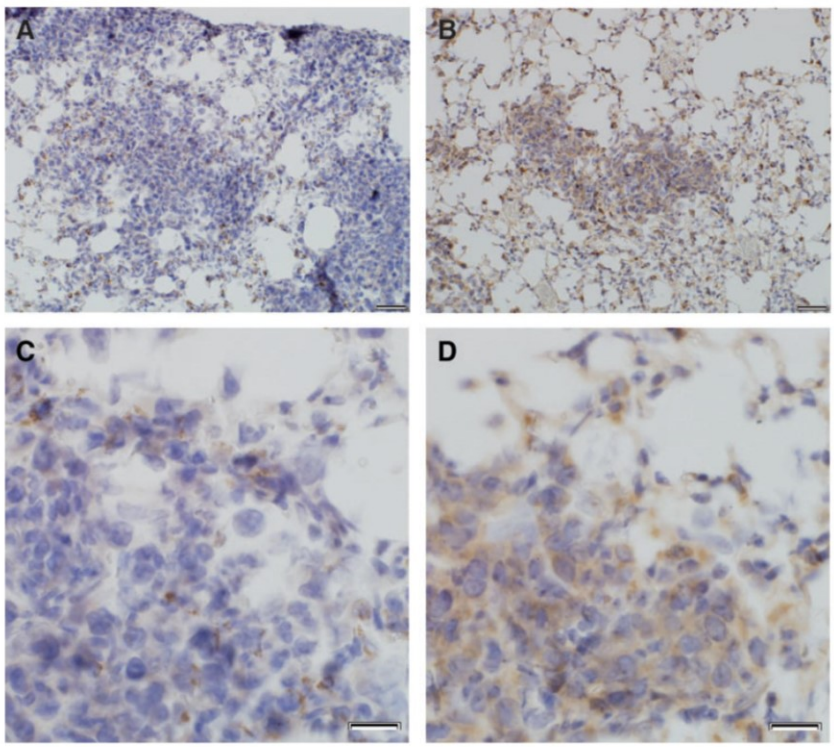
Supplementary Figure S3. Quantification of signal intensity at different time points of tumor growth in 4T1-iRFP720 tumor model. Balb/c mice received 10^5 4T1-iRFP720 cells i.v. and were imaged by epifluorescence imaging at different time points after cell implantation (days 5, 7, and 10; $n=3$).



Supplementary Figure S4. Establishment of instillation fixation. Female Balb/c mice were sacrificed by an overdose of anesthesia, and either intubated and intratracheally fixed by in instillation of formalin **(A** and **C)** or immediately excised and fixed afterwards **(B** and **D)**. Magnification used: **(A** and **B)** 10×; **(C** and **D)** 20×.



Supplementary Figure S5. Histology of whole lungs from transfected 4T1-iRFP720 tumor mice after intratracheal instillation corresponding to Fig. 5. Whole-section images after H&E staining are shown. **(A)** Histology for animal shown in Fig. 5A, D, and G. **(B)** histology for animal shown in Fig. 5B, E, and H. Figures were taken at 2× magnification and were stitched together using CellSens software (Olympus) to get the whole section from both lungs. R and L refer to right and left lung.



Supplementary Figure S6. Luciferase immunohistochemistry of tumor-bearing lung tissue. Luciferase immunohistochemistry of tumor-bearing lung tissue from untransfected tumor mice **(A** and **C)** and transfected tumor mice after polyplex instillation **(B** and **D)**. 4T1-iRFP720 tumor-bearing animals were transfected with LPEI polyplexes, as in Fig. 5. After BLI imaging, lungs were fixed by instillation fixation, processed and sectioned, and histological sections (3 μm) stained with polyclonal goat-anti luciferase antibody, followed by biotinylated rabbit-anti-goat antibody and stained with the Vectastain ABC kit followed by incubation in DAB, as described in the Materials and Methods (*brown staining*). Sections were counterstained with hematoxylin (*blue stain*). Scale bar in **(A** and **B)** 100 μm; in **(C** and **D)** 20 μm.

2.3 Up-Scaled Synthesis and Characterization of Nonviral Gene Delivery Particles for Transient *In Vitro* and *In Vivo* Transgene Expression

Alexander Taschauer, Antonia Geyer, Sebastian Gehrig, **Julia Maier**, Haider Sami and Manfred Ogris. *Human Gene Therapy Methods*, 2016. 27(3):87-97.

Aims:

Protocol setup for a standardized up-scaled polyplex (LPEI-pDNA transfection agent) synthesis, including the assessment of different formulations, and evaluation of transfection after intravenous polyplex administration

1. Protocol generation for up-scaled polyplex production, including rigorous testing of physical properties
2. Quality assessment of *in vitro* and *in vivo* transfection potential for different N/P rations, including comparison to other transfection agents

Hypotheses:

1. Syringe-pump based synthesised polyplexes achieve reproducible physical and biophysical properties
2. Polyplexes show comparable transfection potential to commercially available alternatives, with robust in vitro and in vivo transfection efficiencies

Contributions:

J.M. was involved in experimental design and experimental work (cell transductions, transduced cell sorting), and co-authored.

PROTOCOL

Up-Scaled Synthesis and Characterization of Nonviral Gene Delivery Particles for Transient *In Vitro* and *In Vivo* Transgene Expression

Alexander Taschauer, Antonia Geyer, Sebastian Gehrig, Julia Maier, Haider Sami,* and Manfred Ogris

MMCT Laboratory of Macromolecular Cancer Therapeutics, Department for Pharmaceutical Chemistry, Faculty Center for Pharmacy, University of Vienna, Vienna, Austria.

Polyethylenimine-based polyplexes are promising nonviral gene delivery systems for preclinical and clinical applications. Pipette-based polyplexing is associated with several disadvantages, such as batch-to-batch variability, restriction to smaller volumes, and variable gene delivery results. The present protocol describes syringe-pump-mediated upscaled synthesis of well-defined gene delivery nanoparticles capable of efficient *in vitro* and *in vivo* gene delivery. Syringe-pump-based synthesis ensures controlled mixing, upscaling, and reproducible gene delivery. Nanoparticle tracking analysis of the upscaled formulations involved single nanoparticle tracking, thereby generating highly resolved biophysical characterization. Gene delivery performance was investigated by luciferase gene expression in cells and three-dimensional bioluminescence imaging in mice.

INTRODUCTION

DELIVERY OF GENES TO CELLS is a key step in gene therapy, which is achieved by both viral and nonviral gene carriers.[1] The latter category of gene carriers offers various advantages, including tunable biosafety profile, lack of immunogenicity, and programmability for multiple functions. In addition, owing to the multiple possibilities offered by nanotechnology, development of efficient nonviral gene carriers for preclinical and clinical research is highly promising. Accomplishment of successful and reproducible *in vitro* and *in vivo* gene expression via nonviral gene nanocarriers is a challenging task; it needs fine control on the synthesis of nanocarriers, upscaled synthesis methods, detailed characterization of nanoparticles, and sensitive *in vitro/in vivo* gene expression techniques.

The classical method of generating polyplexes by flash pipetting is often characterized by a distinct batch-to-batch variability of the product.[2] Furthermore, it must be considered that formation of polyplexes using a pipette is limited to relatively small volumes.[3] Moreover, it is also susceptible to operator-induced variability, thereby leading to irreproducible gene delivery. Fine control on the synthesis of polyplexes can be achieved by employment of a syringe pump for controlled mixing of the two components needed for polyplex synthesis, that is, plasmid DNA (pDNA) and the transfection agent (linear polyethylenimine, LPEI).[4] Similarly, a mixing device has been reported for lipid-DNA complexes to generate formulations with reproducible attributes.[5] Also, syringe-pump-mediated polyplex synthesis ensures an upscaled production, characterized by a controlled and reproducible mixing, resulting in nanoparticles with narrow size distribution.[4] Detailed characterization of biophysical properties of the nanoparticle formulations is another key aspect for designing efficacious gene delivery particles. Nanoparticle tracking analysis (NTA) is a relatively recent technique that tracks single nanoparticles via light scattering and brownian motion combined with a video camera, thereby giving more detail on nanoparticle population characteristics for size and zeta potential (ζ-potential), when compared with the routinely used dynamic light scattering system.[6] Because of its ability of detecting individual nanoparticles, NTA results in a high-resolution measurement of both particle size and ζ-potential, even of samples characterized by high polydispersity.[6] Another key

*Correspondence: Dr. Haider Sami, MMCT Laboratory of Macromolecular Cancer Therapeutics, Department for Pharmaceutical Chemistry, Faculty Center for Pharmacy, University of Vienna, Althanstraße 14, A-1090 Vienna, Austria. E-mail: haider.sami@univie.ac.at

© 2016 by Mary Ann Liebert, Inc.
DOI: 10.1089/hgtb.2016.027

parameter affecting the gene delivery process of polyplexes is their biophysical stability, which is directly dependent on the solvent used during polyplexing. For example, an increasing concentration of NaCl in the solution results in an enhanced tendency of LPEI-pDNA complexes to form larger aggregates that would finally affect the transfection efficiency.[7–9] HEPES buffered glucose (HBG) shows a stabilizing effect on the physicochemical properties and therefore leads to a more reproducible quality of the resulting nanoparticles.[7,8,10] Other factors affecting transfection efficiency of polyplexes include size, charge, and amount of DNA within the polyplex formulation.[11–13] However, the amount of pDNA that can be used for transient transfection *in vitro* and *in vivo* is strongly limited by the quantity of LPEI needed for complexation because of its cellular toxicity. Apart from chemical and biophysical properties of polyplexes, the success of transient transfection is also influenced by genotypic and phenotypic properties of different cell types.[14] Therefore, it is important that the whole transfection process is optimized for every individual cell type. Upscaling of the polyplexation is more important for *in vivo* gene delivery owing to the high amounts needed in preclinical gene delivery studies. Upon intravenous administration, LPEI polyplexes tend to interact with blood components leading to the formation of aggregates and thereby transfection of lung tissue (after crossing of pulmonary–endothelial barrier).[15,16]

Here we describe a method for syringe-pump-mediated upscaled production of gene delivery nanoparticles for efficient *in vitro* and *in vivo* transient transgene expression (Fig. 1). LPEI was employed as the transfection reagent owing to its higher biocompatibility in comparison to the branched versions.[7–10] This protocol can be used for delivery of transgenes with both intracellular and secreted protein products *in vitro*. *Firefly luciferase* (intracellular) and *Gaussia luciferase* (secreted) were selected as model/reporter genes for delivering them *in vitro* and investigating luciferase expression as parameter of successful gene delivery. Similarly, by employing the same gene delivery nanoparticles, firefly luciferase was delivered *in vivo* and transient transfection of lung tissue was monitored by bioluminescence imaging. Quality control of the nanoparticle formulations was done by NTA to ensure narrow size distribution.

1. MATERIALS

1.1. Reagents

All reagents are enlisted in Table 1.

1.2. Equipment

1. KDS Legato 210 syringe pump system
2. Nanosight NS500 (Malvern)
3. Tecan Infinite M200 pro
4. MacsQuant VYB
5. Inverted microscope
6. Biological safety cabinet
7. Magnetic stirrer
8. pH Meter
9. Arium Pro VF (Sartorius)
10. Vortex mixer
11. Shaking platform
12. Water bath
13. Incubator 37°C, 5% CO_2
14. Refrigerator (4°C)

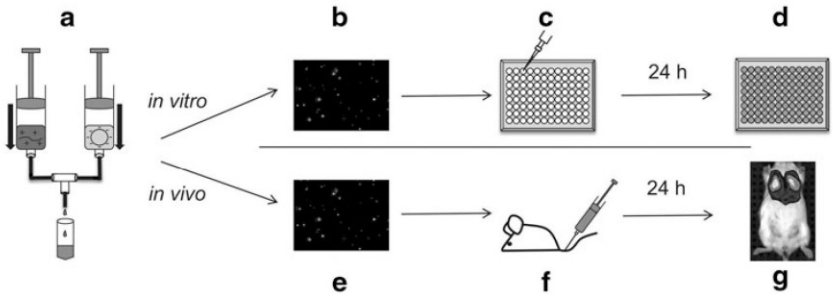


Figure 1. Experimental procedure. **(a)** Prepare polyplexes by mixing equal volumes of pDNA and LPEI-containing solutions using a syringe-pump-based system. **(b, e)** Analyze biophysical properties (particle size; ζ-potential) of polyplexes by NTA. **(c)** For *in vitro* evaluation add polyplexes and control substances (e.g., Lipofectamine 2000 and jetPRIME) to cells. **(d)** Measure luminescence activity after 24 hr. Luminescence signal can be normalized using BCA protein assay or flow cytometry. **(f)** For *in vivo* evaluation, inject polyplex-containing solution into the tail vein of mice. **(g)** After 24 hr measure bioluminescence after s.c. D-luciferin injection and correlate luciferase activity with photons/sec. LPEI, linear polyethylenimine; NTA, nanoparticle tracking analysis.

Table 1. *Reagents*

Reagents	*Supplier*	*Specific handling*	*Storage conditions*
Poly(2-ethyl-2-oxazoline) 50 kDa	Sigma-Aldrich Cat. No. 372846 Lot. No. 09410LH		Room temperature; protected from light in a desiccator
pCMV-Gluc	New England Biolabs Cat. No. N8081S		–20°C
pCpG-hCMV-EF1α-LucSH	Available on request from the authors		–20°C
N-(2-Hydroxyethyl)piperazine-N′-(2-ethanesulfonic acid) (HEPES)	AppliChem Cat. No. A3724,0500		Room temperature
D(+)-Glucose	Merck Millipore Cat. No. 1.08337.1000		Room temperature
Hydrochloric acid 37%	Sigma-Aldrich Cat. No. 30721		Room temperature
Sodium hydroxide	AppliChem Cat. No. A6829,1000		Room temperature
Ethanol absolute	Merck Millipore Cat. No. 1.11727.2500		Room temperature
Cell line: A549 (lung adenocarcinoma)	ATCC		–150°C
RPMI-1640 Medium	Sigma-Aldrich Cat. No. R0883		+4°C
Fetal bovine serum (FBS)	Sigma-Aldrich Cat. No. F7524		–20°C
L-Glutamine 200 m*M*	Sigma-Aldrich Cat. No. G7513		–20°C
Dulbecco's phosphate buffered saline (DPBS)	Sigma-Aldrich Cat. No. D8537		Room temperature
TrypLE express enzyme with phenol red	Gibco Cat. No. 12605–036		Room temperature
2-(4-Amidinophenyl)-6-indolecarbamidine dihydrochloride (DAPI)	Sigma-Aldrich Cat. No. D9542		+4°C; protected from light Aqueous solutions should be stored at –20°C
BCA Compat-Able Protein Assay Kit	Pierce Cat. No. 23229	Danger: reagents can cause severe skin burns and eye damage	Room temperature
Dual-Luciferase Reporter Assay System	Promega Cat. No. E1960		–20°C; once reconstituted the luciferase assay substrate should be stored at –70°C (max. 4 weeks) and the Stop & Glo Reagent at –20°C (max. 15 days)
MACSQuant Running buffer for flow cytometry	Miltenyi Biotec Cat. No. 130-092-747		Room temperature
Beetle luciferin, sodium salt	Promega Cat. No. E464X		–80°C
Isoflurane	CP Pharma Cat. No. 798–932		Room temperature, protected from light
Oxygen	Air liquid—Alphagaz		Room temperature
Scanlux 300	Sanochemia Diagnostics Approval No. 1–23236		Room temperature, protected from light

15. Freezer (–20°C, –80°C, –150°C)
16. IVIS SpectrumCT Preclinical *In vivo* Imaging System (Perkin Elmer)
17. Computer equipped with FlowJo, Microsoft Excel, Living Image, and GraphPad Prism

1.3. Supplies

1. Eppendorf tubes
2. 15 ml centrifuge tubes (Starlab)
3. Syringes:
   a. 3 ml OmniFix (BBraun)
   b. 1 ml Omnican 100 (BBraun)
4. Components of tubing system used for polyplex generation:
   a. Flangeless Nut Delrin 1/4-28 1/16″ Red with Ferrule (Kinesis Abimed)
   b. Female Luer to 1/4-28 Female PEEK (Kinesis Abimed)
   c. Tee HP PEEK 1/16″ (Kinesis Abimed)
   d. PEEK tubing (OD 1/16″) (GE Lifesciences)
5. Pasteur pipettes
6. Pipette tips
7. White 96-well flat-bottom microplate, transparent bottom, sterile (Greiner)

8. Transparent 96-well flat-bottom microplate, sterile (Greiner)
9. Reagent reservoirs

1.4. Reagent setup

HEPES buffered glucose (20 mM HEPES/5% [w/V] glucose). Dissolve 0.4766 g of HEPES and 5 g of glucose in 80 ml ddH_2O; adjust pH to 7.4 by using HCl/NaOH; add ddH_2O to reach a final volume of 100 ml; pass the final solution through a 0.22 μm filter under a biological safety cabinet.

This solution can be made in advance and stored at +4°C for up to 6 months.

Linear polyethylenimine. Linear polyethylenimine (LPEI) with an average molecular weight of 10 kDa was synthesized based on the instructions described by Rödl et al. using poly(2-ethyl-2-oxazoline) as initial compound.[16]

Because of significant batch-to-batch variability of commercially available poly(2-ethyl-2-oxazoline), both ^{1}H-NMR and gel permeation chromatography (GPC) should be conducted for characterizing the product.

LPEI solution in HBG (1 mg/ml). Resuspend 5 mg of LPEI in 4 ml of HBG and readjust the pH to 7.4 with HCl/NaOH under vigorous vortexing to avoid the formation of LPEI precipitates; add HBG to reach a final volume of 5 ml; pass the final solution through a 0.22 μm filter under a biological safety cabinet. Filtering LPEI-containing solutions can cause a reduction of the polymer concentration. Therefore, it is obligatory to quantify the LPEI concentration post-filtration by conducting a copper assay described by Ungaro et al.[17] LPEI-containing stock solutions can be stored at +4°C for up to 2 months and at –80°C for long-term.

Cell culture medium. 500 ml RPMI-1640 is supplemented with 10% (V/V) FBS and L-glutamine at a concentration of 0.3 g/liter. Cell culture medium should be stored at +4°C for up to 2 months. Storing cell culture medium in small aliquots avoids frequent warm-up cycles, which can negatively influence the quality of cell culture medium.

2. EXPERIMENTAL PROCEDURE

2.1. Syringe-pump-based synthesis system for controlled mixing[4]

1. As shown in Fig. 2, connect two 3 ml syringes to a T-connector via polyetherketone tubings with a length of 10 cm, respectively. One syringe is for LPEI and the other syringe is for pDNA.
2. Use one further polyetherketone tubing (5 cm) connected to the T-connector as an outlet tubing.
3. The product can be collected in a centrifuge tube.

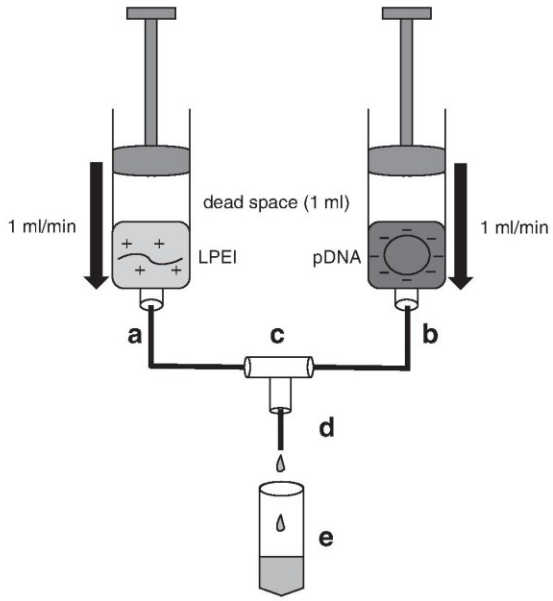


Figure 2. Scheme of syringe-pump-based polyplex generation. Load LPEI- and pDNA-containing solutions into two separate syringes. A dead space of 1 ml in both syringes avoids loss of volume during polyplex generation. Use polyetherketone tubings **(a, b)** to connect both syringes to a T-connector **(c)**. After starting the syringe pump at a flow rate of 1 ml/min, LPEI and pDNA solutions are mixed in the T-connector. The product solution flows through a further polyetherketone tubing **(d)** into a centrifuge tube **(e)**.

2.2. Polyplex formation

1. pDNA and LPEI solutions have to be prepared in different tubes and in same volume as described in steps 2.2.2. and 2.2.3. below.
2. Dilute pDNA (*pCpG-hCMV-EF1α-LucSH* or *pCMVGLuc*) in HBG buffer (20 m*M* HEPES, 5% glucose) to a final concentration of 40 μg/ml for *in vitro* assays or 400 μg/ml for *in vivo* assays.
   a. Note: Generating polyplexes is normally done by mixing equal volumes of pDNA- and LPEI-containing solutions finally resulting in a pDNA concentration of 20 μg/ml for *in vitro* or 200 μg/ml for *in vivo* experiments.

3. The appropriate amount of LPEI according to the total amount of pDNA and the desired N/P ratio can be calculated by using the following equation:

$$m(\text{LPEI}) = \frac{m\ (\text{pDNA}) \times 43 \times \text{N/P}}{330}$$

   a. 43 g/mol is the molecular weight of one subunit in the molecular structure of LPEI and 330 g/mol is the average molecular weight of one nucleotide.
   b. Example: for preparing 500 μl of a polyplex solution with a pDNA concentration of 20 μg/ml and an N/P ratio of 6:
      i. m (pDNA) = 10 μg
      ii. $m(\text{LPEI}) = \frac{10 \times 43 \times 6}{330} = 7.82\ \mu\text{g}$
   c. LPEI has to be diluted in HBG buffer in same volume as used for pDNA.
4. Let both (pDNA solution prepared in 2.2.1. and LPEI solution prepared in 2.2.2.) solutions equilibrate at room temperature for at least 5 min.
   a. Note: For investigating pDNA recovery it is necessary to measure pDNA concentration before and after complexation with LPEI. pDNA concentration and recovery are calculated by using the following equations:

$$c(\text{pDNA};\ \mu\text{g/ml}) = [\text{Abs}(260\ \text{nm}) - \text{Abs}(320\ \text{nm})] \cdot 50$$

$$\text{pDNA recovery}\ (\%) = \frac{c(\text{pDNA};\ \text{after polyplexing})}{[c\ (\text{pDNA};\ \text{before polyplexing})/2]} \times 100$$

5. Transfer each solution into 3 ml syringes
   a. Note: To avoid loss of volume during the mixing process, using a dead space of 1 ml in each syringe is advised.
6. Attach both syringes to the tubing system as shown in Fig. 2 and described in Sec. 2.1, and fix them in the syringe pump.
   a. Note: Controlled mixing should be done by using a flow rate of 1 ml/min.
7. Start the syringe pump to start the polyplexation process and collect the polyplex product in a centrifuge tube after the mixing cycle is complete.
   a. Note: Incubating polyplex-containing solutions over time would result in an increased aggregate formation, which would negatively influence the transfection efficiency of the sample. Therefore, it is advisable to do the biophysical as well as the biological evaluation of LPEI-based polyplexes immediately after generating them.

2.3. Biophysical evaluation by NTA

1. Before doing the first NTA measurement it is necessary to prepare the NanoSight NS500 as follows:
   a. Prime the fluidics with ddH_2O
   b. Before measuring a sample it is mandatory to load the system (at least two times) with the solvent used for diluting the sample to avoid particle movement caused by differences of the ionic strength within the fluidics system.
   c. It is necessary to flush the system 2–3 times between each measurement with ddH_2O for removing remaining particles of the previous sample.
2. NTA measurements require an appropriate dilution of each sample to reach an optimal concentration of 10^8–10^9 particles/ml, which correlates to 10–100 particles in the field of view.
   a. Use either HBG or RPMI 1640 as a diluent for size measurements.
      i. Note: The particle concentration of the prepared polyplex solution correlates directly with both pDNA concentration and N/P ratio. The dilution factors used for this protocol are enlisted in Sec. 4 (troubleshooting).
      ii. Note: Basal RPMI 1640 is used as transfection medium for *in vitro* assays with A549 cells and can therefore be employed as a diluent for the biophysical evaluation to investigate changes in the size of polyplexes that may occur during cell treatment.
   b. Use 2.5 m*M* NaCl as a diluent for investigating the ζ-potential.
      i. Note: The parabolic profile of the particle drift should have a coefficient of determination (R^2 value) of at least 0.95.
   c. Use NTA settings as described in Table 2.

2.4. Reporter activity assay to monitor *in vitro* transgene expression

1. Seed 10,000 cells suspended in 200 μl of complete cell culture medium into each well of a flat-bottom 96-well tissue culture plate.

Table 2. *NTA settings*

Size measurements	*ζ-potential measurements*
Number of captures: 5	Capture duration: 90 sec
Capture duration: 60 sec	Secondary duration: 30 sec
Temperature control: 25.0°C	Applied voltage: 24 V
	Temperature control: 25.0°C

Gently agitate the plate to ensure an even distribution of the cells throughout the whole well surface.

a. Note: The whole *in vitro* transfection protocol is optimized for A549 lung adenocarcinoma cells that have a doubling time of approximately 22 hr. Seeding density and duration should be optimized individually for different cell types.

2. Incubate the cells overnight in a 37°C/5% CO_2 incubator for approximately 16 hr.
3. Check the appearance of the cells under a microscope for morphology and confluence. For efficient transfection, it is advisable that cells are 70–80% confluent at the time of addition of polyplexes (see note in Sec. 2.4.1)
4. Before starting with addition of polyplexes, aspirate the medium of each well and add 90 μl of RPMI-1640 (without FBS) directly on the cells.
5. Add 10 μl of a polyplex solution (containing 20 μg/ml pDNA concentration) to each well containing the 90 μl RPMI-1640.
   a. Note: Always keep untreated cells and cells treated only with pDNA as negative controls. Commercially available transfection agents such as Lipofectamine 2000 or jetPRIME can be used as positive controls.
6. After 4 hr, add 100 μl of complete cell culture medium into each well.
7. Total transfection time (starting from step 5) of 24 hr was followed before investigating the transgene expression.
8. In case of transgenes with intracellular protein products, the procedure described in Sec. 2.5 was followed. For transgenes with secretory protein products, the procedure described in Sec. 2.6 was followed.

2.5. Evaluation of *in vitro* transfection efficiency of intracellular expressed firefly luciferase:

1. After step 7 of 2.4, aspirate the cell culture medium from each well and wash the cells one time with 200 μl DPBS.
2. Lyse the cells using Passive Lysis Buffer (Promega) as per manufacturer's instructions.
3. Use 50% of the total volume of cell lysate for measuring the luminescence of the luciferase protein from the reporter gene.
   a. Apply the following plate reader settings for luminescence measurement:
      i. Substrate volume (Luciferase Assay reagent II; included in Dual-Luciferase Reporter Assay System; Promega): 50 μl
      ii. Integration time: 10,000 msec
      iii. Waiting time (between wells): 2 sec
4. Normalization of the luminescence values based on the amount of protein per well:
   a. Use the remaining 50% of cell lysate for determining the protein concentration by using a BCA protein assay kit.
   b. Mix every sample with 200 μl of BCA working reagent and place the plate in a 37°C/5% CO_2 incubator for 30 min.
      i. Note: While mixing the sample with BCA working reagent, avoid generating air bubbles in the sample as the air bubbles might give rise to erroneous absorption measurements.
   c. After cooling the plate to room temperature measure the absorption of each sample by using the following plate reader settings:
      i. Wavelength: 562 nm
      ii. Bandwidth: 9 nm
      iii. Number of flashes: 25
   d. Note: Use a bovine serum albumin (BSA) standard curve for calculating the protein amount in the cell lysates.

2.6. Evaluation of *in vitro* transfection efficiency of secreted Gaussia luciferase:

Compared with intracellular expressed reporter proteins, secreted reporters offer several advantages, such as the possibility of monitoring transient transfection over a longer duration. Since the luciferase expression is measured only in the medium, the remaining and intact cells can be employed for further analysis, such as the evaluation of cellular toxicity of the transfection reagents by flow cytometry and normalizing the luminescence values by the total number of living cells per well.[18,19]

1. After step 7 of Sec. 2.4, transfer 20 μl of the cell culture medium from each well into a white 96-well flat-bottom microplate for luminescence measurement. Therefore, it is necessary

to use a plate reader for luminescence measurements with the following settings:

a. Substrate volume (Stop & Glo Reagent; included in Dual-Luciferase Reporter Assay System; Promega): 50 μl
b. Integration time: 10,000 msec
c. Waiting time (between wells): 2 sec

2. Normalization of the luminescence values based on absolute cell count per well by flow cytometry:
   a. Aspirate the cell culture medium from the cells and wash them with 200 μl DPBS.
   b. Detach the cells by adding 20 μl of TrypLE to each well and incubating the plate for 5 min in an incubator (37°C/5% CO_2).
   c. Once cells are detached from the surface, resuspend them in 140 μl DPBS.
   d. Add 40 μl of DAPI-HCl dissolved in DPBS (5 μg/ml) to each sample directly before starting the flow cytometer measurement for counting dead and live cells.
      i. Note: Exclude duplicates from your cell population.
      ii. Note: Voltage settings have to be adjusted in a way to set the peak created by the living cells between 10^0 and 10^1.

Note: For normalizing the luminescence to the protein amount, use the protocol described in step 2.5.4.

2.7. Evaluation of *in vivo* transfection efficiency of intracellular expressed firefly luciferase

Balb/c mice were used as models for transfection with firefly luciferase-based polyplexes and bioluminescence imaging studies were performed to investigate the reporter transgene expression *in vivo*. The whole process was carried out in a way similar to the *in vitro* experiments described above.

1. Prepare polyplexes as described in Sec. 2.2. with a final pDNA concentration of 200 μg/ml.
   a. Note: Before injecting, evaluation of biophysical properties of polyplexes such as size and ζ-potential should be conducted to ensure high quality and good transfection efficiency (see Sec. 2.3.).
2. Inject the polyplex product intravenously (tail vein) at a dose of 2.5 mg of pDNA per kg body weight.[13]
3. After 24 hr of polyplex treatment, perform bioluminescence imaging (under anesthesia) as described in steps 4–7.
   a. Note: Induce anesthesia by applying 5% isoflurane in oxygen using a precision vaporizer. Anesthesia can be maintained using 1.5–2% isoflurane in oxygen.
4. Inject D-luciferin (dissolved in DPBS with a concentration of 30 mg/ml) subcutaneously at a dose of 150 mg per kg body weight. Place the animal in the imager in a ventral position and start with bioluminescence imaging after 10 min of luciferin injection. Depending on the imaging device, the bioluminescence can be acquired in either two-dimensional (2D) mode or both 2D and 3D modes.
   a. Use the following Caliper Ivis settings for acquiring 2D bioluminescence images:
      i. Emission open
      ii. Excitation blocked
      iii. Exposure time: 60 sec

Table 3. *Timelines for* in vitro *and* in vivo *transfection*

Task	*Steps*	*Duration*
Timeline for in vitro *transfection*		
Cell seeding for transfection	Sec. 2.4, step 1	30–45 min for cell seeding pprox. 12 hr incubation for cell attachment
Polyplex preparation	Sec. 2.2, steps 1–7	15 min per sample
Biophysical evaluation	Sec. 2.3, steps 1–2	60 min per sample
Cell treatment	Sec. 2.4, steps 3–5	10 min
Reporter activity assay for intracellular luciferase types	Sec. 2.5, steps 1–3	60–90 min
Reporter activity assay for secreted luciferase types	Sec. 2.6, step 1	30–60 min
Normalization via:		
1. Evaluation of the amount of protein per well, or	Sec. 2.5, step 4	90–120 min
2. Absolute count of living cells	Sec. 2.6, step 2	30–60 min
Timeline for in vivo *transfection*		
Polyplex preparation	Sec. 2.2, steps 1–7	30 min
Biophysical evaluation	Sec. 2.3, steps 1–2	30 min
i.v. injection into tail vein	Sec. 2.7, step 2	5 min per mouse
Bioluminescence imaging	Sec. 2.7, steps 3–7	60 min per mouse

Table 4. *Troubleshooting*

Problem	*Possible reason(s)*	*Solution(s)*
ζ-potential measurement shows parabolic drift profile with a coefficient of determination of less than 0.95	Particle concentration too low Measuring chamber of the NTA system is coated with LPEI-based particles.	Increase the concentration of the sample used for ζ-potential measurement. The NTA software needs at least 100 particle tracks per video. The dilution factors that showed optimal measurement conditions are listed in Table 5. Disassemble and clean the chamber as per instructions from the manufacturer.
High toxicity after cell treatment with polyplexes	LPEI concentration too high	Perform cell treatment with different N/P ratios and cell densities for determining the least toxic amount of LPEI.
Low pDNA recovery after polyplex formation	N/P ratio too low	Increase the amount of LPEI used for complexing pDNA.
Low luciferase signal *in vitro*	Low transfection efficiency of polyplexes	Evaluate the biophysical properties of used polyplexes. Aggregate formation could lead to reduced transfection of cells.
	Usage of overgrown cell passage for transfection assay	Subculture cells for regaining optimal cell growth.
	Cells may not be completely lysed	Increase the incubation time for the lysis step.
Low/no luciferase activity after animal treatment detected	Bradycardia induced through anesthesia during injecting of polyplex-containing solution	Side effects like bradycardia may lead to a reduced transfection of lung tissue. Injection without anesthesia is advised.
	Time between subcutaneous injection of D-luciferin and bioluminescence imaging	Optimal duration between injecting D-luciferin and luciferase detection *in vivo* is 10–15 min.
	Exposure time and binning are too low.	Readjust exposure time and binning as per instructions from the manufacturer.

LPEI, linear polyethylenimine; NTA, nanoparticle tracking analysis.

iv. F/stop: 1
v. Binning: 8
vi. Field of view (FOV): 13.4 cm^2

b. Use the following Caliper Ivis settings for acquiring 3D bioluminescence images:
i. Emission filter set range: 560–640 nm
ii. Excitation blocked
iii. Binning: 8
iv. F/stop: 1
v. Filter position: 60 sec
vi. Field of view (FOV): 13.4 cm^2

c. Acquiring 3D reconstructions requires a number of photon counts of 600–60,000 in at least 3 filters (600–640 nm), which cannot be achieved with polyplexes prepared at an N/P ratio of 6.

5. Image processing can be conducted using a program such as Living image.
6. Define the region of interest (ROI) in 2D images around the lung tissue using an automated contour drawing function for analyzing only the intensity of the bioluminescence signal that is significantly higher than the background.
7. Luciferase activity can be correlated with photons/sec.

3. TIMING

All time points are listed in Table 3.

4. TROUBLESHOOTING

Troubleshooting is shown in Tables 4 and 5.

ANTICIPATED RESULTS

Applying a syringe-pump-based controlled mixing method for pDNA/LPEI complexation results in reproducibly controlled formation of nanoparticles with a narrow size distribution as shown in Fig. 3. NTA was used for high-resolution analysis of both size and ζ-potential of the nanoparticulate polyplexes. For investigating changes in polyplex characteristics as a function of solvent used for polyplexing/transfection, the particle size was analyzed after diluting the polyplexes in HBG/serum-free medium (RPMI 1640), respectively (shown in Fig. 3a).

The positive correlation between DNA complexation and the N/P ratio is shown in Fig. 4 in

Table 5. *Troubleshooting: suggested dilution factors for size and ζ-potential measurements by NTA*

	Dilution factor (for samples prepared at final pDNA conc. of 20 μg/ml)		*Dilution factor (for samples prepared at final pDNA conc. of 200 μg/ml)*	
N/P ratio	*HBG*	*RPMI 1640*	*HBG (for size measurement)*	*2.5 mM NaCl (for ζ-potential measurement)*
3	1/10	1/10	—	—
6	1/50	1/50	1/500	1/40
9	1/100	1/100	1/500	1/40

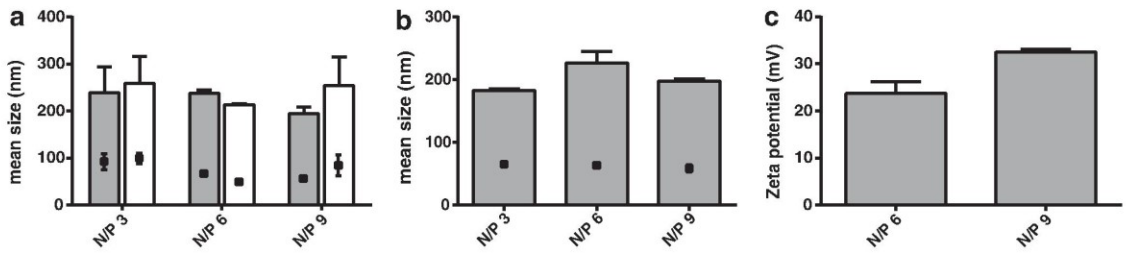


Figure 3. Evaluation of biophysical properties of LPEI-based polyplexes by NTA. All experiments are presented as mean ± SD ($n=3$). **(a)** Size measurement of polyplexes prepared at a final pDNA concentration of 20 μg/ml for *in vitro* transfection. Polyplexes were prepared at different N/P ratios in HBG by controlled mixing and analyzed without incubation time. To investigate changes in the particle size as a function of solvent used for polyplexing/transfection, both HBG (gray bars) and RPMI 1640 (white bars) were used as diluents for NTA measurements. Bars indicate the mean size, and black squares (within each bar) indicate the standard deviation calculated by the NTA software. **(b)** Size measurement of polyplexes prepared at a final pDNA concentration of 200 μg/ml for *in vivo* transfection. All samples were diluted with HBG. Bars indicate the mean size, and black squares (within each bar) indicate the standard deviation calculated by the NTA software. **(c)** ζ-potential measurements were done with samples prepared at 200 μg/ml using 2.5 m*M* NaCl as diluent.

terms of DNA recovery after polyplexation. N/P 3 already leads to full complexation of pDNA at a concentration of 20 μg/ml as indicated by the pDNA recovery of nearly 100%. In case of N/P 3 at a pDNA concentration of 200 μg/ml, the polyplexes precipitated immediately during polyplexation, indicating lower stability. As observed in Fig. 4, the pDNA recovery was also very low in this case, which might be because of lack of full complexation of pDNA, also indicated by precipitation. At higher N/P ratios, the pDNA recovery was 100% irrespective of the pDNA concentration. This indicates the need for applying a certain amount of free LPEI, which is necessary not only to complex pDNA and stabilize the nanoparticles but also to enhance their ability to effectively transfect cells.[13] Therefore, measuring recovery of pDNA after polyplex generation is an important tool for quality assurance.

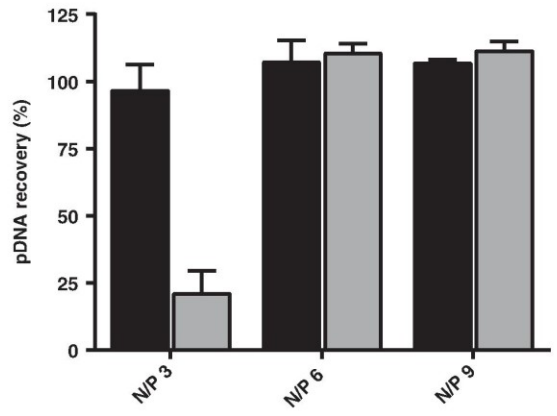


Figure 4. pDNA recovery after polyplex formation. All experiments are presented as mean ± SD ($n=3$). pDNA recovery was evaluated by calculating the percentage ratio between pDNA concentration before and after polyplex formation (black columns: polyplexes prepared at a pDNA concentration of 20 μg/ml; gray columns: polyplexes prepared at a pDNA concentration of 200 μg/ml).

The upscaled polyplex nanoparticles were investigated for efficiency of gene delivery both *in vitro* and *in vivo* models. The optimized *in vitro* transfection protocol was used for A549 lung adenocarcinoma cells just as a model cell type and is expected to work for a broad spectrum of cell lines (with differing transfection efficiency depending on the cell type), as demonstrated in other cell types.[4,20,21] For *in vitro* studies, intracellular and secreted luciferase reporter genes were employed, and expression of respective luciferase proteins was studied as shown in Fig. 5. The upscaled nanoparticles at N/P 6 and N/P 9 showed transfection efficiency comparable to the commercially available transfection agents for both types of luciferases as shown in Fig. 5a and 5b. Activity of intracellularly expressed luciferases needs normalization based on total protein amount. On the other hand, using of secreted luciferases offers advantages of evaluation of the cellular toxicity (Fig. 5c) and total cell count-based normalization of luciferase activity. Upscaled polyplexes (based on firefly luciferase reporter gene) at two different N/P ratios (N/P 6 and 9) were used for monitoring transfection efficiency *in vivo*. Bioluminescence measurement 24 hr post-injection shows a distinct luciferase activity in the chest area (Fig. 6a and 6b), indicating successful gene delivery by the upscaled nanoparticles. Bioluminescence imaging in combination with CT (i.e., 3D mode of acquisition) offers the advantage of localizing the luminescence signal to the lungs of the animal (Fig. 6c). PEI-based polyplexes have been demonstrated to cross pulmonary–endothelial barrier and transfect the

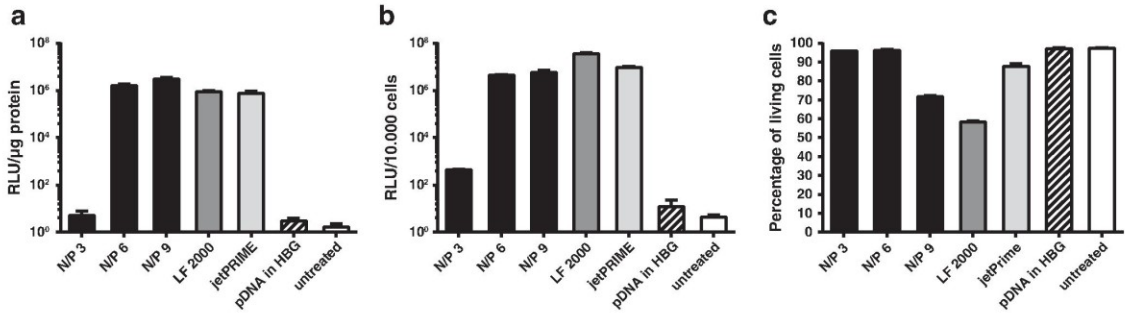


Figure 5. *In vitro* expression of *firefly* and *Gaussia luciferase* reporter transgenes. A549 cells (10,000) were seeded into a 96-well plate and treated with 200 ng pDNA complexed with LPEI (10 kDa) at three different N/P ratios (N/P 3, 6 and 9; prepared at 20 μg/ml) in serum-free medium (RPMI 1640). After 4 hr, RPMI 1640/10% FCS was added to reach a final volume of 200 μl in each well. Both Lipofectamine 2000 (LF 2000) and jetPRIME were used as positive controls. Only pDNA in HBG was used as a negative control. Reporter activity was measured 24 hr after starting the cell treatment ($n=3$). **(a)** Expression of firefly luciferase (*pCpG-hCMV-EF1α-LucSH*) at different N/P ratios: It was detected by lysing the cells followed by measuring luciferase activity. Luciferase activity was normalized according to the amount of protein per well. **(b)** Expression of Gaussia luciferase (*pCMV-Gluc*) at different N/P ratios: It was analyzed in 20 μl of the supernatant. Gaussia luciferase activity was normalized to the total count of living cells per well determined by flow cytometry. The percentage of living cells per well was evaluated using DAPI staining of dead cells as shown in **(c)**.

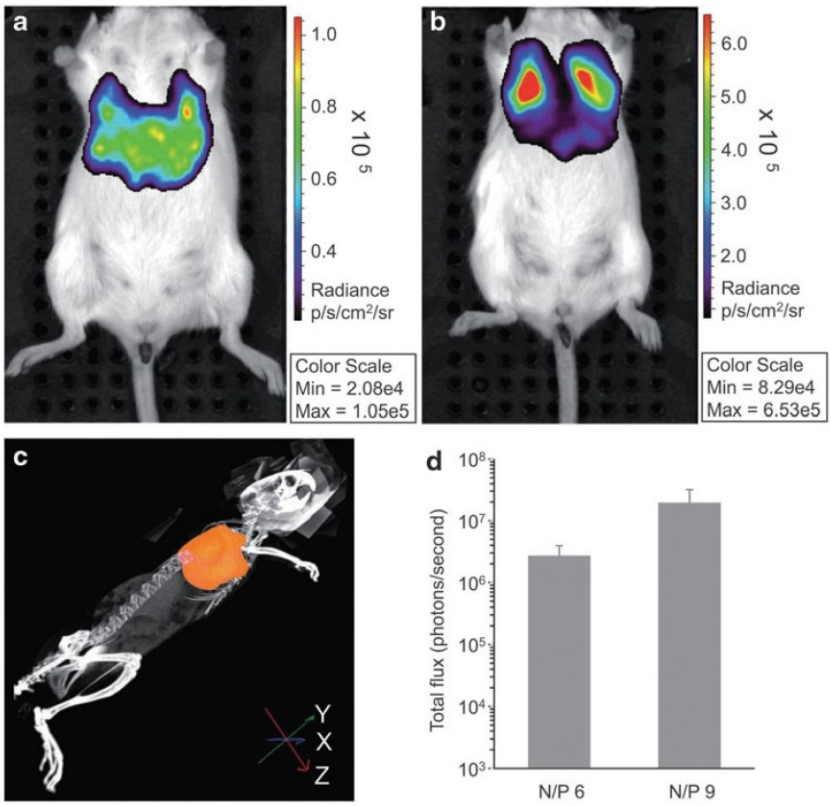


Figure 6. *In vivo* lung expression of firefly luciferase reporter transgene. Polyplexes were prepared at a pDNA concentration of 200 μg/ml using N/P 6 and N/P 9 and immediately injected into the tail vein of BALB/cByJRj mice using a dosage of 2.5 mg/kg. Control mice were injected with 250 μl HBG ($n=3$). After 24 hr of polyplex injection, bioluminescence was measured after administration of D-luciferin (150 mg/kg). CT-based 3D reconstruction enabled localizing the luminescence signal to the lungs. Panels **(a)** and **(b)** show representative 2D bioluminescence images of animals treated with polyplexes at N/P 6 and N/P 9. Panel **(c)** shows representative 3D surface reconstruction of the luminescence signal of an animal treated with polyplexes at N/P 9. Luciferase activity was calculated as photons/sec detected in the region of interest **(d)**.

pulmonary cells as reported in earlier studies.[15,16] Total flux measured in 2D bioluminescence increases with the total amount of polymer used for complexing pDNA as seen in Fig. 6d.

ACKNOWLEDGMENTS

Parts of this work have received support from the EU/EFPIA Innovative Medicines Initiative Joint Undertaking COMPACT Grant No. 115363. J.M. is supported by the uni:docs—fellowship program for doctoral candidates of the University of Vienna.

AUTHOR DISCLOSURE

No competing financial interests exist.

REFERENCES

1. Gehrig S, Sami H, Ogris M. Gene therapy and imaging in preclinical and clinical oncology: Recent developments in therapy and theranostics. Ther Deliv 2014;5:1275–1296.
2. Talsma H, Cherng J, Lehrmann H, et al. Stabilization of gene delivery systems by freeze-drying. Int J Pharm 1997;157:233–238.
3. Anchordoquy TJ, Koe GS. Physical stability of nonviral plasmid-based therapeutics. J Pharm Sci 2000;89:289–296.
4. Kasper JC, Schaffert D, Ogris M, et al. The establishment of an up-scaled micro-mixer method allows the standardized and reproducible preparation of well-defined plasmid/LPEI polyplexes. Eur J Pharm Biopharm 2011;77:182–185.
5. Hirota S, de Ilarduya CT, Barron LG, et al. Simple mixing device to reproducibly prepare cationic lipid-DNA complexes (lipoplexes). Biotechniques 1999;27:286–90.
6. Filipe V, Hawe A, Jiskoot W. Critical evaluation of nanoparticle tracking analysis (NTA) by NanoSight for the measurement of nanoparticles and protein aggregates. Pharm Res 2010;27:796–810.
7. Wightman L, Kircheis R, Rossler V, et al. Different behavior of branched and linear polyethylenimine for gene delivery *in vitro* and *in vivo*. J Gene Med 2001;3:362–372.
8. Goula D, Benoist C, Mantero S, et al. Polyethylenimine-based intravenous delivery of transgenes to mouse lung. Gene Ther 1998; 5:1291–1295.
9. Ferrari S, Moro E, Pettenazzo A, et al. ExGen 500 is an efficient vector for gene delivery to lung epithelial cells *in vitro* and *in vivo*. Gene Ther 1997;4:1100–1106.
10. Goula D, Remy JS, Erbacher P, et al. Size, diffusibility and transfection performance of linear PEI/DNA complexes in the mouse central nervous system. Gene Ther 1998;5:712–717.
11. Di Gioia S, Conese M. Polyethylenimine-mediated gene delivery to the lung and therapeutic applications. Drug Des Devel Ther 2009;2:163–188.
12. Khalil IA, Kogure K, Akita H, et al. Uptake pathways and subsequent intracellular trafficking in nonviral gene delivery. Pharmacol Rev 2006;58:32–45.
13. Boeckle S, von Gersdorff K, van der Piepen S, et al. Purification of polyethylenimine polyplexes highlights the role of free polycations in gene transfer. J Gene Med 2004;6:1102–1111.
14. von Gersdorff K, Sanders NN, Vandenbroucke R, et al. The internalization route resulting in successful gene expression depends on both cell line and polyethylenimine polyplex type. Mol Ther 2006;14:745–753.
15. Goula D, Becker N, Lemkine GF, et al. Rapid crossing of the pulmonary endothelial barrier by polyethylenimine/DNA complexes 965. Gene Ther 2000;7:499–504.
16. Rödl W, Schaffert D, Wagner E, et al. Synthesis of polyethylenimine-based nanocarriers for systemic tumor targeting of nucleic acids. Methods Mol Biol 2013;948:105–120.
17. Ungaro F, De Rosa G, Miro A, et al. Spectrophotometric determination of polyethylenimine in the presence of an oligonucleotide for the characterization of controlled release formulations. J Pharm Biomed Anal 2003;31:143–149.
18. Tannous BA. Gaussia luciferase reporter assay for monitoring biological processes in culture and *in vivo*. Nat Protoc 2009;4:582–591.
19. Tannous BA, Kim DE, Fernandez JL, et al. Codon-optimized Gaussia luciferase cDNA for mammalian gene expression in culture and *in vivo*. Mol Ther 2005;11:435–443.
20. Lenter MC, Garidel P, Pelisek J, et al. Stabilized nonviral formulations for the delivery of MCP-1 gene into cells of the vasculoendothelial system. Pharm Res 2004;21:683–691.
21. Kopp F, Schnoedt M, Haase R, et al. De-targeting by miR-143 decreases unwanted transgene expression in non-tumorigenic cells. Gene Ther 2013;20:1104–1109.

Received for publication February 26, 2016;
accepted after revision May 10, 2016.

Published online: May 11, 2016.

5 Discussion

In the main paper of this thesis, we set the goal to develop a multi-pathway reporter plasmid, focussing on the Wnt, HH and Notch pathways. For this, we generated several reporter plasmids and compared their performance. We utilized various reporter gene constructs that mediated expression of proteins for optical readout, ranging from fluorophores such as eGFP or iRFP720 to bioluminescent enzymes, such as FLuc. In the second work, we transduced breast cancer cells to constitutively express iRFP720^{+}, which then generated lung metastases in an *in vivo* model. We then administered polyplex-aerosol containing FLuc-pDNA to assess the effectivity of intratracheal delivery of polyplexes via microspraying, especially in the breast cancer metastases cells. In a third paper, we generated an up-scaled polyplexing approach, and identified optimal modalities for polyplex-based transfection experiments by investigating expression patterns *in vitro*.

A broad range of different reporter constructs were employed in our projects. This enables a thorough evaluation of the different promoters and reporter genes. Also, we encountered challenges regarding bioluminescent and fluorescent imaging, and observed interesting variations of different normalization methods for transgene expression. In this discussion, we will also look into alternative destabilized and BRET/FRET driven reporter constructs for pathway research, the crosstalk between the Wnt, Notch and HH pathway, and discuss the importance of screening approaches for drug discovery.

Promoter choice is vital for designing reporter systems. Interestingly, even identical promoters by name have been shown to produce different experimental results (115), drawing attention to the need to characterize the expression of any given reporter locally in a laboratory environment. For *in vivo* work, considerations of long-term transgene expression and strength, which are often inversely correlated, are of special concerns. This is well demonstrated by the CMV promoter, which, after providing high expression levels of the transgene at first, is known to be downregulated by methylation

(116). In contrast to this, the PGK promoter has been described to be less methylated (117), but is also a weaker promoter in mammalian cells compared to CMV (118). In our multimodal imaging work, we had issues to separate the relatively weak fluorescence signal from PGK-iRFP720 from the background fluorescence, which persists for example in the digestive tract, despite providing low fluorescent diet seven days prior to the experiment to the mice. As such, switching to a stronger promoter might be required to better investigate far red fluorophores *in vivo*.

In line with the finding that the promoter performance can vary, our results generated with the Notch-pathway sensitive CBF promoter did not match with its description in the literature. CBF:H2B-Venus has been successfully used to image the Notch pathway *in vivo* (119). For Notch pathway induction, we acquired the same plasmid as used in this paper from Addgene, pCAGGS-NICD (#26891). The CBF promoter, as part of the CBFRE-EGFP plasmid, was generated previously to track Notch signalling in brain development, also using NICD for Notch induction (120), corroborating our methodology for pathway activation further. In our hands, non-induced CBF:H2B-Venus had an easily distinguishable Venus signal in flow cytometry, but did not react to Notch induction when co-transfected with pCAGGS-NICD. In contrast, our modified versions CBF-GLuc and CBF-tdTomato did successfully react to Notch induction, even if the fold-increases of signal upon induction were comparatively low. To us, there is no obvious explanation to this phenomenon. For assessing the reasons for this further, we recommend re-cloning of our promoter into the original backbone as well as exchanging the fluorophore on the CBF:H2B-Venus construct, and acquiring the original CBFRE-EGFP construct for rigorous assessment.

We also observed vast differences in the two HH pathway sensitive promoters we evaluated. The promoter PTCH1_WT consists of the original PTCH1 promoter, which encompasses two GLI consensus sequences (5), whereas 12GLI features twelve GLI consensus sequences in front of a truncated thymidine kinase promoter (12, 121). Comparing the performance of the originally acquired promoters for PTCH1_WT and 12GLI directly, which both use FLuc as reporter gene, we saw drastic differences in fold increase upon induction: approximately five times for PTCH1_WT, and around 200 times for 12GLI. While the difference in performance could easily be correlated to the amount

of GLI consensus sites, this stresses the importance of carefully evaluating promoters, and tailoring their choice to the experimental requirements.

In our work on the Wnt, HH and Notch pathway reporters, we had the opportunity to work with three different luciferases. One of them was the relatively novel NLuc, which excels in brightness (20). This brightness led to unforeseen challenges. The NLuc transgene, when driven in preliminary experiments with the CMV promoter, was so bright that the luminescence in a 96-well plate was clearly visible with the human eye in conditions of very dim light. The apparatus used for measuring was unable to evaluate the signal due to its extraordinary strength, falsely registering it as “opened cover” due to its brightness. Furthermore, even in our experiments with TOP-NLuc, we had to take care to distribute the experimental conditions in a sophisticated manner. For example, we could not place wells with low and high NLuc signal too close to each other, as the signal spillover into adjacent wells was considerable.

Interestingly, we also noticed that the machine we used for evaluation of bioluminescence signals carried over signal from one well to the other. This resulted in problems if we first measured a high-signal well, and afterwards any low-signal well, even if the two were spatially distinctly separated. We noticed that this decay in remaining sensor signal was time-dependent. As a result, we resorted to measuring the wells on 96-well plates in several groups, starting with the conditions where we expected the lowest signal. We adopted this procedures of separating conditions spatially and reading them in groups of similar luminescence for all luciferases, as we noticed identical problems, although in less striking magnitudes, for GLuc and FLuc. Even though our method certainly reduced effectiveness in terms of time as well as the number of conditions that could be placed on one well plate, we advocate adopting it generally to increase signal fidelity, in case large variations in signal strength are to be expected within an experiment. This challenge again highlights rigorous assay evaluation, as an oversight of such signal spillover has the potential to severely distort experimental results.

Additionally, the lack of substrate specificity between NLuc and GLuc required a careful assay setup. The GLuc substrate coelenterazine can also be utilized by NLuc, as it is an analogue of furimazine. To complicate matters further, NLuc and GLuc emission spectra are comparable (122). As such, in our single pathway luciferase assays, the conditions in which NLuc signal was normalized with GLuc required special attention. As a solution, we used secreted GLuc, and intracellular NLuc. For the normalization measurement all of the supernatant was removed from the wells and replaced by phosphate buffered saline (PBS), and the original plate was then refrigerated. Of the supernatant, a fraction was measured for GLuc luminescence. In a second step, the cells in the original plate were assessed for their NLuc signal. With this method, we could prevent a spillover of NLuc signal into the GLuc luminescence measurement, which would have been more powerful as NLuc luminescence is very bright. On the other hand, it cannot be excluded that unsecreted, intracellular GLuc signal spilled into the NLuc measurement, but it has been shown that GLuc activity to furimazine is negligible, and thus the NLuc luminescence should not be significantly influenced by GLuc signal (123).

In both papers that focus on imaging, we noticed that working with fluorescence is technically more challenging than luminescence. In our *in vivo* studies, fluorescence values were determined to be comparatively low. Autofluorescence from the digestive tract was an issue, despite switching to low fluorescent diet a week before imaging. In our work focussing on pathway reporter constructs, we faced two main issues with the fluorescent reporter genes utilized. Considerably larger amounts of polyplexes were needed to effectively investigate the signal fold increases upon pathway induction, compared to the luciferase reporter constructs. Whereas we used below 100ng total polyplexes per well in the luminescent conditions, this value increased to a standard of 800ng for investigations of fluorophore-based reporter constructs. Raising the amount of polyplex is associated with higher cytotoxicity, and is thus suboptimal (111). That lower amounts of polyplexes were required for the luciferase reporters could be due to the signal amplification that is present in luciferase assays, with the reporter gene being an enzyme that can convert large amounts of its substrate molecules, with each conversion resulting in a light pulse (27). Still, fluorophores offer considerable advantages, such as

the established possibility to image processes in single cells (119), and even intracellular structures with highly sophisticated methods such as single-molecule fluorescence microscopy (124). As such, choice of reporter gene is again something that needs to be considered wisely.

Employing several fluorophores in our 3P-Fluor construct required subsequent signal compensation of the flow cytometry data. Especially the emission of eGFP was problematic, as it overlapped broadly with other fluorophores, especially tdTomato (see Tab. 1). Furthermore, eGFP was CMV-promoter driven, resulting in a very high eGFP signal. Even after compensation, detection of the other signals was complicated, as eGFP outshone the weaker and rarer signals. In a revision of this construct, we would emit eGFP from the construct, as it was not essential as pathway reporter: it was only included to report positive transcription or transduction.

Signal normalization, as mentioned in the introduction, is often a necessary step in reporter gene assays. In our paper, we noticed large and reproducible differences on the normalized luciferase-based results, which were correlated to the choice of normalization method. Specifically, we found normalized luciferase signal strength to be connected to the either vector or life-cell based normalization. Interestingly, papers that compare different normalization modes are very sparse, and as thus there is value in discussing our findings here.

We used two modes of normalization: (1) vector normalization, in our case a co-transfection with a suitable luciferase; (2) CellTiter-Fluor, a commercially available kit (125, 126). Per default, we used vector normalization, which is also able to take into account transfection efficiency as well as the overall transcription potential of the treated cells. As such, vector normalization is deemed to be a more accurate method (36). We performed normalization with either GLuc or FLuc, depending on the reporter gene used for the pathway. For the evaluation of our 3P-Luc constructs, normalizing with luciferases was not feasible, as all possible luciferases (FLuc, GLuc, NLuc) were already part of the construct. Here, we used CellTiter-Fluor, which is an indicator of cell viability.

In short, this assay assesses the activity of proteases that become labile if cellular membranes are damaged.

We noticed striking differences between the normalized luciferase signals of these two normalization methods (Tab. 2). Interestingly, there is no clear tendency regarding a general increase or decrease upon usage of one or the other method, and the fold increase after pathway induction increases a log scale for TOP-NLuc, decreases half for GLI-FLuc, and disappears in CBF-GLuc. This deviations also indicate that it is not a systemic phenomenon, but that the effect on each individual reporter gene assay was varying, indicating distinct causal chains. If we assume that the baseline pathway-reporter associated luminescence stays the same, then the relative signal of fold increase upon induction increases if the normalization signal decreases, and vice versa.

It has to be said that the two normalization methods evaluate different parameters. In case of CellTiter-Fluor, cell viability is assessed. Vector normalization, in contrast, depends on the number of living cells, their transfectability, and the transgene expression. It thus more directly reflects the subpopulation of cells in which the actual reporter is likely to be expressed. Still, given that the two normalization techniques are similarly different in this respect for all reporter genes investigated, one would assume a similar effect, if this is the only reason for the observed variation of the post-normalization signal.

Reporter gene	**Vector normalization**	**CellTiter-Fluor normalization**
	Fold increase upon pathway induction (approx.)	
TOP-NLuc	100	1000
GLI-FLuc	200	100
CBF-Gluc	3	None

Table 2: Influence of normalization method on luciferase assays*. Two different normalization methods were applied, and the fold-increase of baseline signal versus pathway-induced signal compared for each reporter gene. Shown here are the approximate values of the normalized signals Methods for the induction of reporter genes were identical.*

Communication of our protocols to the manufacturer excluded known assay incompatibilities of our method and CellTiter-Fluor (J. Adam, Promega, personal communication, October 15, 2018). As another explanation, using CMV-driven luciferase variants for vector normalization could have skewered the outcome. CMV promoter, and its enhancer elements, are also receptive towards external and internal stimuli, likely because of the transcription factor binding sites, and the CMV promoter has be shown to be sensitive towards JNK pathway activation (127, 128). Thus it can be speculated that modification of cellular pathways in our induction experiments had an influence on CMV-luciferase expression. As such, investigating if pathway induction of Wnt, HH or Notch also influences CMV-driven expression would be valuable.

Pathway induction could also have affected CellTiter-Fluor, as pathway status could interact with intracellular proteases. Induction of the canonical Wnt pathway has been described to increase protease activity (129). Interestingly, this effect would have an effect contrary to our observations. In our Wnt pathway activation experiments, normalized signal increased for CellTiter-Fluor, which would have meant that protease activity would have to be decreased. Literature for a correlation of protease activity and pathways activation does not exist for the HH or Notch pathway.

Adding a layer of complexity, LPEI actively damages membranes, which in turn is important for the CellTiter-Fluor signal. PEI is internalized a few hours after transfection (130), and disturbances such as destruction of the mitochondrial membrane, and associated activation of caspases which can lead to apoptosis, persist at least up to 24 hours post-transfection (131). As such, results of CellTiter-Fluor in PEI-transfection might be influenced by caspases, and thus protease activity. As the exact proteases required for CellTiter-Fluor readout are proprietary knowledge, we can only speculate that PEI addition might influence this normalization approach. Still, as all conditions received comparable amounts of LPEI, we would again expect a similar signal shift for changes in normalized signal when we compare the two normalization methods over all three pathways. Additionally, as mentioned above, induction of developmental pathways might in turn have influenced apoptosis signalling, and thus the proteases required for CellTiter-Fluor. All three pathways are known to interact with apoptosis (132-134).

Taken together, we suggest that CellTiter-Fluor might be suboptimal for normalization of PEI-transfection experiments. Instead, alternatives that evaluate protein content as surrogate marker for cell viability, such as MTT assay or the Bredford assay, could be used. Furthermore, if constitutively expressed luciferases should be used for normalization, we recommend replacing the CMV-promoter with one that is less prone to react to numerous transcription factors.

In our reporter design for the three developmental pathways, we utilized the expression of reporter genes to visualize pathway signalling. While this is a straightforward approach, accumulation of reporter proteins within the cells has a negative impact on the reporter signal dynamics. Fluorescent reporter proteins often exhibit half-lives or around 24 hours (135). As such, the measured signal is an accumulation of protein stability and promoter activity, and reporters with long half-lives are not especially well suited to determine kinetics, which would be ideal for pathway signalling. The luciferases used in our experiments show half-lives from 3 hours (FLuc), <6 hours (NLuc) to 6 days (GLuc) (18, 136).

As a solution, reporter variants with shorter half-lives can be utilized to increase the dynamic range. For this, native proteolysis signals can be used. A well-known example is the PEST destruction domain, a peptide sequence consisting of proline (P), glutamate (E), serine (S) and threonine (T). The PEST sequence leads to rapid degradation when present in proteins (137). A short-lived variant of NLuc, NLucP, features such a PEST sequence. It shows an intracellular stability of around 20 minutes, with a reduced signal intensity (138). As we experienced issues with extremely high NLuc signals, replacing NLuc with NLucP thus holds promise for our approach regarding both improved signal dynamics and a more convenient signal strength. Another variant, FLucP, has a half-live of around 2 hours (138). For GLuc, a destabilized variant exists, which utilizes three PEST sequences, for which the half-live has not yet been published (139).

For the fluorophores, PEST-modified versions exist of eGFP with a half-life of 2 hours (140), and tdTomato, with unknown half-life (141). Usage of destabilized versions could thus increase the accurate measuring of the signal dynamics, to the cost of signal

intensity. As low signal intensity was especially a challenge in our fluorophore reporters, it would have to be seen if using destabilized reporter versions would be feasible overall.

An alternative would be the usage of a system which only gives a short-lived signal upon active signalling. This would offer detection of pathway activity at a much finer resolution. For this, BRET/FRET based approaches could be employed. In the literature, BRET/FRET has been widely used to investigate signalling pathways.

Several discoveries regarding the HH pathway have been made by using BRET/FRET (142). Same goes for the Wnt pathway (143, 144). FRET has also been used to show gene regulation by investigation the formation of transcriptional complexes. In a paper, the dimerization of the notch transcription complex on DNA was researched using FRET, illuminating notch gene regulation (145). Interestingly, BRET as well as FRET seem to be rather uncommon in Notch pathway research.

BRET/FRET is mainly used to investigate protein-protein interactions. For example, investigating the HH signalling pathway, Praktiknjo et al. used the EPAC-BRET system, which is sensitive to changes in cAMP (146). Here, RLuc and GFP10 were used as donor/acceptor pair (147), comparable to the natively occurring BRET observed in *R. reniformis*. Similar to our approach, the HH pathway was induced by n-terminal *D. melanogaster* HH protein. Here, upon binding of cAMP to the BRET system, the BRET signal decreases. Also, in this work BRET was used to uncover molecular interactions within the HH pathway, not to show induction per se.

In an experimental series investigating the Wnt pathway, different central proteins of this pathway were fashioned into BRET pairs, such as β-catenin-RLuc and GSK3-GFP2, using HEK293T cells. For pathway induction, purified Wnt3a protein was used. Unfortunately, no statistical analyses was performed, and as such the effectiveness of this approach is unclear (148). This approach would be interesting for visualizing pathway induction, also in HH and Notch.

BRET can also be used to investigate the interplay between different signalling modules. To explore the interaction of β-catenin and glucagon, the involvement of LRP5 and the glucagon receptor was investigated by using BRET (149). Here, LRP5 was tagged with RLuc and the glucagon receptor with YFP, showing direct interaction of these two molecules, indicating cross-talk of Wnt and glucagon signalling.

Regarding sensitivity, the work of van Unen et al. has shown that at least for their assessed FRET pairs, single-cell quantification of histamine signalling is possible (150)

Our literature research shows that a lot of exciting BRET/FRET approaches for uncovering signalling pathway protein interaction exist, but no readily available and statistically verified BRET/FRET pair is used for detecting Wnt, HH and Notch signalling activity in general, and any existing system would need to be optimized for this use first. At the same time, not all fluorophores utilized in our research exist as destabilized versions. As such, any update of our system with one of these two solutions for enhancing signal dynamics would require novel sets of experiments for first establishing any such system for our aim of visualizing pathway activity of these three pathways.

While BRET/FRET based approaches could increase the signal dynamics remarkably, detection of several pathways at once would be challenging. Several BRET/FRET pairs would need to be employed in parallel to detect the activity of the Wnt, HH and Notch pathway, increasing the complexity of such a system, as well as the interplay of the individual components. Additionally, the size of our total plasmid constructs 3P-Fluor and 3P-Luc is large, but still allows for lentivirus generation. In contrast, a BRET/FRET based approach would need to include more genetic information to contain all necessary donor/acceptor pairs, thus rendering lentivirus generation unlikely. Taken together, BRET/FRET approaches enable interesting insight into signal dynamics, while destabilized reporter gene versions can be seen as compromise between signal dynamics, complexity and size of the genetic payload when lentivirus generation is aimed at.

Another challenge is the cross-talk of the Wnt, HH and Notch pathway (Fig. 5). Especially in cancer stem cells (CSC), where the modulation of these pathways is estimated to be central to therapeutic success, this intense cross talk is researched (45, 47). As mentioned in the introduction, the effect of Notch signalling is conditional, and depends also on its interplay with the Wnt and HH pathway.

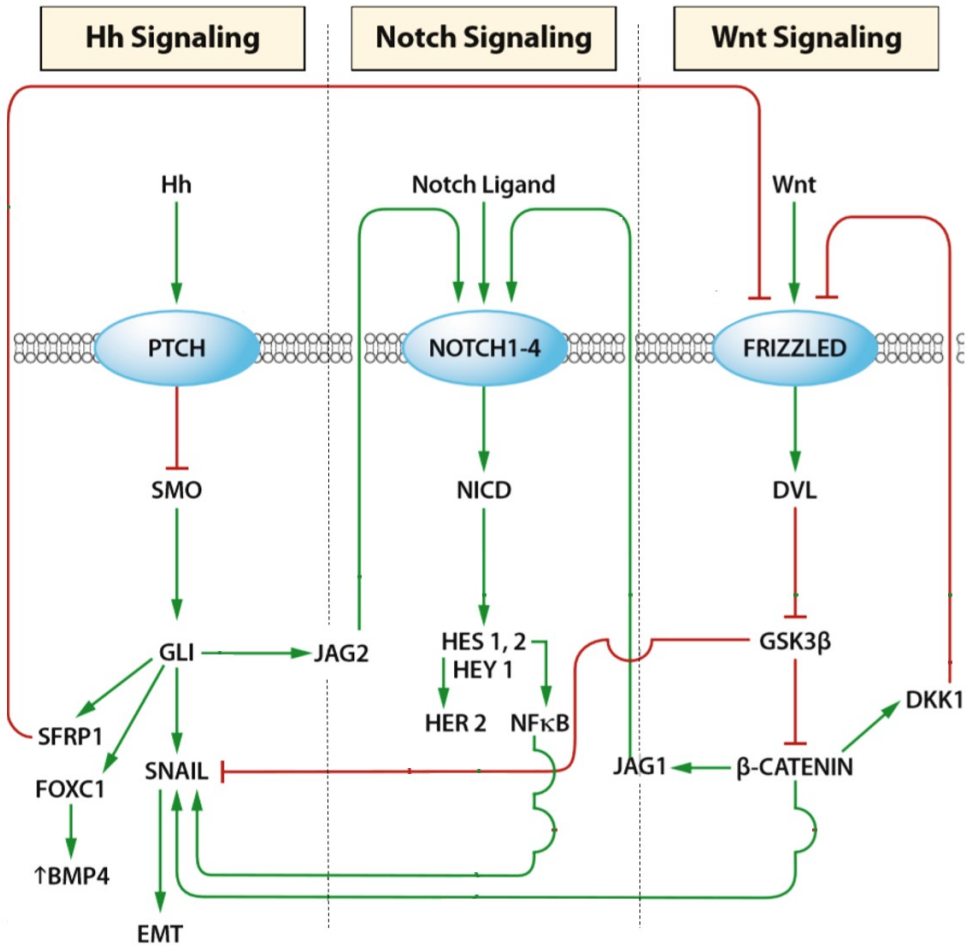


Figure 5: Interplay between the HH, Notch and Wnt signalling pathways. Green colour depicts activating, red inhibiting interactions. Modified from (151).

A close interaction between Notch and Wnt activation has been shown in several studies. In colourectal cancer, progastrin is secreted, which in turn activates the Wnt and Notch pathway (152). Similarly, in breast CSC, Mel-18 knockdown increases Wnt and Notch signalling, leading to self-renewal of the CSC (153). In other studies, HH signalling was shown to inhibit Wnt in gastric cancer (154). Interestingly, in glioblastoma cells, Notch inhibition has been shown to upregulate the HH and Wnt pathway (155).

This insight points out the concept of therapeutic resistance, in which cancer cells compensate for the effects of therapeutic interventions, such as downregulation of one pathway, by modulation of other pathways. As such, hopes rest in clinical approaches that target several pathways at once. This method is also under investigation in clinical

cancer stem cell eradication, as CSC are suspected to evade therapy by modification of an interconnected pathway (45). CSC are thought to be especially resistant to radio- as well as chemotherapy. They are thought to play an important part in disease relapse, and as such, suppression of this cell type in cancer is estimated to be of high importance (156). Numerous clinical trials with compounds modulating these three pathways in cancers, partly also in combination, are set in motion or have already ended (45). In this respect, targeting developmental signalling pathways remains a promising approach, and it remains to be seen how well the insights from the bench can be translated to the bedside.

A reporter system in which the reaction of several pathways upon treatment can be analysed at once would be of advantage. Other efforts at designing multi-pathway reporter systems have already been made. Some commercial kits, for example the multi-pathway reporter solution by Qiagen, utilizes dual luciferases (FLuc as reporter and RLuc for normalization), but performs the analysis for each pathway in separate, duplicate wells (157). GM Biosciences markets a similar assay (158). In a kit that co-expresses destabilized copepod GFP and a luciferase, System Biosciences sells both plasmid and virus variants of various reporter constructs, such as a Notch reporter system (159). In an RNA-sequencing focussed approach, Zhang *et al.* investigated the status of 917 pathway reporter genes to determine the state of 154 signalling cascades, but this approach requires an intricate bioinformatics analysis (160). Ammeux *et al.* researched the activity of seven signalling pathways in *Drosophila melanogaster* cell lines, by using quantitative qPCR as well as other methods which inspect mRNA levels (161). It seems that constructing multi-pathway lentiviral constructs, as we did in our work, remains a novel approach.

As mentioned above, the search for effective assays for drug discovery is still a highly relevant topic. In recent years, tremendous progress has been made with phenotypic drug discovery (PDD). In contrast to target-based drug discovery, were a target molecule of interest is first defined and then screens are performed to find modulating substances, PDD approaches this process more broadly. For example, PDD looks at the response of signalling pathways upon compound addition, without setting a pre-defined molecular target (162). Reporter constructs which could screen several pathways at once

hold high value for PDD. Due to its broadness, the PDD approach is more likely to uncover serendipitous findings, and aims to first discover an effect, only then proceeding to unravel its molecular basis and/or therapeutic effect. Of course, PDD approaches still suffer from translating *in vitro* findings to clinically effective drugs. However, in some areas such as anti-infective or monogenetic disease compound research, translatability of PDD derived findings is high. In contrast, disease types which feature highly interconnected and partly evading systems such as oncology, PDD-based assays are less effective. In such disease areas, a rational assay setup is especially important and challenging, and should include e.g. replication of external factors such as 3D-environments, and should be highly disease-specific, as laid out in Vincent *et al.* in their "rule of 3" publication (163). Future work in the area of drug discovery will need to implement solutions to both allow serendipitous as well as therapy-relevant discoveries.

Taken together, refining of our pathway reporter system is possible in several ways. Most promising is a modification for improved signalling dynamics of the luciferase reporters by exchanging the reporter proteins to destabilized versions. Also, an optimized solution for 3P-Luc normalization should be implemented in the future. All in all, we are hopeful that our insights into reporter construct design and assay implementation will move us into the direction of a combined Wnt, HH and Notch reporter system, which holds promise for PDD-driven drug discovery.

6 References

1. Niu G, Chen X. Molecular imaging with activatable reporter systems. Theranostics. 2012;2(4):413.
2. Schenborn E, Groskreutz D. Reporter gene vectors and assays. Molecular biotechnology. 1999;13(1):29-44.
3. Alam J, Cook JL. Reporter genes: application to the study of mammalian gene transcription. Analytical biochemistry. 1990;188(2):245-54.
4. Xiao Y-L, Redman JC, Monaghan EL, Zhuang J, Underwood BA, Moskal WA, et al. High throughput generation of promoter reporter (GFP) transgenic lines of low expressing genes in Arabidopsis and analysis of their expression patterns. Plant Methods. 2010;6(1):18.
5. Winklmayr M, Schmid C, Laner-Plamberger S, Kaser A, Aberger F, Eichberger T, et al. Non-consensus GLI binding sites in Hedgehog target gene regulation. BMC molecular biology. 2010;11(1):2.
6. Stadhouders R, van den Heuvel A, Kolovos P, Jorna R, Leslie K, Grosveld F, et al. Transcription regulation by distal enhancers: who's in the loop? Transcription. 2012;3(4):181-6.
7. Rushton PJ. What Have We Learned About Synthetic Promoter Construction? Plant Synthetic Promoters: Springer; 2016. p. 1-13.
8. Qin JY, Zhang L, Clift KL, Hulur I, Xiang AP, Ren B-Z, et al. Systematic comparison of constitutive promoters and the doxycycline-inducible promoter. PloS one. 2010;5(5):e10611.
9. Ede C, Chen X, Lin M-Y, Chen YY. Quantitative analyses of core promoters enable precise engineering of regulated gene expression in mammalian cells. ACS synthetic biology. 2016;5(5):395-404.
10. Veeman MT, Slusarski DC, Kaykas A, Louie SH, Moon RT. Zebrafish prickle, a modulator of noncanonical Wnt/Fz signaling, regulates gastrulation movements. Current Biology. 2003;13(8):680-5.
11. Hsieh J, Henkel T, Salmon P, Robey E, Peterson MG, Hayward SD. Truncated mammalian Notch1 activates CBF1/RBPJk-repressed genes by a mechanism resembling that of Epstein-Barr virus EBNA2. Molecular and cellular biology. 1996;16(3):952-9.
12. Kogerman P, Grimm T, Kogerman L, Krause D, Undén AB, Sandstedt B, et al. Mammalian suppressor-of-fused modulates nuclear–cytoplasmic shuttling of Gli-1. Nature cell biology. 1999;1(5):312.
13. Powell SK, Rivera-Soto R, Gray SJ. Viral expression cassette elements to enhance transgene target specificity and expression in gene therapy. Discovery medicine. 2015;19(102):49.
14. Silhavy TJ, Beckwith JR. Uses of lac fusions for the study of biological problems. Microbiological reviews. 1985;49(4):398.
15. De Wet JR, Wood KV, Helinski DR, DeLuca M. Cloning of firefly luciferase cDNA and the expression of active luciferase in Escherichia coli. Proceedings of the National Academy of Sciences. 1985;82(23):7870-3.
16. Fan F, Wood KV. Bioluminescent assays for high-throughput screening. Assay and drug development technologies. 2007;5(1):127-36.
17. Andreu N, Zelmer A, Fletcher T, Elkington PT, Ward TH, Ripoll J, et al. Optimisation of bioluminescent reporters for use with mycobacteria. PloS one. 2010;5(5):e10777.
18. Thorne N, Inglese J, Auld DS. Illuminating insights into firefly luciferase and other bioluminescent reporters used in chemical biology. Chemistry & biology. 2010;17(6):646-57.
19. Haddock SH, Moline MA, Case JF. Bioluminescence in the sea. Annual Review of Marine Science. 2010;2:443-93.
20. England CG, Ehlerding EB, Cai W. NanoLuc: a small luciferase is brightening up the field of bioluminescence. Bioconjugate chemistry. 2016;27(5):1175-87.

21.Lu B, Green BA, Farr JM, Lopes F, Van Raay TJ. Wnt drug discovery: weaving through the screens, patents and clinical trials. Cancers. 2016;8(9):82.
22.Chalfie M, Tu Y, Euskirchen G, Ward WW, Prasher DC. Green fluorescent protein as a marker for gene expression. Science. 1994;263(5148):802-5.
23.Rodriguez EA, Campbell RE, Lin JY, Lin MZ, Miyawaki A, Palmer AE, et al. The growing and glowing toolbox of fluorescent and photoactive proteins. Trends in biochemical sciences. 2017;42(2):111-29.
24.Shaner NC, Steinbach PA, Tsien RY. A guide to choosing fluorescent proteins. Nature methods. 2005;2(12):905.
25.Smith AM, Mancini MC, Nie S. Bioimaging: second window for in vivo imaging. Nature nanotechnology. 2009;4(11):710.
26.Roederer M. Spectral compensation for flow cytometry: visualization artifacts, limitations, and caveats. Cytometry: The Journal of the International Society for Analytical Cytology. 2001;45(3):194-205.
27.Ozawa T, Yoshimura H, Kim SB. Advances in fluorescence and bioluminescence imaging. Analytical chemistry. 2012;85(2):590-609.
28.Boute N, Jockers R, Issad T. The use of resonance energy transfer in high-throughput screening: BRET versus FRET. Trends in pharmacological sciences. 2002;23(8):351-4.
29.Wu P, Brand L. Resonance energy transfer: methods and applications. Analytical biochemistry. 1994;218(1):1-13.
30.Xu Y, Piston DW, Johnson CH. A bioluminescence resonance energy transfer (BRET) system: application to interacting circadian clock proteins. Proceedings of the National Academy of Sciences. 1999;96(1):151-6.
31.Morin JG, Hastings JW. Energy transfer in a bioluminescent system. Journal of cellular physiology. 1971;77(3):313-8.
32.Miyawaki A. Development of probes for cellular functions using fluorescent proteins and fluorescence resonance energy transfer. Annual review of biochemistry. 2011;80:357-73.
33.Xie Q, Soutto M, Xu X, Zhang Y, Johnson CH. Bioluminescence resonance energy transfer (BRET) imaging in plant seedlings and mammalian cells. Molecular Imaging: Springer; 2011. p. 3-28.
34.Goyet E, Bouquier N, Ollendorff V, Perroy J. Fast and high resolution single-cell BRET imaging. Scientific reports. 2016;6:28231.
35.Dyer BW, Ferrer FA, Klinedinst DK, Rodriguez R. A noncommercial dual luciferase enzyme assay system for reporter gene analysis. Analytical biochemistry. 2000;282(1):158-61.
36.Schagat T, Paguio A, Kopish K. Normalizing genetic reporter assays: approaches and considerations for increasing consistency and statistical significance. Cell Notes. 2007;17:9-12.
37.Weber K, Thomaschewski M, Warlich M, Volz T, Cornils K, Niebuhr B, et al. RGB marking facilitates multicolor clonal cell tracking. Nature medicine. 2011;17(4):504.
38.Weber K, Bartsch U, Stocking C, Fehse B. A multicolor panel of novel lentiviral "gene ontology"(LeGO) vectors for functional gene analysis. Molecular therapy. 2008;16(4):698-706.
39.Gomez-Nicola D, Riecken K, Fehse B, Perry VH. In-vivo RGB marking and multicolour single-cell tracking in the adult brain. Scientific reports. 2014;4:7520.
40.Thomaschewski M, Riecken K, Unrau L, Volz T, Cornils K, Ittrich H, et al. Multi-color RGB marking enables clonality assessment of liver tumors in a murine xenograft model. Oncotarget. 2017;8(70):115582.
41.Mohme M, Maire CL, Riecken K, Zapf S, Aranyossy T, Westphal M, et al. Optical barcoding for single-clone tracking to study tumor heterogeneity. Molecular Therapy. 2017;25(3):621-33.
42.Albers J, Danzer C, Rechsteiner M, Lehmann H, Brandt LP, Hejhal T, et al. A versatile modular vector system for rapid combinatorial mammalian genetics. The Journal of clinical investigation. 2015;125(4):1603.
43.Katzen F. Gateway® recombinational cloning: a biological operating system. Expert opinion on drug discovery. 2007;2(4):571-89.
44.Giancotti FG. Deregulation of cell signaling in cancer. FEBS letters. 2014;588(16):2558-70.

45.Takebe N, Miele L, Harris PJ, Jeong W, Bando H, Kahn M, et al. Targeting Notch, Hedgehog, and Wnt pathways in cancer stem cells: clinical update. Nature reviews Clinical oncology. 2015;12(8):445-64.
46.Peitzsch C, Tyutyunnykova A, Pantel K, Dubrovska A, editors. Cancer stem cells: the root of tumor recurrence and metastases. Seminars in cancer biology; 2017: Elsevier.
47.Koury J, Zhong L, Hao J. Targeting signaling pathways in cancer stem cells for cancer treatment. Stem cells international. 2017;2017.
48.Nusse R, Clevers H. Wnt/β-catenin signaling, disease, and emerging therapeutic modalities. Cell. 2017;169(6):985-99.
49.Kusserow A, Pang K, Sturm C, Hrouda M, Lentfer J, Schmidt HA, et al. Unexpected complexity of the Wnt gene family in a sea anemone. Nature. 2005;433(7022):156.
50.Willert K, Brown JD, Danenberg E, Duncan AW, Weissman IL, Reya T, et al. Wnt proteins are lipid-modified and can act as stem cell growth factors. Nature. 2003;423(6938):448.
51.Gilbert SF. Developmental biology. Sunderland, Mass.: Sinauer; 2006.
52.Rubinfeld B, Souza B, Albert I, Muller O, Chamberlain SH, Masiarz FR, et al. Association of the APC gene product with beta-catenin. Science. 1993;262(5140):1731-4.
53.de Sousa e Melo F, Vermeulen L. Wnt signaling in cancer stem cell biology. Cancers. 2016;8(7):60.
54.Briscoe J, Thérond PP. The mechanisms of Hedgehog signalling and its roles in development and disease. Nature reviews Molecular cell biology. 2013;14(7):416.
55.Merchant AA, Matsui W. Targeting Hedgehog—a cancer stem cell pathway. Clinical cancer research. 2010:1078-0432. CCR-09-2846.
56.Cochrane C, Szczepny A, Watkins D, Cain J. Hedgehog signaling in the maintenance of cancer stem cells. Cancers. 2015;7(3):1554-85.
57.Rubin LL, de Sauvage FJ. Targeting the Hedgehog pathway in cancer. Nature reviews Drug discovery. 2006;5(12):1026.
58.Chamoun Z, Mann RK, Nellen D, von Kessler DP, Bellotto M, Beachy PA, et al. Skinny hedgehog, an acyltransferase required for palmitoylation and activity of the hedgehog signal. Science. 2001;293(5537):2080-4.
59.Vokes SA, Ji H, McCuine S, Tenzen T, Giles S, Zhong S, et al. Genomic characterization of Gli-activator targets in sonic hedgehog-mediated neural patterning. Development. 2007;134(10):1977-89.
60.Kopan R, Ilagan MXG. The canonical Notch signaling pathway: unfolding the activation mechanism. Cell. 2009;137(2):216-33.
61.Liu J, Sato C, Cerletti M, Wagers A. Notch signaling in the regulation of stem cell self-renewal and differentiation. Current topics in developmental biology. 92: Elsevier; 2010. p. 367-409.
62.Aster JC, Pear WS, Blacklow SC. The varied roles of Notch in cancer. Annual Review of Pathology: Mechanisms of Disease. 2017;12:245-75.
63.Venkatesh V, Nataraj R, Thangaraj GS, Karthikeyan M, Gnanasekaran A, Kaginelli SB, et al. Targeting Notch signalling pathway of cancer stem cells. Stem cell investigation. 2018;5.
64.Schwanbeck R. The role of epigenetic mechanisms in Notch signaling during development. Journal of cellular physiology. 2015;230(5):969-81.
65.Lu FM, Lux SE. Constitutively active human Notch1 binds to the transcription factor CBF1 and stimulates transcription through a promoter containing a CBF1-responsive element. Proceedings of the National Academy of Sciences. 1996;93(11):5663-7.
66.Kovall RA, Gebelein B, Sprinzak D, Kopan R. The canonical Notch signaling pathway: structural and biochemical insights into shape, sugar, and force. Developmental cell. 2017;41(3):228-41.
67.Jahan-Tigh RR, Ryan C, Obermoser G, Schwarzenberger K. Flow cytometry. Journal of Investigative Dermatology. 2012;132(10):e1.
68.BD Biosciences . BD Flow Cytometry Technical Bulletin2008 30.12.2018:[4 p.]. Available from: https://www.bdbiosciences.com/documents/BD_Research_FlowCyto_TechBulletin.pdf. Accessed 31.03.2019

69.Cook E, Stahl J, Lowe L, Chen R, Morgan E, Wilson J, et al. Simultaneous measurement of six cytokines in a single sample of human tears using microparticle-based flow cytometry: allergics vs. non-allergics. Journal of immunological methods. 2001;254(1-2):109-18.
70.Zinchenko A, Devenish SR, Kintses B, Colin P-Y, Fischlechner M, Hollfelder F. One in a million: flow cytometric sorting of single cell-lysate assays in monodisperse picolitre double emulsion droplets for directed evolution. Analytical chemistry. 2014;86(5):2526-33.
71.O'Donnell EA, Ernst DN, Hingorani R. Multiparameter flow cytometry: advances in high resolution analysis. Immune network. 2013;13(2):43-54.
72.Goedhart J, Von Stetten D, Noirclerc-Savoye M, Lelimousin M, Joosen L, Hink MA, et al. Structure-guided evolution of cyan fluorescent proteins towards a quantum yield of 93%. Nature communications. 2012;3:751.
73.Branchini BR, Southworth TL, Fontaine DM, Kohrt D, Florentine CM, Grossel MJ. A Firefly Luciferase Dual Color Bioluminescence Reporter Assay Using Two Substrates To Simultaneously Monitor Two Gene Expression Events. Scientific reports. 2018;8(1):5990.
74.Novus Spectra Viewer: Novus Biologicals; 2018. Available from: https://www.novusbio.com/spectraviewer . Accessed 31.03.2019
75.Stacer AC, Nyati S, Moudgil P, Iyengar R, Luker KE, Rehemtulla A, et al. NanoLuc reporter for dual luciferase imaging in living animals. Molecular imaging. 2013;12(7):7290.2013. 00062.
76.Yankeelov TE, Abramson RG, Quarles CC. Quantitative multimodality imaging in cancer research and therapy. Nature Reviews Clinical Oncology. 2014;11(11):670.
77.Choi YJ, Oh S-G, Singh TD, Ha J-H, Kim DW, Lee SW, et al. Visualization of the biological behavior of tumor-associated macrophages in living mice with colon cancer using multimodal optical reporter gene imaging. Neoplasia. 2016;18(3):133-41.
78.Park W, Yang HN, Ling D, Yim H, Kim KS, Hyeon T, et al. Multi-modal transfection agent based on monodisperse magnetic nanoparticles for stem cell gene delivery and tracking. Biomaterials. 2014;35(25):7239-47.
79.Villate-Beitia I, Zarate J, Puras G, Pedraz JL. Gene delivery to the lungs: pulmonary gene therapy for cystic fibrosis. Drug development and industrial pharmacy. 2017;43(7):1071-81.
80.Templeton NS. Gene and cell therapy: therapeutic mechanisms and strategies: CRC Press; 2015.
81.Davies LA, McLachlan G, Sumner-Jones SG, Ferguson D, Baker A, Tennant P, et al. Enhanced lung gene expression after aerosol delivery of concentrated pDNA/PEI complexes. Molecular Therapy. 2008;16(7):1283-90.
82.Gautam A, Densmore C, Waldrep J. Pulmonary cytokine responses associated with PEI–DNA aerosol gene therapy. Gene therapy. 2001;8(3):254.
83.Griffith F. The significance of pneumococcal types. Epidemiology & Infection. 1928;27(2):113-59.
84.Avery OT, MacLeod CM, McCarty M. Studies on the chemical nature of the substance inducing transformation of pneumococcal types: induction of transformation by a desoxyribonucleic acid fraction isolated from pneumococcus type III. Journal of experimental medicine. 1944;79(2):137-58.
85.Hardee CL, Arévalo-Soliz LM, Hornstein BD, Zechiedrich L. Advances in non-viral DNA vectors for gene therapy. Genes. 2017;8(2):65.
86.Nayerossadat N, Maedeh T, Ali PA. Viral and nonviral delivery systems for gene delivery. Advanced biomedical research. 2012;1.
87.Ginn SL, Amaya AK, Alexander IE, Edelstein M, Abedi MR. Gene therapy clinical trials worldwide to 2017: An update. The journal of gene medicine. 2018;20(5):e3015.
88.Desfarges S, Ciuffi A. Retroviral integration site selection. Viruses. 2010;2(1):111-30.
89.Naldini L, Blömer U, Gallay P, Ory D, Mulligan R, Gage FH, et al. In vivo gene delivery and stable transduction of nondividing cells by a lentiviral vector. Science. 1996;272(5259):263-7.
90.Landau NR, Warton M, Littman DR. The envelope glycoprotein of the human immunodeficiency virus binds to the immunoglobulin-like domain of CD4. Nature. 1988;334(6178):159.

91. Zufferey R, Nagy D, Mandel RJ, Naldini L, Trono D. Multiply attenuated lentiviral vector achieves efficient gene delivery in vivo. Nature biotechnology. 1997;15(9):871.
92. Milone MC, O'Doherty U. Clinical use of lentiviral vectors. Leukemia. 2018:1.
93. Dull T, Zufferey R, Kelly M, Mandel R, Nguyen M, Trono D, et al. A third-generation lentivirus vector with a conditional packaging system. Journal of virology. 1998;72(11):8463-71.
94. Vink CA, Counsell JR, Perocheau DP, Karda R, Buckley SM, Brugman MH, et al. Eliminating HIV-1 packaging sequences from lentiviral vector proviruses enhances safety and expedites gene transfer for gene therapy. Molecular Therapy. 2017;25(8):1790-804.
95. Merten O-W, Hebben M, Bovolenta C. Production of lentiviral vectors. Molecular Therapy-Methods & Clinical Development. 2016;3.
96. Hoffmann M, Wu Y-J, Gerber M, Berger-Rentsch M, Heimrich B, Schwemmle M, et al. Fusion-active glycoprotein G mediates the cytotoxicity of vesicular stomatitis virus M mutants lacking host shut-off activity. Journal of General Virology. 2010;91(11):2782-93.
97. Sanber KS, Knight SB, Stephen SL, Bailey R, Escors D, Minshull J, et al. Construction of stable packaging cell lines for clinical lentiviral vector production. Scientific reports. 2015;5:9021.
98. Tomás H, Rodrigues A, Carrondo M, Coroadinha A. LentiPro26: novel stable cell lines for constitutive lentiviral vector production. Scientific reports. 2018;8(1):5271.
99. Shearer RF, Saunders DN. Experimental design for stable genetic manipulation in mammalian cell lines: lentivirus and alternatives. Genes to Cells. 2015;20(1):1-10.
100. Ellis J. Silencing and variegation of gammaretrovirus and lentivirus vectors. Human gene therapy. 2005;16(11):1241-6.
101. Yin H, Kanasty RL, Eltoukhy AA, Vegas AJ, Dorkin JR, Anderson DG. Non-viral vectors for gene-based therapy. Nature Reviews Genetics. 2014;15(8):541.
102. Fraley R, Subramani S, Berg P, Papahadjopoulos D. Introduction of liposome-encapsulated SV40 DNA into cells. Journal of Biological Chemistry. 1980;255(21):10431-5.
103. Lam A, Dean D. Progress and prospects: nuclear import of nonviral vectors. Gene therapy. 2010;17(4):439.
104. Dean D, Strong D, Zimmer W. Nuclear entry of nonviral vectors. Gene therapy. 2005;12(11):881.
105. Jäckel C, Nogueira MS, Ehni N, Kraus C, Ranke J, Dohmann M, et al. A vector platform for the rapid and efficient engineering of stable complex transgenes. Scientific reports. 2016;6:34365.
106. Boussif O, Lezoualc'h F, Zanta MA, Mergny MD, Scherman D, Demeneix B, et al. A versatile vector for gene and oligonucleotide transfer into cells in culture and in vivo: polyethylenimine. Proceedings of the National Academy of Sciences. 1995;92(16):7297-301.
107. Mao S, Neu M, Germershaus O, Merkel O, Sitterberg J, Bakowsky U, et al. Influence of polyethylene glycol chain length on the physicochemical and biological properties of poly (ethylene imine)-graft-poly (ethylene glycol) block copolymer/SiRNA polyplexes. Bioconjugate chemistry. 2006;17(5):1209-18.
108. Kircheis R, Wightman L, Schreiber A, Robitza B, Rössler V, Kursa M, et al. Polyethylenimine/DNA complexes shielded by transferrin target gene expression to tumors after systemic application. Gene therapy. 2001;8(1):28.
109. Densmore CL, Orson FM, Xu B, Kinsey BM, Waldrep JC, Hua P, et al. Aerosol delivery of robust polyethyleneimine–DNA complexes for gene therapy and genetic immunization. Molecular Therapy. 2000;1(2):180-8.
110. Breuzard G, Tertil M, Goncalves C, Cheradame H, Geguan P, Pichon C, et al. Nuclear delivery of NFκB-assisted DNA/polymer complexes: plasmid DNA quantitation by confocal laser scanning microscopy and evidence of nuclear polyplexes by FRET imaging. Nucleic acids research. 2008;36(12):e71-e.
111. Hall A, Lächelt U, Bartek J, Wagner E, Moghimi SM. Polyplex evolution: understanding biology, optimizing performance. Molecular Therapy. 2017;25(7):1476-90.
112. Wightman L, Kircheis R, Rössler V, Carotta S, Ruzicka R, Kursa M, et al. Different behavior of branched and linear polyethylenimine for gene delivery in vitro and in vivo. The journal of gene medicine. 2001;3(4):362-72.

113. Zhao Q-Q, Chen J-L, Lv T-F, He C-X, Tang G-P, Liang W-Q, et al. N/P ratio significantly influences the transfection efficiency and cytotoxicity of a polyethylenimine/chitosan/DNA complex. Biological and Pharmaceutical Bulletin. 2009;32(4):706-10.
114. Gebhart CL, Kabanov AV. Evaluation of polyplexes as gene transfer agents. Journal of Controlled Release. 2001;73(2-3):401-16.
115. Zheng C, Baum BJ. All human EF1α promoters are not equal: markedly affect gene expression in constructs from different sources. International journal of medical sciences. 2014;11(5):404.
116. Hsu C-C, Li H-P, Hung Y-H, Leu Y-W, Wu W-H, Wang F-S, et al. Targeted methylation of CMV and E1A viral promoters. Biochemical and biophysical research communications. 2010;402(2):228-34.
117. Herbst F, Ball CR, Tuorto F, Nowrouzi A, Wang W, Zavidij O, et al. Extensive methylation of promoter sequences silences lentiviral transgene expression during stem cell differentiation in vivo. Molecular therapy. 2012;20(5):1014-21.
118. Johnston JM, Denning G, Doering CB, Spencer HT. Generation of an optimized lentiviral vector encoding a high-expression factor VIII transgene for gene therapy of hemophilia A. Gene therapy. 2013;20(6):607.
119. Nowotschin S, Xenopoulos P, Schrode N, Hadjantonakis A-K. A bright single-cell resolution live imaging reporter of Notch signaling in the mouse. BMC developmental biology. 2013;13(1):15.
120. Mizutani K-i, Yoon K, Dang L, Tokunaga A, Gaiano N. Differential Notch signalling distinguishes neural stem cells from intermediate progenitors. Nature. 2007;449(7160):351.
121. Almlöf T, Gustafsson J-A, Wright A. Role of hydrophobic amino acid clusters in the transactivation activity of the human glucocorticoid receptor. Molecular and cellular biology. 1997;17(2):934-45.
122. Wires ES, Henderson MJ, Yan X, Bäck S, Trychta KA, Lutrey MH, et al. Longitudinal monitoring of Gaussia and Nano luciferase activities to concurrently assess ER calcium homeostasis and ER stress in vivo. PloS one. 2017;12(4):e0175481.
123. Heise K, Oppermann H, Meixensberger J, Gebhardt R, Gaunitz F. Dual luciferase assay for secreted luciferases based on Gaussia and NanoLuc. Assay and drug development technologies. 2013;11(4):244-52.
124. Shashkova S, Leake MC. Single-molecule fluorescence microscopy review: shedding new light on old problems. Bioscience reports. 2017:BSR20170031.
125. Niles AL, Moravec RA, Hesselberth PE, Scurria MA, Daily WJ, Riss TL. A homogeneous assay to measure live and dead cells in the same sample by detecting different protease markers. Analytical biochemistry. 2007;366(2):197-206.
126. Promega. CellTiter-Fluor™ Cell Viability Assay Technical Bulletin. 2017.
127. Rodova M, Jayini R, Singasani R, Chipps E, Islam MR. CMV promoter is repressed by p53 and activated by JNK pathway. Plasmid. 2013;69(3):223-30.
128. Stinski MF. Cytomegalovirus promoter for expression in mammalian cells. Gene expression systems. 1999:211-33.
129. van den Bosch MH, Blom AB, Sloetjes AW, Koenders MI, van de Loo FA, van den Berg WB, et al. Induction of canonical Wnt signaling by synovial overexpression of selected Wnts leads to protease activity and early osteoarthritis-like cartilage damage. The American journal of pathology. 2015;185(7):1970-80.
130. Godbey W, Wu KK, Mikos AG. Tracking the intracellular path of poly (ethylenimine)/DNA complexes for gene delivery. Proceedings of the National Academy of Sciences. 1999;96(9):5177-81.
131. Moghimi SM, Symonds P, Murray JC, Hunter AC, Debska G, Szewczyk A. A two-stage poly (ethylenimine)-mediated cytotoxicity: implications for gene transfer/therapy. Molecular therapy. 2005;11(6):990-5.
132. Bilir B, Kucuk O, Moreno CS. Wnt signaling blockage inhibits cell proliferation and migration, and induces apoptosis in triple-negative breast cancer cells. Journal of translational medicine. 2013;11(1):1.

133. Thibert C, Teillet M-A, Lapointe F, Mazelin L, Le Douarin NM, Mehlen P. Inhibition of neuroepithelial patched-induced apoptosis by sonic hedgehog. Science. 2003;301(5634):843-6.
134. Zweidler-McKay PA, He Y, Xu L, Rodriguez CG, Karnell FG, Carpenter AC, et al. Notch signaling is a potent inducer of growth arrest and apoptosis in a wide range of B-cell malignancies. Blood. 2005;106(12):3898-906.
135. Snapp EL. Fluorescent proteins: a cell biologist's user guide. Trends in cell biology. 2009;19(11):649-55.
136. Terry L. Riss PD, Promega Corporation. NanoLuc®: A Smaller, Brighter, and More Versatile Luciferase Reporter 2010.
137. Rechsteiner M, Rogers SW. PEST sequences and regulation by proteolysis. Trends in biochemical sciences. 1996;21(7):267-71.
138. Hall MP, Unch J, Binkowski BF, Valley MP, Butler BL, Wood MG, et al. Engineered luciferase reporter from a deep sea shrimp utilizing a novel imidazopyrazinone substrate. ACS chemical biology. 2012;7(11):1848-57.
139. Zeng Z, Huang B, Huang S, Zhang R, Yan S, Yu X, et al. The development of a sensitive fluorescent protein-based transcript reporter for high throughput screening of negative modulators of lncRNAs. Genes & Diseases. 2018;5(1):62-74.
140. Li X, Zhao X, Fang Y, Jiang X, Duong T, Fan C, et al. Generation of destabilized green fluorescent protein as a transcription reporter. Journal of Biological Chemistry. 1998;273(52):34970-5.
141. Mezan S, Feuz JD, Deplancke B, Kadener S. PDF signaling is an integral part of the Drosophila circadian molecular oscillator. Cell reports. 2016;17(3):708-19.
142. Fu L, Lv X, Xiong Y, Zhao Y. Investigation of Protein–Protein Interactions and Conformational Changes in Hedgehog Signaling Pathway by FRET. Hedgehog Signaling Protocols: Springer; 2015. p. 61-70.
143. Kim S-E, Huang H, Zhao M, Zhang X, Zhang A, Semonov MV, et al. Wnt stabilization of β-catenin reveals principles for morphogen receptor-scaffold assemblies. Science. 2013;340(6134):867-70.
144. Mao B, Wu W, Davidson G, Marhold J, Li M, Mechler BM, et al. Kremen proteins are Dickkopf receptors that regulate Wnt/β-catenin signalling. Nature. 2002;417(6889):664.
145. Severson E, Arnett KL, Wang H, Zang C, Taing L, Liu H, et al. Genome-wide identification and characterization of Notch transcription complex–binding sequence-paired sites in leukemia cells. Sci Signal. 2017;10(477):eaag1598.
146. Praktiknjo SD, Saad F, Maier D, Ip P, Hipfner DR. Activation of Smoothened in the Hedgehog pathway unexpectedly increases Gαs-dependent cAMP levels in Drosophila. Journal of Biological Chemistry. 2018;293(35):13496-508.
147. Cheng S, Maier D, Hipfner DR. Drosophila G-protein-coupled receptor kinase 2 regulates cAMP-dependent Hedgehog signaling. Development. 2012;139(1):85-94.
148. Yokoyama N, Yin D, Malbon CC. Abundance, complexation, and trafficking of Wnt/β-catenin signaling elements in response to Wnt3a. Journal of molecular signaling. 2007;2(1):11.
149. Ke J, Zhang C, Harikumar KG, Zylstra-Diegel CR, Wang L, Mowry LE, et al. Modulation of β-catenin signaling by glucagon receptor activation. PLoS One. 2012;7(3):e33676.
150. van Unen J, Rashidfarrokhi A, Hoogendoorn E, Postma M, Gadella TW, Goedhart J. Quantitative single cell analysis of signaling pathways activated immediately downstream of histamine receptor subtypes. Molecular Pharmacology. 2016:mol. 116.104505.
151. Takebe N, Warren RQ, Ivy SP. Breast cancer growth and metastasis: interplay between cancer stem cells, embryonic signaling pathways and epithelial-to-mesenchymal transition. Breast cancer research. 2011;13(3):211.
152. Pannequin J, Bonnans C, Delaunay N, Ryan J, Bourgaux J-F, Joubert D, et al. The wnt target jagged-1 mediates the activation of notch signaling by progastrin in human colorectal cancer cells. Cancer research. 2009;69(15):6065-73.
153. Won H-Y, Lee J-Y, Shin D-H, Park J-H, Nam J-S, Kim H-C, et al. Loss of Mel-18 enhances breast cancer stem cell activity and tumorigenicity through activating Notch signaling mediated by the Wnt/TCF pathway. The FASEB Journal. 2012;26(12):5002-13.

154. He J, Sheng T, Stelter AA, Li C, Zhang X, Sinha M, et al. Suppressing Wnt signaling by the hedgehog pathway through sFRP-1. Journal of Biological Chemistry. 2006;281(47):35598-602.
155. Schreck KC, Taylor P, Marchionni L, Gopalakrishnan V, Bar EE, Gaiano N, et al. The Notch target Hes1 directly modulates Gli1 expression and Hedgehog signaling: a potential mechanism of therapeutic resistance. Clinical cancer research. 2010;16(24):6060-70.
156. Batlle E, Clevers H. Cancer stem cells revisited. Nature medicine. 2017;23(10):1124.
157. Qiagen. Cignal 45-Pathway Reporter Array webpage 2018. Available from: https://www.qiagen.com/us/shop/protein-and-cell-assays/cignal-45-pathway-reporter-array/#productdetails. Accessed 31.03.2019
158. Biosciences G. Pathway Scan Multi-Pathway Reporter Kit 2019. Available from: https://www.gmbiosciences.com/products_PathwayScan_Multi.htm. Accessed 31.03.2019
159. Biosciences S. pGreenFire1-Notch Lentivector 2019. Available from: https://www.systembio.com/products/imaging-and-reporter-vectors/signaling-pathway-reporters/pgreenfire1-notch/. Accessed 31.03.2019
160. Zhang JD, Küng E, Boess F, Certa U, Ebeling M. Pathway reporter genes define molecular phenotypes of human cells. BMC genomics. 2015;16(1):342.
161. Ammeux N, Housden BE, Georgiadis A, Hu Y, Perrimon N. Mapping signaling pathway cross-talk in Drosophila cells. Proceedings of the National Academy of Sciences. 2016;113(35):9940-5.
162. Moffat JG, Vincent F, Lee JA, Eder J, Prunotto M. Opportunities and challenges in phenotypic drug discovery: an industry perspective. Nature reviews Drug discovery. 2017;16(8):531.
163. Vincent F, Loria P, Pregel M, Stanton R, Kitching L, Nocka K, et al. Developing predictive assays: the phenotypic screening "rule of 3". Science translational medicine. 2015;7(293):293ps15-ps15.

Disclaimer

Figures and images were cited according to the common regulations and citation rules to the best of my knowledge, and permission was obtained whenever possible. However, in case of any suspicion of copyright violation, please do not hesitate to notify me.